NERSC

MPI

European Commission Environment and Climate Programme 1994-98-
Topic 1.1.1

Acoustic monitoring of the Ocean Climate in the Arctic Ocean

AMOC

Subtask 3.1

Simulation of the effect of integrated temperature change on acoustic propagation

NERSC Technical Report no. 197

January 2001

SPRI

NIERSC

Project coordinator: Ola M. Johannessen,
Nansen Environmental and Remote Sensing Center,
Edv. Griegsvei 3a,
N-5059 Bergen
Norway

Authors:

Hanne Sagen, Ola M. Johannessen, Halvor Hobæk, Torill Hamre and Stein Sandven

Contract Number: ENV4-CT97-0463

Nansen Environmental and Remote Sensing Center

Edv. Griegsvei 3a,
N-5059 Bergen
NORWAY.
Phone: +47 55 29 72 88 Fax: +47 55 20 00 50
e-mail: administrasjonen@nrsc.no
Internet: http://www.nrsc.no/

a non-profit environmental research center affiliated with the university of Bergen

NERSC Technical Report

TITLE	**REPORT IDENTIFICATION**
AMOC Subtask 3.1 Simulation of the effect of integrated temperature changes on acoustic propagation	NERSC Technical Report no. 197
CLIENT European Commission Environment and Climate Programme 1994-1998. Topic 1.1.1	**CONTRACT** ENV4-CT97-0463
CLIENT REFERENCE Claus Bruning	**AVAILABILITY** Open
PRINCIPAL INVESTIGATORS Ola M. Johannessen Klaus Hasselmann Peter Wadhams Leonid Bobylev	**AUTHORISATION** Bergen, January 2001 DIRECTOR Ola M. Johannessen

AMOC partners:

Nansen Environmental and Remote Sensing Center, Bergen, Norway
Max Planck Institute for Meteorology, Hamburg, Germany
Scott Polar Research Institute, United Kingdom
Nansen International Environmental and Remote Sensing Center, Russia

Contents

CHAPTER 1: INTRODUCTION TO AMOC TASK 3

The overall objective of the AMOC project is to

Develop and design an acoustic system for long-term monitoring of the ocean temperature and ice thickness in the Arctic Ocean, including the Fram Strait, for climate variability studies and global warming detection.

The AMOC project consists of the following tasks:

Task 1: Arctic Ocean data analysis.
Task 2: Climate and ice modeling.
Task 3: Acoustic modeling of Arctic basin.
Task 4. Acoustic modeling of the Fram Strait.
Task 5: Acoustic monitoring.

This report presents the results of the work carried out in Task 3.

OBJECTIVE AND SUBTASKS

The main objective of Task 3 is

Simulation of present and future basin-wide acoustic propagation using natural variability and global warming scenarios (input from climate and ice modeling) to investigate the sensitivity of acoustic methods for global warming detection.

Task 3 consist of two subtasks:
Subtask 3.1 Simulate the effect of integrated temperature change on acoustic propagation
Subtask leader: Dr. Hanne Sagen.

Subtask 3.2. Study the effect of sea ice thickness and roughness on acoustic propagation.
Sub- Task leader: Dr. Peter Wadhams, Scott Polar Research Institute (SPRI).

This report present the work performed in sub-task 3.1. The results from subtask 3.2 are presented in a separate report by SPRI.

SUMMARY OF METHODOLOGY

The reported study applies three main methods: (1) analysis of data from provided from Task 1 (2) analysis of climate modeling results from task 2 and (3) use of existing acoustic propagation models.

WORK PACKAGE DESCRIBTION

The work package description, as defined in the AMOC contract Technical Annex (Johannessen et al, 1997) for the two subtasks are as follows.

Subtask 3.1 Simulate the effect of integrated temperature change on acoustic propagation

* The SAFARI model (Seismo Acoustic Fast Field Algorithm for Range Independent environments) will be used to study the sensitivity of travel time, amplitude and phase to changes in average ocean temperature, salinity and sea ice thickness. The study of range dependent ice conditions will be performed in subtask 3.2.

* In order to perform sensitivity tests, the approach is to use the present unperturbed sound speed field and the perturbed sound speed fields as caused by the predicted global warming scenarios from Task 2 as input to the acoustic propagation models. The result of the SAFARI model studies, together with a range dependent ray trace model (HARPO) or a parabolic approximation formulation including elastic ice cover using finite difference scheme (ELF model) will be used in the sensitivity studies.

* In a permanent Arctic AMOC system it is necessary to locate the sources and receivers on a shelf in order to connect cables to the shore. The ELF model will be used to study the effect of a discontinuous ice cover associated with the ice edge on acoustic propagation.

Subtask 3.2. Study the effect of sea ice thickness and roughness on acoustic propagation.

* Data on ice thickness and roughness along selected acoustic ray paths will be analyzed and interpreted. The data, which are obtained from submarine profiling and airborne laser profiling, will be made available in Task 1.

* The effect of frequency dispersion and variability of sound speed values in different ice types will be incorporated in the acoustic models. Single reflection will be modeled using an analytical technique and generalized to take account of the probability density function of the ice thickness.

* The sensitivity of changes in ice thickness and roughness distribution on acoustic propagation will be studied using input from data as well as from climate simulations in Task 2 to acoustic propagation models accounting for elastic properties and roughness.

ORGANIZATION OF THE REPORT

First an overview description of activities within Task 3 and their respective methods are provided in Chapter 2. Then work and results are given for each activity in Chapter 3-5. Finally a summary and major conclusions are presented in Chapter 6 along with recommendations for a future monitoring system in the Central Arctic.

Chapter 2: Overview of Activities and Methodolgy

In order to meet the objective of Task 3 and Task 3.1 the main activities in Task 3.1 was to

1. Describe the Arctic environment and evaluate existing acoustic propagation models for use in the Arctic
2. Modelling acoustic propagation characterstics for the Arctic .
3. Sensitivity study of climate related changes in ocean temperature

The methods used in each activity is described in this chapter, while the results are given i

ACTIVITY 1. EVALUATION OF ACOUSTIC PROPAGATION MODELS FOR USE IN THE ARCTIC OCEAN

In order to pick the best acoustic propagation model for the Arctic it is necessary to have fundamental knowledge of the of the Arctic ocean climate and how the environment is expected to change. This knowledge was obtained by using the results of Task 1 and by searches in literature. In order to take the benefit existing knowledge of Arctic acoustic, literature and internet was used to read about previous and ongoing acoustic studies in the Arctic. Several public domain acoustic models were evaluated for use in the interior Arctic and the Fram Strait. For ice studies the licensed OASES model was bought for the AMOC project.

ACTIVITY 2. MODELLING ACOUSTIC PROPAGATION IN THE ARCTIC OCEAN

Environmental data input to the Acoustic models

Sea ice

The sea ice were in this task generally modelled as a elastic homogeneous solid plate using typical compressional and shear wave speeds and corresponding absorpsions. Scattering was included using typical valuse for correlation rates and rms roughness.

Ocean

In Task 1 in AMOC existing ocean, ice and acoustic data were compiled through Internet search, scientific and technical literature, and the archives of the respective project partners. The contents of these data sets, and the parameters extracted for model runs in the first year of the AMOC project, are described in the technical report for task 1 (T. Hamre et al., 1998).
Based on the work done in Task 1 we have selected the Arctic Ocean Atlas CDs to be our main source of data for the interior Arctic. The CDs contain oceanographic data from a number of U.S. and Russian sources. The two CDs contain winter and summer data for the Artic region in the period from 1950-1989 in form of (1) annual fields, (2) station statistics and profiles for winter/summer periods for each of the four decadal periods 1950-59, 1960-69, 1970-79 and 1980-89 and (3) interpolated to a 50x50 km grid over the entire region.
In task 1 three Arctic sections were selected.

1. TAP A: The TAP-B track starts at 83^0 30' ^{0} N and 23^0 E ends at the receiver camp "SIMI" at 72^0. 59.9′ N 149^0 35.8′W
2. TAP-B: The TAP-B track starts at 83 30' ^{0} N and 23 ^{0} E ends at the receiver camp "NARWHAL" at 83 62.5' ^{0} N, 26 ^{0} W.
3. Fram Strait along 79 N.

The oceanographic environment along the tracks were establish and converted to 2 dimentional sound speed fields in Task 1. The sound speed fields were transferred into the

formats required for the Acoustic programs. The Fram Strait is generally not considered in this report, but in the task 4 report

Interface to acoustic models.

Software have been developed using Matlab to make data from US-Russian data atlas available for use in RAY, OASES and RAM. The sound speed profiles are not interpolated for use in OASES due to a rapidly increasing need of computer time when the number of sectors increases. In the case of RAY the sound fields and bathymetry are interpolated within the program. The RAM program has to be provided by an interpolated sound speed field, and a program doing this has recently been developed. Bathymetry is available from TerrainBase for use in RAY and RAM. The major difficulty has been to avoid problems with randomly missing data points in the environmental data from the US-Russian Atlas. The programs are found in /usr/users/amoc/apl/Matlab, /usr/users/amoc/ram/Matlab

Acoustic simulations

Sea ice sensitivity study

The objective was to investigate how sea ice changes effect the reflectivity at low frequencies, and furthermore how this will modify the open water acoustic thermometry Algorithms (traveltime, phase and loss). A side effect could be new algorithms for detection and estimation of changes in averaged sea ice thickness. Acoustic simulations were performed using the OASES model which includes a full elastic describtion of the sea ice cover. The OASES model where used both to study the reflection coeffisient, transmission loss and pulse propagation.

Ocean temperature sensitivity study.

The objective was to find the optimum source frequency for basin wide acoustic thermometry in the Arctic, which in practice is the optimum frequency of propagation. Several source depths and receiver positions were considered in order find the best configuration to detect typical seasonal/decadal changes in the sound speed profiles. The sesonal and decal changes in acoustic propagation using historical data from the US-Russian Atlas as input to the acoustic model.
Acoustic insonification is influenced by the bottom topography and this will be considered for each of the three Arctic sections.

ACTIVITY 3. SENSITIVITY STUDY OF CLIMATE RELATED CHANGES IN OCEAN TEMPERATURE

Acoustic simulations

One of the important issues in Task 3.1, has been to investigate if a shallow (60 m) and low frequency source (19.6 Hz), will provide the optimal information about the averaged ocean temperatures. Therefore one deep source (500 m) and one shallow source has been considered in the acoustic simulations in addition to 6 selected receiver depths.
Results from two climate change scenarios were produced and delivered from Task 2. The first production, antrophynic and control run, was delivered in June 2000. After analysing the results it was found that the salinity forcing field was wrong. A new production run were started (August 2000) and the results arrived NERSC in the end of Octobber, 2000.The climate modelling results were provided as monthly means of ice thickness, salinity, and

temperature fields from January 1950 through December 2050 along three acoustic tracks: TAP-A, TAP-B and Fram strait along 79 N. Then the oceanographic output data is converted to sound velocity field on a data format used by the RAY model.

Environmental data input to the Acoustic cmodels

The data deliverables obtained from MPI included monthly averages of the environmental fields aaalong the preselected acoustic tracks.

Sea ice

Sea ice thickness was provided with a resolution of 10 km along the tracks. The available ice parameters are shown in Table 2.1.

Ocean.

Salinity and temperature fields (depth and geographical position) was provided with 10 km horizontal resolution. The depth layers are shown in Table 2.2

Sea floor topography.

For each of the geograpical positions of the track the water depth was obtained from the TOPO5 data base. RAY and an absorption bottom condition was used.

The Acoustic model

Based on the results from the above activities the RAY model was selected for the production run using the climate modelling results as input. The RAY model obtains travel times for resonable CPU time, but still the production requires a lot of computer time. The calculations were therefore performed on the super computer ORIGON 2000.

An interface to the climate modelling results from Task 2 was developed for the RAY model using MATLAB. The programs are found in /usr/users/amoc/apl/Matlab.
The acoustic experiment was kept to the same for all the scenarios.
Two source depths 60 m and 500 m. Six receiver depths 50, 100, 200, 300, 400 and 500 m.

The production run algorithm.

In this study the following rough algorithm was used
For each scenario
Select track
Obtain depth for each position included in the scenario
Extract and read the oceanographic field as function of geographic position and depth
For each month **do** /*1200 months
Convert the oceanographic fields to sound speed profiles

For source depth (60 and 500 m) **Do**
Calculate Eigenrays and eigenfronts for the receiver depths:50, 100, 200, 300 400 and 500 m
Store arrival times for each Eigenfront
End

Then arrival times were then plotted as function of years for each source and receiver pair. This sequence was repeated for each 100 year scenario.

Table 2.1 Climate model parameters

Table shows the available output from the climate model, the parameters outlined in *italics* has been provided for TAP-A, TAP-B and the Fram Strait.

Content	Level	Variable	Unit	Code
temperature	40	THO	C	2
salinity	40	SAO	psu	5
zon. velocity	40	UKO	m/s	3
mer. velocity	40	VKE	m/s	4
freshwaterflux New.C.	1	EMINPO	m/s	67
total heatflux	1	FLUM	W/m**2	70
total freshwaterflux	1	PEM	m/s	79
ice thickness	1	SICTHO	m	13
ice compactness	1	SICOMO	%	15
zon. ice velocity	1	SICUO	m/s	35
mer. ice velocity	1	SICVE	m/s	36
snow thickness	1	SICSNO	m	141
heat flux shortwave	1	QSWO	W/m**2	176
heat flux longwave	1	QLWO	W/m**2	177
heat flux latent	1	QLAO	W/m**2	147
heat flux sensible	1	QSEO	W/m**2	146
net freshwater flux + runoff	1	PRECO	m/s	65
sealevel	1	ZO	m	1
hor. bar. streamfunction	1	PSIUWE	Sv	27
mixed layer depth	1	AMLD	m	83
seaice transport x	1	SICTRU	m**2/s	142
seaice transport y	1	SICTRV	m**2/s	143

Table 2.2 The 40 depth levels are listed in the table below.

20 first layers	20 first depths	20 last layers	20 last depths
1	5.0	21	445.0
2	15.0	22	520.0
3	25.0	23	605.0
4	35.0	24	700.0
5	45.0	25	805.0
6	55.0	26	920.0
7	65.0	27	1045.0
8	75.0	28	1185.0
9	85.0	29	1340.0
10	95.0	30	1510.0
11	107.5	31	1700.0
12	122.5	32	1910.0
13	140.0	33	2145.0
14	160.0	34	2420.0
15	182.5	35	2745.0
16	210.0	36	3120.0
17	242.5	37	3570.0
18	280.0	38	4120.0
19	325.0	39	4770.0
20	380.0	40	5620.0

Chapter 3.

Activity 1: evaluation of acoustic propagation models for use in the Artic ocean

Contents

3.1 Review of the Arctic Ocean Environment

Observing the Arctic Ocean

The structure of the water-masses in the Arctic and Antarctic oceans is impossible to measure by remote sensing techniques from satellites, since the electromagnetic- and micro- waves used in remote sensing do not penetrate the ice cover, and if it does the waves are attenuated within a few centimeters in the sea water. In order to observe the water-masses within the Arctic by existing methods expensive expeditions have been carried out using icebreakers, aircraft or submarines to collect a large number of in situ observations. The time it takes to get an overview of the water-masses in an area, makes short term variations in the water-masses unavailable by existing methods. The today knowledge of the water-mass structure of the Arctic Ocean is based on a high number of in situ measurements obtained during different experiments at different time and geographical grid.

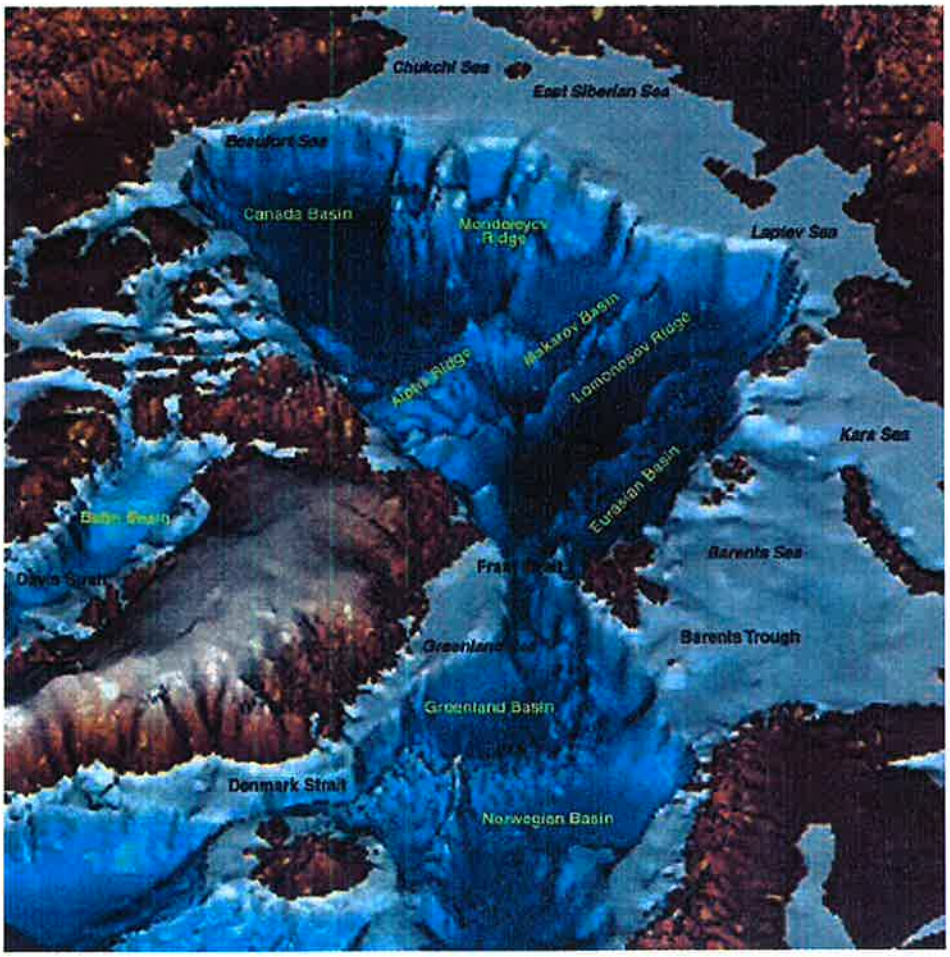

Figure 3.1. Bathymetric map of the Arctic Ocean and Nordic seas

Arctic Ocean bathymetry

As seen in Figure 3.1 the Arctic Ocean has one large deep basin surrounded by several shallow marginal seas (30-200m) above broad continental shelves (600-800 km). The large deep basin has two major sub-basins, the Eurasian Basin and the Canadian Basin which are separated by the Lomonosov Ridge. The Arctic Ocean is connected to the Pacific Basin by the shallow Bering Strait and to the North Atlantic and Nordic Seas by Fram Strait.

The watermasses in the Arctic Ocean

Oceanographical sections in the interior Arctic show water structures with small horizontal gradients and small temporal variations (Anderson, et al. 1994), in contrast to the strong gradients found in the MIZ (Johannessen et al., 1983). The MIZ is described in detail in the Task 4 report abot the Fram Strait. In this report we concentrate on the typical conditions in the central Arctic.

The water mass structure of the Arctic Ocean is characterized by relatively cold and less saline waters in the surface layer which are determined by seasonal variability of the ice cover (melting and freezing) and outflow of fresh water from rivers. The temperature structure in the upper few hundred meters defines a very strong vertical gradient in the sound speed profiles at a depth between 80 and 150 m; this gradient defines the lower boundary of the characteristic surface duct in the Arctic ocean. Warmer and more saline waters are found at intermediate depths originating from inflow of Atlantic water. The deep water masses, which occupy most of the water column, are quite homogeneous with variability in temperature of order 0.1°C and in salinity of order 0.02 ‰.

The surface mix layer

A surface mixed layer (SML) with a rather constant temperature close to freezing (-1.8 ^{0}C) is present over the entire central deep basin, whereas the layer thickness and salinity vary from region to region over the Arctic basins. The thickness of the SML can roughly be defined as the depth to which the salinity is constant to within 0.1, while the temperature is close to freezing (-1.8^0 C). The horizontal variation in salinity was found to vary between 31.5 and 33 in Oden91 which is significant (Anderson, 1994). On the other hand according to the US-Russian data there has been no large changes from the 1950s to the 1980s, See Figure 3.2.

There have been no virtual current measurements within the SML, but the mean circulation is generally reflected by the sea ice drift. The sea ice drift have been observed to flow in a large anti-cyclonic gyre over the Canadian Basin with an outflow to Fram Strait as part of the Trans Polar Drift. Chemical tracers have shown a second drift from the Laptev sea region, which follows the Nansen-Gakkel Ridge and through the western Fram Strait. (Anderson, 1994)

The halocline water layer.

Below the SML in the Arctic Basin we find a water-layer called the cold halocline water layer (CHL) The halocline is defined to be water-masses where the density gradient, with respect to depth, is due to salinity rather than temperature. The CHL represents a transition between two core water masses: cold, fresh waters and the cold, salty, Lower Halocline Water (LHW). CHL derives from river and Bering Strait inflows. The source of the LHW is unknown, but has been related to the ice growth on the shelves of the Eurasian Basin, and to the air-ice ocean exchange found in the MIZ in the Fram Strait.

Steel and Boyd (1998) reported saltier surface waters in the Eurasian Basin in the 1990s than any time since 1950s. The result is a retreat of the cold halocline layer from the Eurasian Basin into the Makarov Basin. The CHL layer insulates SML and the ice pack from the warmer and saltier Atlantic/Pacific Water throughout the Arctic Ocean (Anderson, 1994), and the reported change may cause a thinning of the sea ice cover.

The circulation of Atlantic and Pacific water

The circulation and distribution of the Atlantic water layer and deeper water in the Arctic Ocean are strongly connected to the complex bathymetry briefly described in the introduction. In the Eurasian basin waters the ventilation of water is good, whereas the deep water in Canadian Basin is more isolated. Results from Oden91 indicated that the two main basins maintain distinct circulation's separated by a front in the central region over the Lomonosov ridge (Anderson, et al 1994). Furthermore, Oden91 indicated a possible communication between the two circulation systems at the two southern boundaries. This communication was confirmed by a later expedition Larsen93 (McLaughlin et al, 1996). On the otherhand Larsen93 reported the Atlantic/Pacific boundary to be found well within the Canadian Basin, over the Mendeleyev Ridge. These data indicate that a rapid reposition of the Atlantic/Pacific boundary has occured. Based on historical data and the Larsen 93 a circulation scheme was proposed by McLaughlin et al 1996 (figure 3.2).

The Fram Strait and the Barents Sea are the main areas for exchange of water masses, heat flux and sea ice between the Arctic Ocean and the Greenland Sea and Norwegian Sea (Sandven and Johannessen, 1990). About 240 km of the 600 km wide Fram Strait at 79° N is more than 2000 m deep (Sandven and Johannessen, 1990). The maximum sill depth between the Greenland Sea and the Arctic Ocean is 2600 m (Coachman and Aagaard, 1994), allowing deep water masses to be exchanged through the Fram Strait. A 300 km wide continental shelf of less than 400 m depth covers the Greenland side of the strait. On the Svalbard side the shelf is less than 100 km wide. The width of the Fram Strait allows inflow of warm water to the Arctic Ocean and outflow of cold water and ice to be separated horizontally. The current system is dominated by the northward flowing warm and saline Atlantic water in the West Spitsbergen Current (WSC) and the shallow southward flowing cold and low salinity East Greenland Current (EGC) which exports ice and polar water out of the Arctic Ocean.

The WSC is a continuation of the Norwegian North Atlantic current which branches northwards (WSC) and eastwards (North Cape Current) off the northern cost of Norway (Pfirman et al., 1994). These currents bring relatively warm coastal and Atlantic water into the Barents Sea, keeping a large part of it ice-free during the winter. The Atlantic water flowing via the Barents Sea and Atlantic water in the eastward going extinction of the WSC entering the Arctic Basin through the Fram Strait are recombined in the Nansen Basin. This recombination have strongest effect on the intermediate depth waters.

In ***Figure 3.3***.3 the temperature at 300 m depth is shown for 1950s and 1980s. The warmer water occupies a larger part of the waters north of Svalbard, and there is a change in the Canadian basin as the colder water has moved westwards. There are no major changes in the Fram Strait..

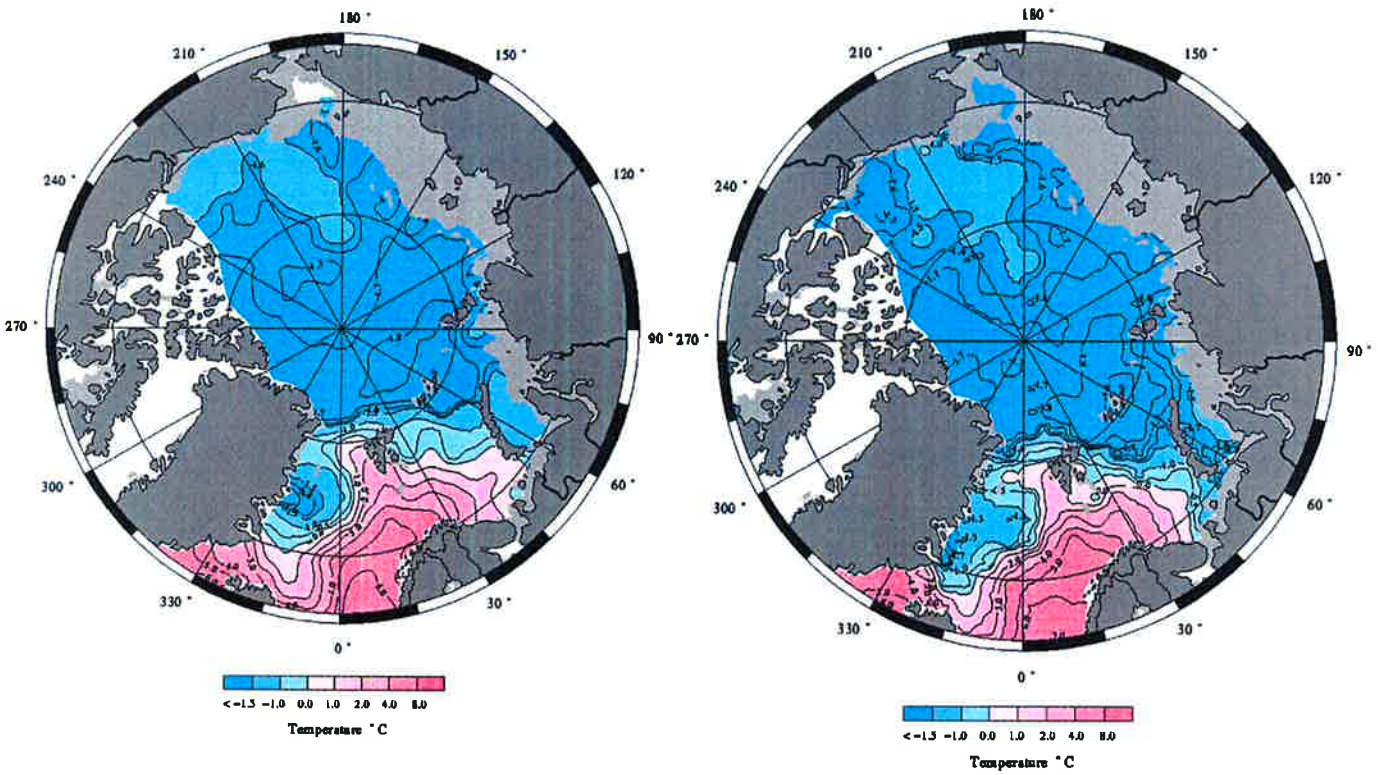

Figure 3.2 Data from US-Russian Data Atlas: Winter Temperature at 50 meters depth. Left: 1950s and Right 1980s

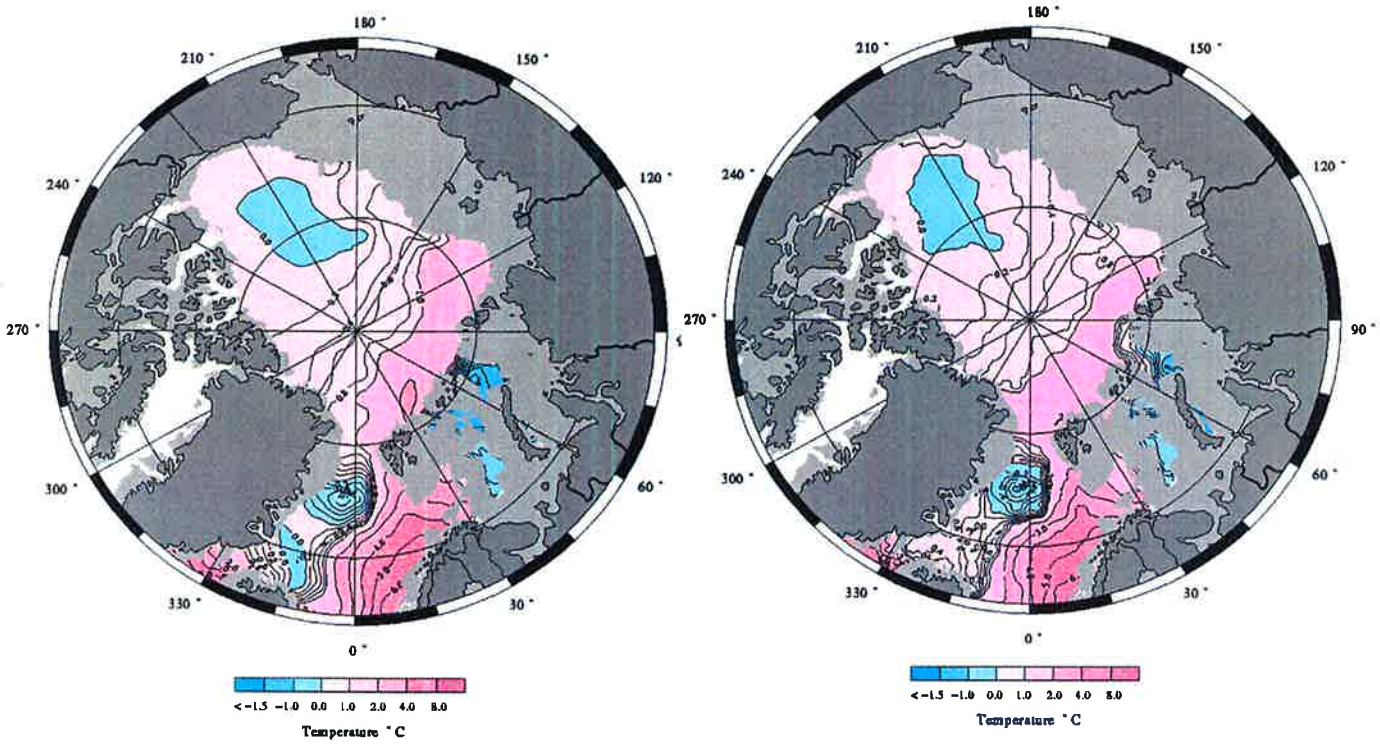

Figure 3.3 US-Russian Data Atlas: Winter Temperature at 300 meters depth. Left 1950s and right 1980s

Tidal currents

It has been known from the time of Nansen that tidal currents, forming elliptical trajectories, produce periodic convergence and divergence in the ice pack. The tidal current oscillations in the Arctic Ocean influence the ice distribution and generate periodic leads in the ice cover. Tidal currents consist of many constituents, the semidiurnal M_2 and S_2 and diurnal K_1 and O_1 constituents and diurnal components. The diurnal components can be trapped due to non-uniform bottom topography as found at the shelf break where the tidal current can be enhanced. Johannessen et al. (1992) have used Gjevik's tidal current model (Gjevik et al., 1990) with two diurnal and two semidiurnal components to estimate tidal ice motion. A high cross correlation is found between tidal current derived from Gjevik's model and the ice motion measured by Argos drifters. These results confirm that the ice floe motion is strongly determined by the tidal motion (Johannessen et al 1992a). The ice-tide interaction affects not only the ice distribution but also changes amplitude and phase of the tidal current significantly in shallow water under shore-fast ice (Kowalik and Proshutinsky, 1994).

Kowalik and Proshutinsky (1994) have modeled the dynamical interactions in the ice-water system using a space grid of about 14 km, which is of higher resolution than the Gjevik model used by Johannessen et al. (1992a). Numerical experiments show that the ice cover in the Arctic ocean is of minor importance for the tidal wave propagation, and the model was unable to reproduce the phase lag and amplitude change in very shallow water under shore-fast ice (Kowalick and Proshutinsky, 1994). Figure 3.4 shows the maximum shear of ice velocity due to the $M_2+S_2+K_1+O_1$ components. A considerable velocity shear, between 50 - 100 x 10^{-7} s^{-1} is found in all ice covered regions on the shelves surrounding the Arctic Ocean. A high shear (above 10^{-6}) favors the generation of leads and regions of high internal ice stress. The interaction between tidal current and the ice cover causes strong periodic fluctuations in low frequency ambient noise, where maximum ambient noise coincide with maximum tidal velocity (Johannessen, et. al. 1992; Bourke and Parsons 1993). The tidal current will be a predictable influence of the signal to noise ratio on the shelf.

Mesoscale processes

High-frequency internal waves can occur anywhere in the ocean where there is vertical stratification and generating mechanisms. Studies in ice covered regions show that internal waves can be generated by several mechanisms such as current interaction with seamounts, ice keels moving relative to the underlying water masses, and interaction with eddies and current shear (Sandven and Johannessen, 1987). In the MIZ internal waves can be manifested by SAR observations at the surface and underwater arrays of temperature profiles. Investigations of internal waves in the Fram Strait MIZ show that density and corresponding temperature surfaces in the pycnocline can oscillate vertically with amplitudes up to 5 m and a frequency of typical 3 - 4 cycles per hour, which is near the buoyancy frequency for internal waves. These oscillations will have impact on the sound velocity profiles and the acoustic propagation conditions (Dyer et al., 1987, Lynch et al., 1996) as well as on low frequency ambient noise (Makris and Dyer, 1991).

Intense small eddies appear to be ubiquitous in at least in the Canadian Basin (Aagaard and Carmack,1994). Typical eddy diameters are in the range of 10-20 km and their tangential speeds can exceed 30 cm/s. The eddies are generally embedded in the pycnoclineor within the Atlantic layer, and their thickness does not usually exceed 400-500 m. The eddies have little or no surface manifestation, their water properties anomalous, suggesting a distant origin. They are most reasonable formed near the margins of the Artic Ocean, and they have very long lives, probably many years.

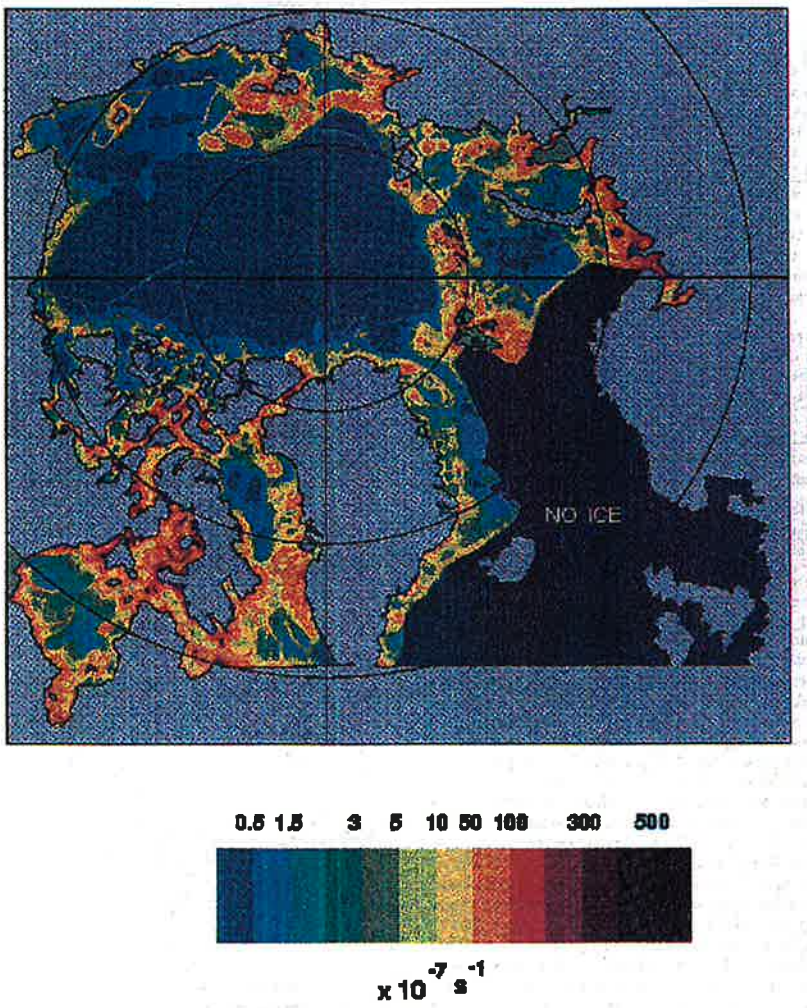

Figure 3.4. Distribution of maximal shear of ice velocity in the Artic Ocean caused by four components M2,S2,K1 and O1 (From Kowalik and Proshutinsky, 1994)

The Arctic Sea ice

Sea ice is an integral component of the polar climate system. Ice area and thickness are the two fundamental parameters for estimation of ice mass balance, which shows the response of sea to climate change. Data from polar orbiting satellites provide the most consistent, reliable means of deriving quantitative information on the global ice cover, such as sea ice extent and ice classification maps. are used extensively in monitoring of sea ice area, extent, concentration and ice types. Whereas ice thickness is not available by the remote sensing techniques used to day.

Therefore, improved methodology for global ice thickness measurements is therefore of primary importance in monitoring the global ocean and climate system (Allison and Moritz, 1995).

The sea ice *in the interior Arctic ocean* is generally described as a mixture of continuous ice cover, which can be broken up by leads, and numerous ice floes of varying size. Average thickness of the multiyear ice, which is the ice surviving one or more summer seasons, is about 3 m, but the maximal thickness can exceed 20 m in areas of heavy ridges and ice keels. The leads can be open water or covered with new frozen ice. The surface topography is determined by the amount and size of ridges and the presence of edges surrounding floes and leads.

Sea ice extent

Johannessen et al, 1997 and Parkinson et al 1999 analyses a time-serie total sea ice extent, derived from satellite passive microwave data for November 1987 through December 1996, using the limit of at least 15 % ice concentration. These data show that the Arctic Ocean is fully ice covered in a least 1 month of the year and generally for at least 3 months, most typically, February-April. The average seasonal cycle shows near full ice coverage from December through April, followed by a slight opening in the three months from May through December. An overall negative trend in the minimum sea ice extent observed during the summer time, whereas full sea ice coverage is still observed during the winter time. This also indicate increasing seasonal variation in sea ice extent, which again implies changes in the sea ice composition.

Two decades, of continuous brightness temperature (T_B) data obtained from the satellite-borne Scanning Multichannel Microwave Radiometer (SMMR) and Special Sensor Microwave Imager (SSMI), have been analysed (Johannessen et al., 1999). It is found that the total ice extent and area in the Arctic have decreased about 6% during the two decades (1978-98), consistent with reduction rate found in studies to 1996 (Bjørgo et al., 1997). This represents a reduction of over 600,000 km^2 in the total ice area. It is also found that the multi-year ice area in winter has decreased more rapidly, about 9% per decade, i.e., 18% over the observation period, representing a reduction of nearly 900,000 km^2, of which about half is replaced by first-year ice. This is the first time that quantitative changes in the *character* of the sea ice cover have been derived from passive microwave satellite data. These findings show an Arctic ice cover in apparent transformation, and suggest a thinner winter ice cover, consistent with very recent analyses of two decades of submarine sonar transect data (Wadhams, 1998). However, it must be noted that even two decades of observations, whether satellite or in situ, are inadequate to establish whether these represent long-term trends.

Sea ice thickness

Sea ice thickness distribution in the Arctic and Antarctic oceans is difficult to observe by any existing methods unless expensive expeditions with icebreakers, aircraft or submarines are carried out collecting a large number of in situ observations by upward looking sonar's repeatedly over many years (Wadhams, 1998). Polar orbiting satellites are the most cost efficient platforms for observing ice parameters, because they can provide data coverage of all ice areas in both hemispheres with sufficient temporal and spatial. However, the satellite sensors and processing techniques are not yet developed for retrieval of ice thickness directly. The reason is that it is difficult to establish significant relations between ice thickness and remotely sensed parameters with the data which have been available so far (Wadhams et al., 1992, Wadhams, 1994).

Definition of ice thickness distribution

Sea ice thickness on local scale is highly variable due to a number of ridges and corresponding ice keels To characterize the ice cover it is necessary to estimate a thickness probability distribution function (PDF) which require a number of observations of each thickness category (Wadhams, 1994, Wadhams, 1998).

The ice thickness PDF g(h) is defined by

$$\int_{h_1}^{h_2} g(h)dh = \frac{1}{R}\{A(h_1,h_2)\}$$

Correspondingly, the draft PDF is defined by

$$\int_{h_1}^{h_2} f(D)dD = \frac{1}{R}\{A(h_1,h_2)\}$$

where f(D)=g(h)/k and the factor k is varying with ice type and season Wadhams (1998) uses the factor k=1.36. This provide a method for measuring the ice thickness by means of ice draft measurement using acoustic sonars.

Sonar data

Most sonar data published so far have been obtained by upward looking sonar profiling from submarines whose exact positions are classified (Wadhams, 1994). Upward looking sonar's mounted on moorings obtain valuable time series of the ice thickness, derived form ice draft measurements, at selected locations, such as in the Fram Strait (Vinje et al., 1998). Sonar data are severely restricted by high cost, limited spatial coverage, inability to provide global data sets, and military constraints. The data are very valuable site specific observations and for validation of model estimates and new satellite monitoring techniques.

In a paper a recent submitted paper by Rothrock, et al, 1999 summer sea ice draft data from the SCICEX submarines cruises from 1993, 1996 and 1997 are analysed and compared to summer and fall data obtained during cruises between 1958 and 1976. The study show that the mean draft data from a large portion of the Artic have decreased on average by about 1.3 meters, roughly 6.5 cm a year. An objection to the result is that the SCICEX experiments were carried out with in years with minimum in sea ice extent in the summer time (Rothrock, 1999, Johannessen, 1999) which can cause the reduction a year to be overestimated (Johannessen, et al, 1999).

Gravity waves

Elastic gravity waves in ice are caused by ocean swell waves generated in ice-free oceans, strong wind zones and ridging processes. Long surface waves (200-500m) couples to the sea ice cover and can propagate hundreds to thousands of kilometers with weak dampening (Wadhams, 1987). Long surface wave propagation is not disturbed by non-uniform ice conditions, such as hummocks, thin ice and water patches, which have a relatively small horizontal dimension compared to wavelength. Ice thickness can be obtained from measured dominant wavelength, wave period and direction using the dispersion relationship for a thin elastic plate given the plate stiffness of the sea ice (eq. Sagen, 1998). The thickness obtained will be a characteristic ice thickness for an area big enough to be sensed by the travelling wave.

Spatially-averaged regional ice thickness estimates have been made using directional surface elastic-gravity wave measurements from Russian *North Pole* drifting stations (Naugurnyc). Measurements of surface oscillations of the ice cover were carried out regularly in the Eurasian Basin from 1972 to 1991. Using a wave algorithm, based on measuring the frequency of resonant waves, directional ice thickness estimates are derived with an error less than 10 % using an averaged elastic property of the sea ice is used. Furthermore, by averaging the directional ice thickness' obtained during April-May each year a spatially-averaged effective ice thickness for each year is obtained. The ice thicknesses obtained vary between 3.02 m and 2.8 m. Furthermore, the data show an on the average decrease of 1 cm in mean effective ice thickness pr year from 1978 to 1990. A more detailed inspection of the time series show two periods of significant reduction of sea ice thickness the first between 1978 and 1982 (10 cm-2.5cm pr year) and the second between 1987 and 1990 (22.5 cm-7.5 cm pr year). Between these two periods there is a period with significant increase in ice thickness (1.5 cm-3cm pr year). Only the period between 1987 and 1990 have a decrease corresponding to decrease pr year observed by Rothrock et al, 1999. This certainly show the difficulties in picking out trends from 20 years of data and sparse data sets.

The ice thickness data from the Russian work has been correlated with the mean extent area of multiyear ice in April-May derived from Micro wave data, and a correlation factor of 0.77 was obtained (Johannessen et al., 1999). This implies that the effective ice thickness variability obtained by the wave method can be explained by variations in the extent of multi year ice. It would be interesting to redo the analysis with total sea ice coverage variation to see if the effective ice thickness retrieved by the wave method is mainly reflecting the multi year ice.

3.2 PREVIOUS ACOUSTIC STUDIES IN THE ARCTIC

The open ocean is usually considered as an acoustic wave guide limited by the sea floor and the sea surface, and the main problem is to model a rough free surface and a rough sea floor with varying geo-acoustic conditions. Several advanced range dependent numerical models have been developed during recent years, see reviewed by Buckingham, (1991) and Jensen et al., (1994).

The waveguide description is also adequate for the Arctic Ocean, but there are three dominant features of the Arctic which affect sound propagation compared to open ocean:

1) the sea ice cover
2) the very strong vertical gradient in ocean temperature at a depth between 80-200m,
3) the small horizontal gradients in the oceanographic parameters (temperature, salinity and density)

Propagation effects in a typical Arctic Ocean are summarized in Table 3.1. Sound at frequencies below a cut off frequency (domain) leaks out of the channel and interacts with the bottom and surface, causing reflection loss due to two boundaries. Higher frequency sound is trapped within the surface duct, and repeatable exposed to a angular and frequency dependent reflection coefficient at the water ice boundary. This corresponds to first a high pass filtering and then a filtering of higher frequencies due to the interaction with the ice cover.

The transmission loss in the Arctic generally follows the law of cylindrical spreading at long ranges (Diachoke, 1976), this is due to the small horizontal variation in ocean layering and the strong vertical stratification of the upper ocean. Deviation from the cylindrical spreading or correspondingly the wave guide model, will vary with range and frequency due to the reflection and scattering from the sea ice cover and non-geometrical loss mechanisms. Most often the loss model include only scattering from a rough free surface (ex. Diachoke, 1976, Rubenstein and Greene, 1991), but several studies underlines the importance of including the elastic properties in the description of the reflection coeffisient (Fricke, 1991, 1993, Le Page and Schmidt). The inclusion of rough sea ice cover complicates the modeling work of the reflection and scattering significantly (e.q. Fricke, 1991, 1993; Schmidt, 1994; LePage and Schmidt, 1994).

Table 3.1 Summarized propagation effects in a ice covered ocean with strong surface duct

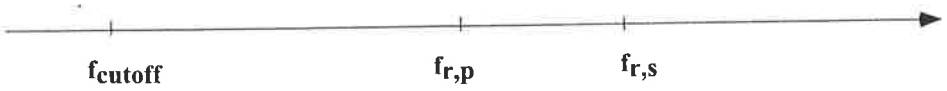

$f<f_{cutoff}$	Sound leaks out of the surface duct and significant bottom interaction occurs at shallow and intermediate water depths. The cutoff frequency increases as the duct depth reduces.
$f > f_{cutoff}$	The sound is trapped in the surface duct, and influenced by the interaction with the ice cover. The number of interactions with the ice cover increases as the duct depth reduces, this will increase the attenuation.
$f_{cutoff}<f<fr,p$	The transmission loss is dominated by scattering from the ice cover or rough sea surface. The reflection coefficient is one (or close to one) and causes no transmission loss.
$fr, p <f<f_r, s$	P waves starts to be refracted into elastic p waves in the ice cover this corresponds to an reflection coefficient less than one for angles above critical grazing angle for p waves. The reflection coefficient causes an steadily increase in attenuation for frequencies above this frequency.
$f_{s,p} <f< F$	Reflection loss due to energy conversion to elastic shear waves are introduced for a very broad range of angles, and the reflection loss increases very rapidly above this frequency and up to a frequency F from where the Reflection loss as a function of grazing angle is constant with increasing frequency.

An overview of acoustic studies carried out the last 25 years are listed in Table 3.2

Table 3.2. Summary of previous studies in the Arctic ocean

References	Geographical location - Study objective - Methodology used - Main Results
Diachoke,1976	Experiment in Lincoln Sea in combination with a environmental/acoustic model. The main objective was to present a theoretical model of under ice reflectivity which is consistent with the statistical and geometrical models of sea ice ridges, and furthermore to use the concept to show the effect of under ice reflection loss on long range transmission loss. A pressure release boss scattering models were used developed by Twersky. The sea ice ridges was modeled as infinitely long, randomly distributed elliptical half-cylinders. (Statistic parameters describing the distribution of ridges are average keel depth and width, number of ridges/km and grazing angle.). Diachoke reported a good agreement between experiment and theory at frequencies above 200 Hz. Acoustic transmission loss calculations are made for 40 Hz, 50Hz and 200 Hz using a ray model including 1000 rays with a source fan of +/- 15^0. This gives reasonable good agreement between theory and measurements for ranges up to 150 km, where the results starts to become less consistent.
Jin and Wadhams, 1989	Ray theory was used to predict the intensity and travel time changes due to sea ice cover. According to this work a travel time change has two contributing components: the physical reduction in the path length due to the reflection occurring at a depth equal to the ice draft rather than at the surface; and a change in travel time due to a horizontal beam displacement which occurs at reflection. They found that in many cases there is a travel time decrease which is monotonic and is almost proportional to ice thickness; their estimates were for the geometry of the 1989 Greenland Sea tomography experiment, with a path length of about 200 km, and they predicted a travel time decrease of about 1 ms per metre of ice thickness. In other cases, however, the use of a range of possible compressional and shear velocities in the ice led to travel time changes which were not necessarily monotonic with thickness and which therefore could not be used for thickness measurement. A need was identified for better measurements of sound velocities in sea ice, for which only very sparse data exist. Jin and Wadhams also estimated the scattering loss in a rough Greenland Sea-type (i.e. MIZ - marginal ice zone) ice field, using both the method of small perturbations and the tangent plane method, estimating some 15 dB over 200 km for steeper rays. This would be enough to reduce the signal-to-noise ratio so as to cause a deterioration in the timing precision of the order of 0.5-1 ms.
Kupermann and Schmidt, 1989	Elastic perturbation approach is developed. By introducing a boundary condition operator formulation, the effect of scattering on the mean field is accounted for by replacing the boundary conditions for the smooth interface with a set of effective boundary conditions involving matrix operation. The "new" boundary conditions are compatible with existing propagation models for stratified media.
Rubenstein, 1991	A theoretical study which provide the exact solution of scattering off a flat surface with a single semi-elliptical cylindrical boss of infinite extent. This study assumes a Rayleigh distribution of ridge-keel depths. The most important results from this study are that at frequencies below 200 Hz scattered incoherent acoustic energy is directed towards the bottom where it is absorbed, while energy at frequencies above 200 Hz is directed towards shallow angels where it becomes a propagating incoherent component. Above 400 Hz the scattering loss becomes relatively constant. Furthermore it is clear from this study that the scattering loss depends on how the distribution of keel depths are modeled. Rubenstein and Greene also studied the sensitivity of surface scattering to the statistical distribution of ice-ridge keel depths, which shows that constant keel depth gives more reflection and scattering losses than by assuming a Rayleigh distribution of keel depths.

Fricke, 1991, 1993.	The motivation of this study was the in ability in existing scattering theories to explain observed losses at low frequencies , 10-100 Hz in long range propagation experiments. A numerical acoustic propagation model using finite difference solution to the elasto-dynamic equations of motions was developed. Then the model was used to calculate the scattered field from the elemental scatters with different elastic properties. The major result was the documentation of the strong effect of the elastic properties of the sea ice on scattering. The simulations indicate that young keels can be modeled as fluid structures which give rise to a dipolar scatter field. Furthermore it was found that older keels are better modeled as elastic structures which causes the sound to scatter in a quadro polar field. For these low frequencies the simulations indicate that the loss depend on frequency as $f^{3.5}$ in the case of young ice while in the case of old ice the dependence is $f^{4.5}$. The observed frequency dependence is close to $f^{3.5}$. From this it was suggested that the observed long range propagation loss is best explained by scatter from large, young pressure ridges.
Jin et al. 1993	The objective of this study was to investigate the effects of sea ice on acoustic ray travel times, with applications to the Greenland Sea tomography experiment. Generalized ray theory were used to study the effect of sea ice cover on travel time using a source with a center frequency of 250 Hz. In this work it was shown that for a non uniform ice thickness, the travel time changes can be estimated approximately by adding the time changes due to individual reflections. For higher shear velocities in the ice the travel time changes can simply be estimated from the beam displacements and time delay of the reflection at the central frequency instead of using the generalized ray method. For lower shear velocities in the ice the sound may penetrate into the ice and large errors will be introduced if resonant reflection is present for a large number of reflections. In these cases the generalized ray theory has to be used. Furthermore it was found from simulations that the shear velocity, ice thickness are most important for changes in travel time. At resonant reflection absorption will be important. The travel time change over a 121 km long track is in the order of milli seconds. This lead to the conclusion that the effect of sea ice cover negligible in a tomographic inversion scheme for the Greenland Sea.
Le Page and Schmidt, 1994	The Elastic perturbation approach is used together with KRAKEN to study the low frequency propagation in the Arctic (10-100 Hz). It is shown that by using a fully elastic, two dimmentional perturbation theory greater coherent loss is predicted than if the free surface assumption is used. The scattering is sensitive both to the type of surface spectra and by tuning the individual spectra.
Fricke and Unger, 1995	The main objective of this study was to test the results in Fricke, 1993 with laboratory experiments. The measurements of the scattered field from the two models shows that young keels behave very different from old keels in terms of how they scatter sound. The young keels have a dipolar like scattered field while the scattered field from old ice is closer to a quadro polar. Furthermore the results leads to the conclusion that the internal properties determines the dominant pole of the scattered field and the roughness determines the amplitude. Therefore, it was recommended that the internal structure of the ice has to be included if proper scattering loss prediction should be made for long range propagation.

Laible and Rajan, 1996	A year long acoustic tomography experiment, April 1992-April 1993, in multi year ice was conducted in Sabine Bay of Melville Iceland. The Reflection coefficient at water ice interface has been determined as function of time, displaying seasonal variations. Two theoretical models, a model based on Biot theory and an elastic model, are used to calculate the compressional and shear wave speeds given the temperature and salinity structure. The temperature and salinity profiles are obtained from a on-dimensional thermodynamic model. Compressional and shear wave speed profiles are then used as input to theoretical model for the magnitude of the acoustic reflection coefficient. From simple Numerical calculations of the plane wave reflection coefficient at 12 kHz are performed by OASES, using monthly wave speeds (10 cm layers) obtained from the thermodynamic model. Differences are observed at grazing angles close to the angle where conversion to shear waves occur. The shear waves speeds are sensitive to temperature changes in the sea ice. Roughness of 0.01m rms is considered showing an significant effect in reflectivity at the frequency considered. Based on the numerical study the seasonal variations in reflectivity was concluded to be an combined effect of changes in the reflection coefficient, roughness and in the water column.
Pawlowics et al, 1996	Results from the Trans Arctic Propagation Experiment performed in April 1994 using a low frequency source. Track from TURPAN to NARWHALE, 1000 Km long. CW and M sequence transmissions are performed. The study shows that stable phase measurements are obtained and that these can be used to measure changes in the less stable travel time. Coupled normal mode theory is used as forward model. Adiabatic approximation works well for mode 1 and 2 but not for higher modes. Several scattering theories was explored, ending up with the Le Page and Schmidt elastic scattering theory as the best. The main conclusion is that the forward problem is well enough understood to launch an acoustic monitoring program in the Arctic.
Mikalevsky et al., 1999	During a pilot Transarctic Acoustic Propagation experiment (TAP) conducted by Mikhalevsky in the spring of 1994, long range propagation (2600 km) in the Arctic Basin was performed. . Track from TURPAN to SIMI, 2600 Km long. 1994 using a low frequency source. Track from TURPAN to NARWHALE, 1000 Km long This experiment showed that transmission across the Arctic basin is possible. The approach of this study was to use the normal mode code to analyse the experimental results. It was observed that mode 2-5 is sensitive to changes in ocean temperture. Furthermore, the results of this study show that the travel time and phase measurements are more than accurate enough to pick up changes caused by climate change in the Arctic basin (Mikhalevsky et al. 1999). By comparing simulated historical and present travel times to travel times measured during the TAP experiment, it is found a clear increase in travel time. This corresponds to the observed increase of the ocean temperature found in the oceanographic data. Despite the lack of "simultaneously" obtained oceanographic data and acoustic measurements, TAP demonstrates the feasibility of using travel-time measurements to monitor changes in averaged ocean temperature, which was the one of the main objectives of this experiment. The sea ice has an dampening effect on acoustic waves due to reflection loss and scattering, and and it was concluded, without any sensitivity study, that the attenuation of the lowest modes contains information about the sea ice properties.

3.3 General Definitions in Ocean Acoustic Propagation

Sound speed

The speed of sound in water depends on temperature, salinity and density and depth, c(T,s,δ,z). Several empirical functions has been developed and one simplified expression is

$$c = 1449.2 + 4.6T - 0.055T^2 + 0.00029T^3 + (1.34 - 0.01T)(S - 35) + 0.016z$$

As a rule of thumb the sound speed increases by about: 4m/s per Celsius degree, 1.5 m/s per 100 m depth increment and 1m/s for a salinity increase of 1.0 %.

In the Arctic Ocean the temperature in the upper 50-80m is constant and close to freezing (-1.8 ^{0}C), while a strong vertical gradient in temperature occurs at a depth between 80 and 200 m. This defines the surface duct the Arctic ocean which trapp much of the acoustic energy close to the sea ice cover. Using a salinity around 0.31% gives a sound speed close to 1436 m/s. The direct path between a source and receiver separated with 2600 km within the duct corresponds to a travel time 32.3 minutes.

Acoustic travel time

Ray theory

The simple example above corresponds to calculation of travel time for a signal travelling along one single ray, whereas a large number of rays are needed to describe the sound propagation from a source through the ocean. The ray construction follows from a solution of dz/dx=tanθ(z) where θ is found from Snells law.

$$x(z) = \int \frac{dz}{\tan\theta(z)}$$

Travel time along the ray element ds is given by $\frac{ds}{dt} = \frac{1}{S(z)}$, $\frac{dz}{ds} = \sin\theta(z)$. S(z) is the slowness.

Travel time along the ray path is given by

$$\tau(z) = \int \frac{S(z)dz}{\sin\theta(z)}$$

Time fronts are everywhere normal to the rays, and they portray where a pulse is heard at a given instant t in the r,z space, or at a fixed range in t,z. Ray arrivals correspond to the intersections of the time front and the receiver depths.(Munk et al., 1995)

Eigenrays are rays that intersect both source and receiver. The travel time of a nearly horizontal eigenray in a moving range independent ocean can be written

$$\tau_n^{\pm} = \int_{\Gamma_n^{\pm}} \frac{ds}{C(z) \pm u(z)}$$

for propagation in the positive/negative x direction respectively. A source/receiver pair is located at both the starting point and end point. u is the flow velocity component along the ray in positive direction. The paths of integration $\Gamma_n^{\pm}$ are along the trajectories of the nth ray and are generally functions of C(z) and u(z).

Mode theory

Normal mode theory is very accurate for calculations in range independent wave guides, and can be extended to range dependent case by adiabatic approximation or coupling of modes.

In normal mode theory the acoustic field is found by using the technique of separation of variables to solve the Helmholtz equation. Briefly is the total field is found by a summation of all modes, and approach described detailed in the book by Jensen. Each mode is described by a distinct shape function $\phi_m(z)$ and a distinct horizontal wavenumber k_m.

For each mode the horizontal wavenumber relates to a *phase velocity* through

$$v = \frac{\omega}{k_m}, \text{ where } \omega = 2\pi f$$

The modal phase velocity is the speed at which a constant wave front propagates horizontally through the wave guide. The phase velocity vary with mode (through the distinct mode wave number) and frequency (geometrical dispersion).
Group velocity is the most important parameter for pulse propagation and given by

$$u_m = \frac{d\omega}{dk_m}$$

This is the horizontal velocity at which the energy each mode travels in the wave guide.

Sound intensity

The standard measure of change in acoustic signal intensity with range is transmission loss defined as

$TL = 10\log_{10}\frac{I(r,z)}{I_0}$, I_0 is the intensity 1m from the source.

The transmission losses may be considered to be the sum of a loss due to geometrical spreading and a loss due to attenuation. Geometrical spreading loss is simply a measure of the signal weakening as it propagates out from the source, and it includes effects like reflections and leakage from surface ducts. The second loss part includes absorption, scattering and other non-geometrical effects.
Transmission loss measurements are often compared to transmission loss function describing propagation in simple geometry's and sources. The two most common models are 1) a point source in a free space and 2) a line source in a wave-guide.
For the free space model we have spherical spreading loss given by
TL=20log r [dB re 1m]
For the wave guide model we have cylindrical spreading loss given by
TL=10log r [dB re 1m]
Deviations in transmission loss from the simple transmission loss rules is mainly due the difference between the simple geometrical model and the actual physical model and due to the non-geometrical effects. Acoustic sound propagation models to day are made so that they model the actual physical situation more accurate, and thereby the theoretically obtained transmission loss differ less from the measured transmission loss.

Active sonar equation

The most important use of transmission loss calculations are to study the signal to noise ratio in order to use a good enough source and to find the best positions of the source and receivers. In thermometry usually a bi-static sonar is considered, that is source and receiver at different position. For such a sonar the signal to noise ratio (SNR) at a single receiver is obtained by
SNR=SL-TL-N
where SL is the source level , TL is the predicted/calculated transmission loss and N is the noise level measured at the receiver. In order to get a good enough signal the signal to noise ratio should be close to +20 dB. As an example we use the configuration in the Trans Arctic Propagation Experiment (Mikhalevsky, 1999), where the source level was 195 and the center frequency was 19.6 Hz. In the Arctic ocean the ambient noise around 20 Hz is between 80-85 dB, so if we use the worst case
SNR=110 -TL

which leads to the fact that TL should not exceed 90 dB if a signal to noise ratio of 20 dB should be hold.
A sonar system usually consists of an array of hydrophones which are easily beamformed to obtain signal to noise enhancement (DI-directivity index) of many dB for example 20 dB (Munk, et al. 1995).
SNR_{BF}=SL-TL-N+DI=130-TL
Using the same noise and source level as above the TL should not exceed 120dB.

3.4 AVAILABLE ACOUSTIC PROPAGATION MODELS FOR THE ARCTIC

The AMOC program relies on using existing acoustic models. An appropriate acoustic model for the central Arctic has to include the effect of elastic ice cover, elastic bottom and range dependence in all layers. This Chapter provide a short presentation of the actual models to be used in this Task.

Acoustic propagation models

The open ocean is ususally considered as an acoustic wave guide limited by the sea floor and the sea surface, and the main problem is to model a rough free surface and a rough more or less solid sea floor with varying geo-acoustic conditions. Several advanced numerical models have been developed during recent years, see reviewed by Buckingham, (1991) and Jensen et al., (1994).
In the Arctic ocean the ice covered regions can also be considered as a waveguide limited by a solid rough surface and a solid rough bottom. The inclusion of the reflection and scattering from rough elastic surfaces complicates the modeling work significantly (e.q. Fricke, 1991, 1993; Schmidt, 1994; LePage and Schmidt, 1994).

Ocean acoustic models.

Ray trace models have a long history in underwater acoustics and are still the most widely used technique in operational underwater acoustic. Much of the physical interpretation of more advanced numerical models are based on the concept of rays. A ray path is given as the solution of the eikonal equation, whereas the solution of the transport equations gives the amplitude for each ray. The complex pressure field is found by summing up the contributions of each ray passing through a point (eigenrays). Several ray trace models have been developed using different numerical algorithms to solve the ray equations and different methods to correct for the anomalies obtained by the traditional ray trace model. Ray theory has reduced validity in the following cases:

- in shadow zones where the pressure is found to be zero,
- near and within caustics,
- if the acoustic wavelength is larger or of comparable size to any of the length scales of the problem on hand, and
- at interfaces not correcting for beam displacement.

The most important advantages of the ray trace theory are :

- simple physical interpretation,
- efficient numerical codes,
- the ability to model in range dependent environments, and
- the ability to model in three dimensions

Generalized ray trace, which includes correction of beam displacement, has been used to study the effect of ice cover on travel times (Jin et al., 1993).

The most popular models for range dependent problems in ocean acoustics solve a parabolic equation by discretisizing the area and using a finite difference scheme or a marching solution technique. The development of the parabolic equations is based on the assumption of outgoing waves (one way propagation) which means that the interface interaction is not handled generally. Far field assumption ($k_0 r >> 1$) and angle restrictions are introduced by the paraxial approximation (wide angle parabolic equation). The angle restrictions have been improved by using other approximations. Another drawback is that the results have to go through a post processing to present physical interpretation capabilities. Elastic parabolic equations have been developed recently, but they still need to be verified (Goh, 1998).

Range independent seismo acoustic models.

Wave motion in a solid, described as a elastic media, is described completely by displacement vector which can be written as a sum of the gradient of a scalar potential and the curl of a vector potential (see Schmidt, 1988 for details).

$$\mathbf{u} = \left[u_1, u_2, u_3\right] = \nabla\Phi + \nabla \times \Psi \qquad 3.1$$

Each of the potentials in the displacement representation can be shown to satisfy the wave equation (See any text book on elastic waves)

$$\nabla^2\Phi = \frac{1}{c_L^2}\frac{\partial^2\Phi}{\partial^2 t}, \text{ where } c_L^2 = \frac{\lambda + 2\mu}{\rho} \qquad 3.2$$

$$\nabla^2\Psi = \frac{1}{c_T^2}\frac{\partial^2\Psi}{\partial^2 t}, \text{ where } c_T^2 = \frac{\mu}{\rho} \qquad 3.3$$

λ, μ are the Lame′constants, and ρ is the material density.

The first equation describes the longitudinal (pressure or volume) wave propagation, and the second one describes the transverse (shear) wave. These equations also cover the case of waves in a fluid. By solving the wave equations for the displacement potentials, and using constitutive equations the stress components can be found.

The potentials (sound field), assuming small amplitudes, from a point source of strength s(t) is a solution of the in-homogenous wave equation. If the source term s(t) is a pulse wave form, the

solution can be by found by Fourier transforming the wave equation. The resulting Helmholtz equation is then transformed to the inhomogeneous depth separated wave equation by a Hankel transform. The solution of the depth separated wave equation, the depth separated Greens function, is written as

$$g(k,z) = \overbrace{\hat{g}(k,z)}^{\text{The field produced by the sources in absence of boundaries}} + \underbrace{A^-(k)g^-(k,z) + A^+(k)g^+(k,z)}_{\text{Linear combinatiotwo solutions to the homogeneous depth separated wave equation}} \qquad 3.4$$

where the arbitrary coefficients A^- and A^+ are determined from the boundary conditions. k is the horizontal wave number, while z is the depth component. When the unknown coefficients are found, the total field at the angular frequency (ω) is found at any range by carrying out the inverse Hankel transform. The time response is obtained by evaluating the inverse Fourier transform.

The basic property of the full wave field solution is to restrict the depth dependence of sound speed to cases where the depth separated wave equation can be solved analytically, limiting the numerical effort to determine the unknown coefficients from the boundary conditions and to evaluate the inverse integral transforms.

This concept is used in SAFARI and OASES models (Schmidt, 1988, 1997). The SAFARI model (Schmidt, 1988) and the OASES model (Schmidt, 1997) calculate the depth separated Green functions using direct global matrix approach, and a Fast Fourier Transform to obtain the inverse Hankel transform. In order to evaluate the wavenumber integral the Hankel transform is approximated to a Fourier integral. This approximation is good a few wavelengths away from the source. Numerical errors are introduced by truncation of the wavenumber integration domain and by under-sampling of the integrand. The theory and numerical method is described in detail by Jensen et al. (1994) and Schmidt (1988). The advantage of SAFARI and OASES is the inclusion of multi-layers which can be described both as a fluid and an elastic solid.

Scattering from rough surfaces was not originally included in the model theory. Elastic roughness conditions have recently been introduced in the models by transforming the boundary conditions given on an elastic rough surface into a mean horizontal surface through a matrix formulation of a perturbational approach (Kupermann and Schmidt, 1989; LePage and Schmidt, 1994).

Range dependent solutions including elastic ice cover.

Scattering due to surface roughness is a "statistical constant" range dependence included in the boundary conditions. Discontinuity in the boundary description such as the ice edge separating open water from ice is not covered by this theory. Diffraction/scattering models dealing with changes in formulation of boundary condition matrices and complicated boundary geometries involve partial differential equations with mixed boundary conditions and/or boundary conditions involving singularities which cannot be solved by elementary mathematical or numerical models.
An ice-edge diffraction problem has been studied by Dahl (1989) using the Wiener Hopf technique (Noble, 1958). The achievements of using this method was a better understanding of

the physics behind scattering, but due to numerical difficulties it is not useful as a numerical approach. A direct numerical way to obtain a solution in a range dependent ocean environment is to discretezise the governing equations and using a finite element or a finite difference schemes to calculate the solutions. Fricke (1991,1993) developed and used a finite difference method to solve the heterogeneous elasto-dynamic equations in two dimensions in order to calculate the scattered field from the elemental scatterers. The model permits arbitrary roughness, unrestricted slope, displacement or radius of curvature. The model is well suited to study broadband sources and produces the solution in time domain. Generally, finite element or finite difference schemes are very time and space demanding solution methods because of dense sampling of a large area. Additional large calculation areas are needed due to the problem of false reflections from the numerical boundaries.

Another approach is to develop hybrid schemes involving a combination of wavenumber integration and boundary integral methods, (BEM) as described by Gerstoft and Schmidt (1991). BEM combines an integral representation of the wave field within a volume with a point representation of stresses and displacements on the boundary between the two domains. The need for a dens mesh is limited to the boundary alone, eliminating the problem of discretely representing the wave field throughout the volume. In contrast to discrete methods, such as the finite element and finite difference approaches, the solution obtained with the hybrid scheme is efficient for short as well as long range reverberation. The total solution is decomposed in the temporal and spatial spectral components, which is important to the basic physical understanding of the factors affecting seismo-acoustic facet reverberation.

Recently, by using *spectral super element methods* it has been possible to model strong range dependence in both ocean waveguides (Goh and Schmidt, 1995), and in wave guides with seismo-acoustic boundaries (Goh and Schmidt, 1996). The spectral super element approach is an hybridization of the finite elements, boundary integrals and wavenumber integration to solve the Helmholtz equation in a range dependent environment. The environment is first divided into a series of range dependent sectors or super elements, separated by vertical boundaries or cuts. Within each sector the ocean environment is horizontally stratified and will allow for fluid-elastic stratification's. The field in each sector is now expressed as a superposition of the field produced in the stratified element in absence of the vertical boundaries $\mathbf{u}^*$, the field arising from the left boundary, $\mathbf{u}^-$, and the field arising from the right boundary, $\mathbf{u}^+$,

$$\mathbf{u}(x,z) = \mathbf{u}^*(x,z) + \mathbf{u}^-(x,z) + \mathbf{u}^+(x,z) \tag{3.5}$$

where $\mathbf{u}$ is taken to denote contributions from the displacement potentials. $\mathbf{u}^*$ is calculated by using the SAFARI/OASES model. The wave fields from the vertical boundaries are found by using a indirect boundary integral method, based on Greens theorem for the semi-infinite virtual element obtained by eliminating the other vertical boundary and letting the element continue to infinity. For fluid super elements the boundary conditions are the continuity of pressure and particle displacement, for elastic super elements the boundary conditions are the continuity of stresses and displacements.

While the spectral super element approach solves the coupled integral equation using a high-order panel-boundary-element formulation, an approximate approach is to solve reflections and

transmission locally at a discrete number of depths, yielding a description of virtual panel sources (VISA), (Schmidt, 1997). This method has been used to provide a range dependent version of OASES. The results from this model correspond well to canonical benchmark results obtained by the spectral super element approach (Goh et al., 1997).

Models to be used in AMOC

Based on the above review the models in Table 3.3 have been selected for use in the AMOC project. The range dependent version of OASES was licenced to be used witin AMOC (Johannessen et al. 1997). The range independent version of OASES is a public domain model. This model is basically a expanded version of SAFARI, and allows for arbitrary stratification's incorporating fluids with depth dependent sound speed profiles, linearly visco elastic solids, transversely isotropic solids and poro-elastic layers. All common source representations are handled, including plane waves, point and line explosive sources, line arrays, and a variety of plane or axis symmetric seismic moment sources. The licenced OASES model includes the possibility to have range dependence both in sea ice in water and bottom properties. However, later in the project when considering the oceanographic data from the US-Russian data atlas it became clear that the calculations including several sound speed profiles (up to 50 for the TAP-A profile) the computer time became very high and increasing with frequency. The KRAKEN model is just as time consuming as OASES (Schmidt personal communication), and was therefore not included further studies in AMOC.

During the first phase of the project the OASES model was found to replace the use of SAFARI and the ELF model in the case of studying the effect of sea ice on acoustic propagation. KRAKEN. The OASES model were extensively for the ice thickness sensitvity study(see chapter covering the activity 2). The problem with long simulation times in the time domain was in the ice sensitivity study solved by selecting shorter ranges (120-300 km). One of the major results (see next chapter) of this study was that low frequency sound (20-100 Hz) was insensitive to ice thickness with respect to travel times and to transmission loss. Therefore, a simpler acoustic model which do not include sea ice can be selected for the study of the sensitivity to ocean temperature.

RAM- was used for transmission loss calculations to study the insonification of the water masses
RAY- was used for travel time calculations for the ocean temperature sensitivity study.

Table 3.3 Overview of acoustic models used in AMOC

Model	Theory	Range dependent	Ice ?	Elastic bottom?	Comments
OASES	Full wave	Yes	Yes	Yes	The effect of sea ice
SUPERSNAP	Normal mode	Yes	No	No	Only used as a supplement
RAY	Ray trace	Yes	No	No	Coupled to the climate model
RAM	Parabolic approximation	Yes	No	Yes	Study the insonification of the ocean.

A brief description of these well documented acoustic models are found in Task 1 Technical report [6].

Chapter 4

Activity 2. Modelling acoustic propagation in the Arctic ocean

Contents

4.1 SET UP AND PREPARATION OF MODEL EXPERIMENTS

The acoustic monitoring system for averaged ocean temperature will be designed to full fill the following requirements

1) the signal to noise ratio is as good as possible without having to use a too energetic acoustic sources,
2) the acoustic signal travels though the regions and water layers where significant changes in ocean climate are predicted by climate modelling,
3) the effects of averaged temperature changes are separated from the effects caused by changes in the ice conditions.

After these pre-investigations a sensitivity study using the historical data from the US-Russian data Atlas will be used to study the effect of changing oceanographic conditions.

Ambient Noise in the Interior Arctic

In order to meet these requirements ambient noise frequency spectra from different regions have been analyzed and the acoustic propagation are studied by numerical simulations.

N.C. Makris and I. Dyer, 1991 reports that the ambient noise frequency spectrum has a maximum between 15-25 Hz in the interior Arctic. At frequencies between 20-50 hz the ambient noise level is generally between 80 and 90 dB//1μPa^2 , the highest levels are found close to the ice edge during strong on ice wave conditions and in connection with ice edge eddies (Sagen, 1998, Johannessen et al 1988). One should also be aware of the strong effect of inertial oscillations and tidal current on low frequency ambient noise levels (less than 125 Hz) in ice covered shallow water(Johannessen et al, 199. The noise level may rise as much as 10 dB.

The optimum frequency of propagation in ice covered deep ocean

In Figure 4.1 the OASES model has been used to calculate the transmission loss as function of range and frequency. In the interior Arctic Ocean it is often assumed small horizontal gradient in the oceanographic parameters, and therefore the ocean model is considered range independent. The sea ice is modelled as a homogeneous thin and smooth elastic plate. The water depth is 3800 m. The Arctic sound speed profile and the other data used in these calculation is shown in Fig. 4.2 . In Fig. 4.1 the transmission loss as a function of range and frequency for different source and receiver positions. It is clear from Fig. 4.1 that the decrease of acoustic intensity is much less in a band limited frequency domain than for other frequencies. This is called the optimum frequency domain of propagation.

By comparing the different cases in Fig. 4.1 show that the optimum frequency of propagation is most sensitive to the depth of the receiver relative to the surface duct and less sensitive to the position of the source. When both the source and receivers are positioned within the surface duct (as in the upper plot in Fig. 4.1) the center of optimum frequency domain of propagation is 65 Hz. At 1000 km from the source the transmission loss at frequencies below 20 Hz are more than 96 dB, while above 20 Hz the loss is around 84 dB. The reason is that the surface duct has a cutoff frequency below which the energy leaks out of the duct and interacts with the bottom, while above the cutoff frequency the energy is trapped within the duct.

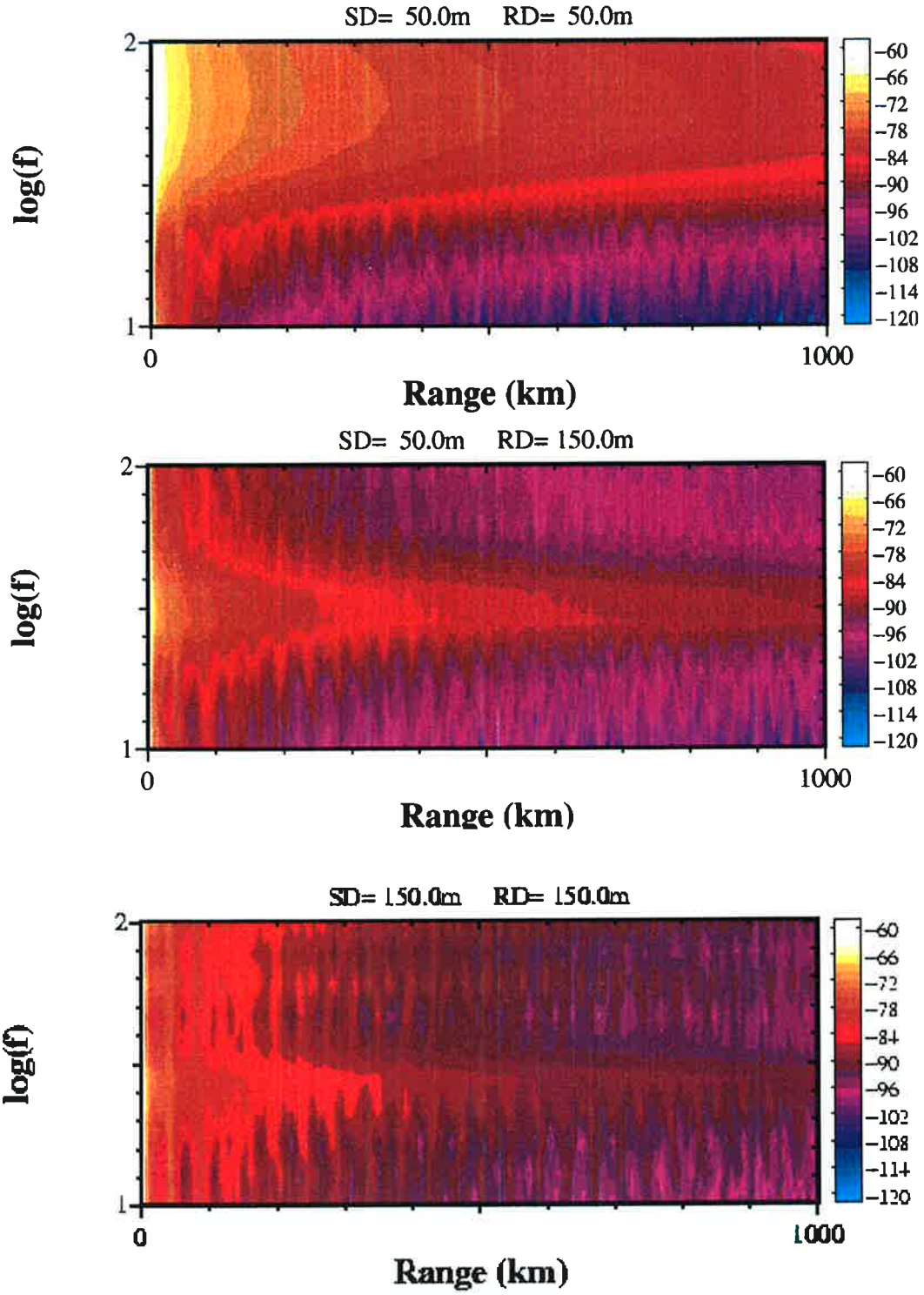

Figure 4.1. Transmission loss as a function of frequency and range for different source and receiver depths.

Transmission loss as a function of frequency and range for different source and receiver depths. In these cases the smooth ice cover is 2m thick (cc=3600m/s, cs=1800 m/s ac=0.5dB/wavelength as= 0.5 dB/wavelength and density=0.92 g/ cm^3). The water depth is 3800m and the sea floor has a 300 m thick bedrock layer overlying a high absorption layer which protects against false reflections. The color table gives transmission loss in dB relative to the level 1 m from the point source. Please note that the frequency axis is given as Log (f) so that 1 is 10 Hz, 1.3 is 20 Hz, 1.5 is 31.6 Hz, 1.7 is 50 Hz and 2 is 100 Hz.

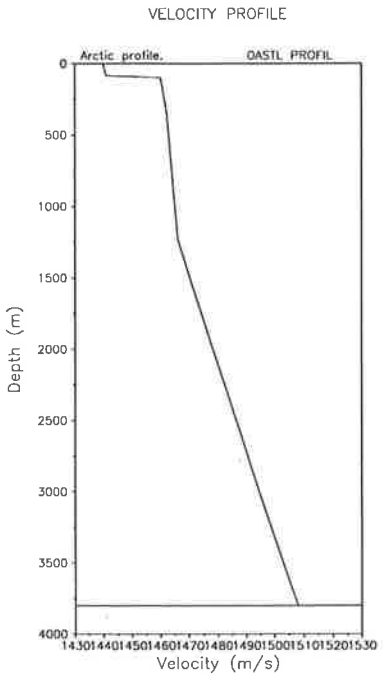

a

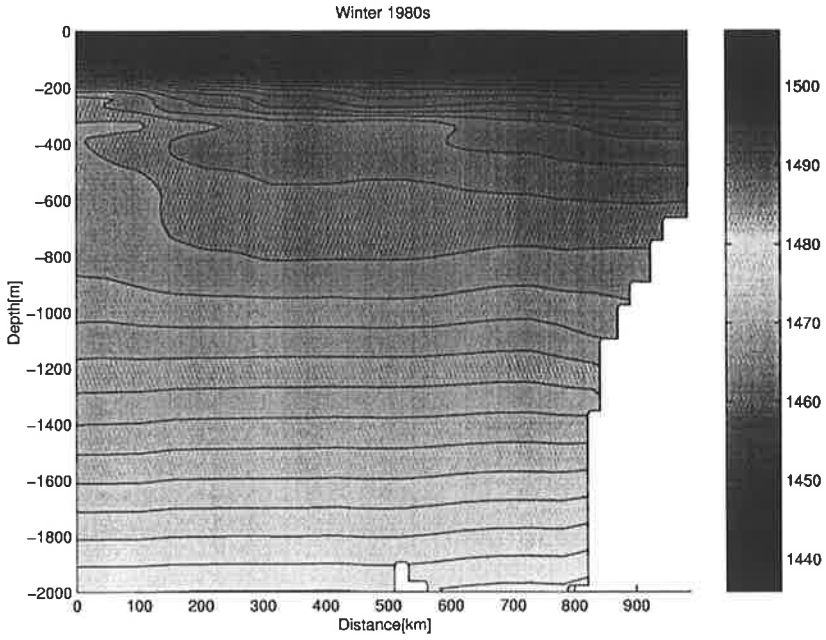

b

Figure 4.2. (a) The input sound velocity profile to OASES used for generation of transmission loss in Figure 4.1. (b) Vertical ssection of sound speed along TAP-B track used as input to the RAM model based on mean winter data for 1980s.

If the receiver is positioned below the duct, as in the figure in the middle, much less energy at frequencies above 30 Hz will reach this receiver because most of the energy is ducted in the surface duct. Also in this case high losses are seen at frequencies below 20 Hz due to bottom interaction. The optimum frequency of propagation is between 20-30 Hz. If the frequency is selected within the optimum frequency band the loss is around 88 dB while if the frequency is outside the loss is 96-100 dB. When the source and the receiver is positioned below generally 90-96 dB transmission loss for frequencies outside the interval from 25 to 30 Hz, while within the interval the loss is less than 90 dB.

In order to monitor changes in the watermasses below the surface duct the above results suggest that a relatively *low frequency source should be selected* to avoid ducting of the energy in the

surface duct. Furthermore to get the best signal to noise ratio for the part of the acoustic field which traces the intermediate water depths (corresponding to mode 2 and mode 3) *the source should be positioned below the duct.* The last statement will be further documented below.

The Acoustic Insonification of the Arctic Basin

In this section the acoustic insonification of the Arctic Basin for the selected tracks are studied by calculating the transmission loss as function of depth and range has been calculated. As oceanographic model the mean sound speed section for TAP B (Fig. 4.2 b) as well as for TAP-A for the 1980s winter were used. In the calculations two source depths have been considered, 60 m and 500 m. A source frequency of 20 Hz is considered. In this study the RAM model was used to calculate transmission loss as function of depth and range. The transmission loss for TAP A and TAP B is plotted in Figure 4.3 and Figure 4.4, respectively. The figures show that the transmission loss plots is different when comparing the two source depths. If a relatively shallow source depth is used the acoustic energy is generally trapped within the 200 m thick surface duct. Whereas for a deep source the energy is more concentrated between 300 and 1000 m. Therefore: the deeper source probes the water masses between 300 and 1500m. On the other hand the shallow source should be excellent for monitoring the surface water layer.

The transmission loss at deeper depths are less influenced by the position of the source and more related to changes in the bathymetry. The part of the acoustic field which penetrates to the deeper part of the basin is very influenced by the topographical conditions, while the acoustic field in the upper part of the ocean is less influenced. In order to avoid influence by the sea floor on the important part of the acoustic field (which probes the 250-1500m water masses) one should keep the receiver array away from shelves and other shallow water regions. For the TAP B track one should be aware of that positioning a receiver array in shallow water (around 500m) will cause additional transmission loss of the modes/rays which goes through the watermasses between 250-1500m. In the TAP-B and the ACOUS experiment the receiver array has been positioned in relatively shallow water.

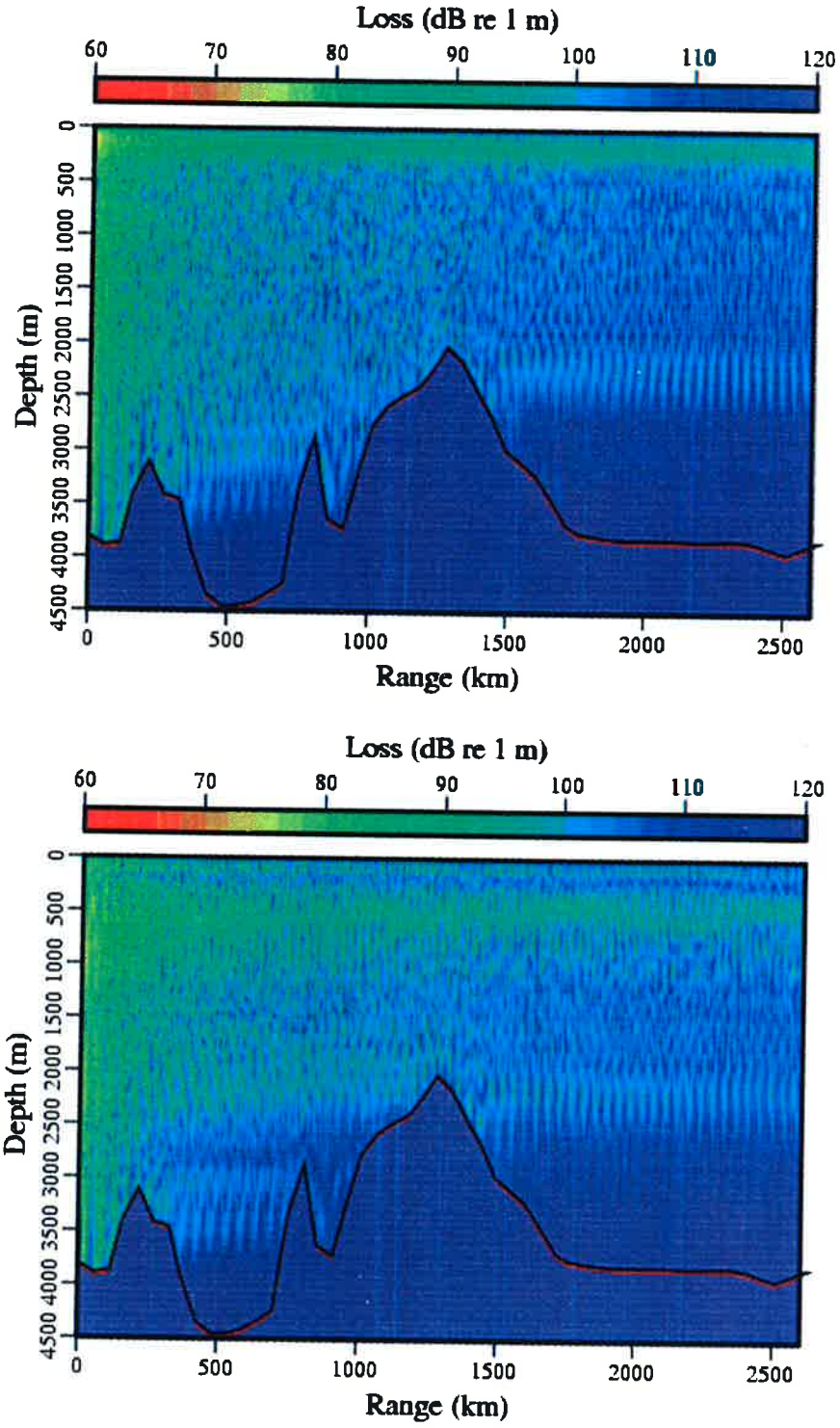

Figure 4.3 Transmission loss calculated for TAP-A using mean oceanographic conditions of winters in the 1980s obtained from the US-Russian data Atlas. Source depth is 50 m in the upper plot and 500 m in the lower plot. Source frequency is 20 Hz.

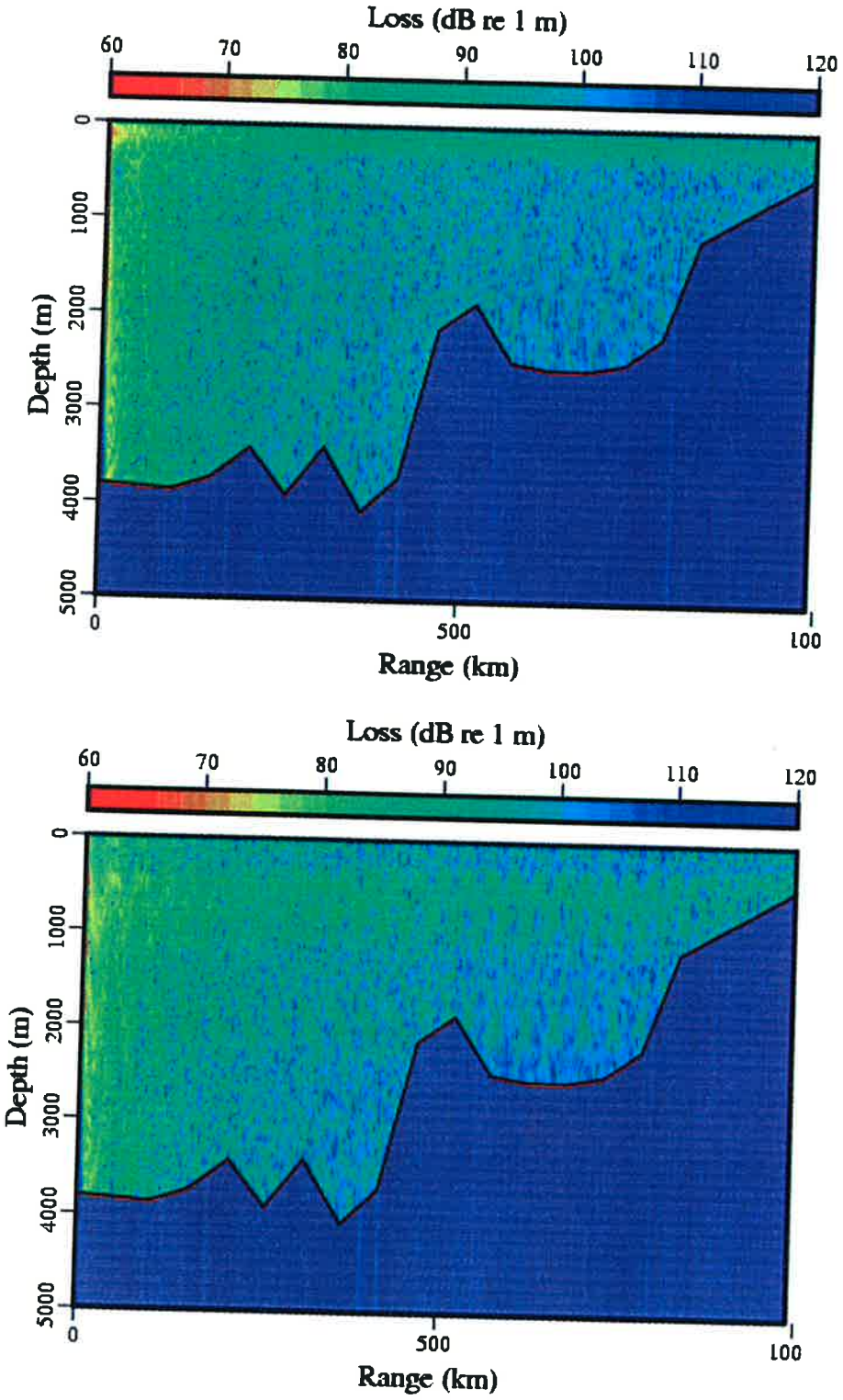

Figure 4.4. Transmission loss calculated for TAP-B using mean oceanographic conditions of winters in the 1980s obtained from the US-Russian data Atlas. Source dept is 50 m in the upper plot and 500 m in the lower plot. Source frequency is 20 Hz.

Mode decomposition

The normal mode model SUPERSNAP was used to calculate the 6 lowest modes corresponding to the sound speed profile shown in Fig. 4.5. The five lowest mode functions are plotted for 70 Hz and 20 Hz in Fig. 4.6 For 70 Hz it is clearly seen that the 3 first modes are not penetrating deeper than 400 m, while mode 4-5 penetrate down to 1000 m.

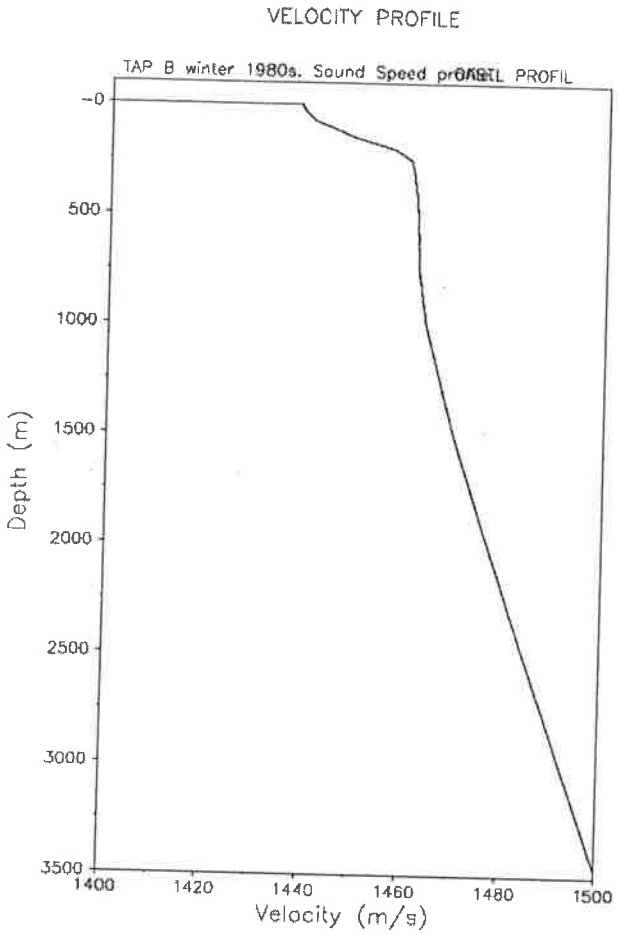

Figure 4.5. Sound speed from the first "station" in the TAP-B track winter 1980 plotted as function of depth. The oceanographic data is obtained from the US-Russian data Atlas.

When 20 Hz is considered the mode 1 is generally excited in the upper 250 meters, and is presumable the part of the acoustic field which is most sensitive to the sea ice. Mode 2 – 6 are the modes which generally establishes the sound field below 250 m and down to 2000 m, but some energy of these modes are also found in the upper part of the ocean. The Mode 2 and 3 is found to represent the acoustic field between 300m and 1400 m, and are not influenced by the bottom if

the water depth along the track is deeper than around. The higher modes, which penetrates deeper, will be strongly influenced in areas with such water depths, these are the modes which constructs the reflected acoustic field.

In the case of a 20 Hz shallow source the acoustic energy goes mainly into mode 1 and less energy into mode 2 and 3 and the higher modes. By lowering a source to 500 m the major part of the acoustic energy goes into mode 2 and 3, and dominates over the generation of mode 1. The amount of energy going into the higher modes will be relatively the same independent of source depth this can also be seen in the transmission loss plots as the deep part of the acoustic field is less influenced by the position of the source.

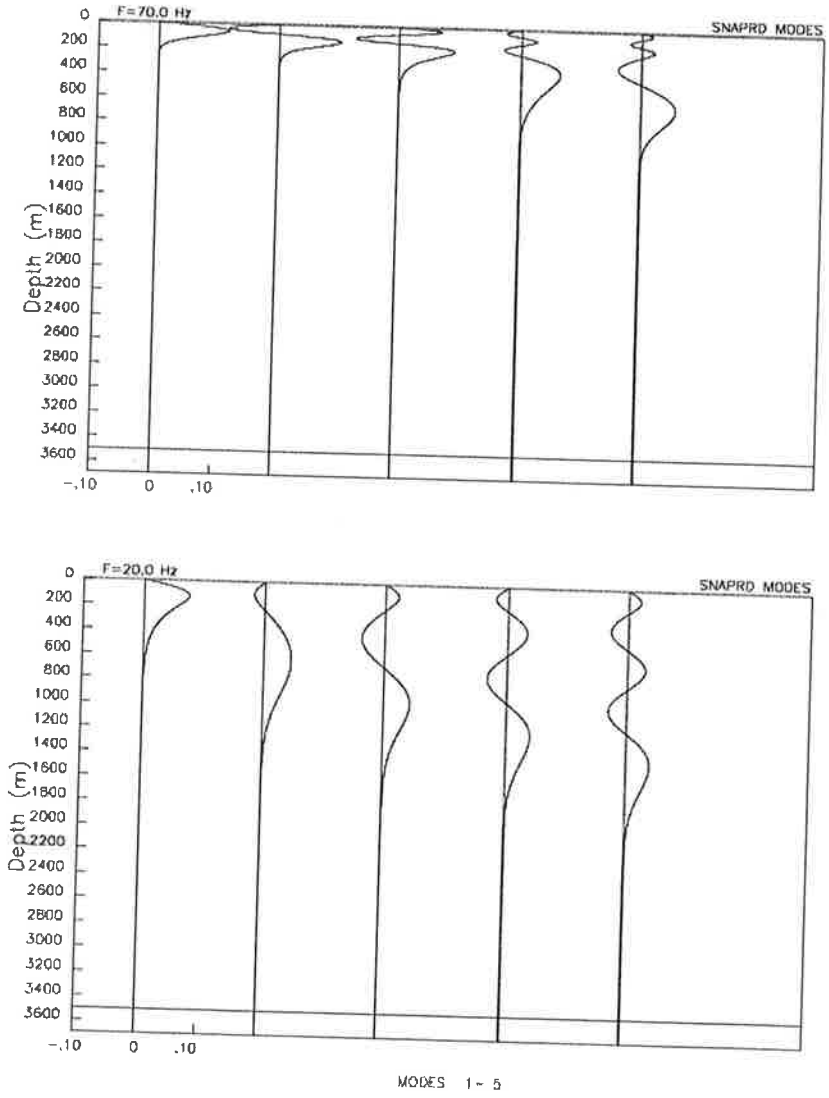

Figure 4.6. The first 6 modes calculated for 20 Hz (lower) and 70 Hz (upper) by SUPERSNAP using the sound speed profile at the source location for the TAP-B track (Winter 1980s).

As mode 2 and 3 are the part of the acoustic field which probes the water masses between 250-1400m the source should be positioned below the surface duct so that relatively more of the available energy goes into these modes.

The surface ducted energy (Mode 1) will arrive later than the energy which propagates in the intermediate water layers (mode 2 and 3) because it goes through a layer with lowest sound speed. This suggest that the modes can be time separated and this will be studied by using ray traceing.

Ray pattern

In order to obtain some general knowledge about the expected arrival structure for receivers in the above defined oceanographic model a ray model have been used. The ray model, RAY, accounts for range dependence in the ocean, rang dependent variation in the bathymetry. The model do not treat the effect of sea ice or surface roughness.

The source is in all cases positioned at 60 m. In the first case the receiver is positioned 60 km away from the source 173.3 m below the sea surface. In these simulations the bottom is perfect reflecting. There is four families of rays: A big family which is trapped in the duct, a smaller which penetrates a little deeper and interacts with the surface approximately 6 times, one family which interacts 3 times with the sea floor and 2 times with the surface, and finally a family which interacts one time with surface and two times with bottom (Fig 4.7).

The lower plot in Fig. 4.7 shows the corresponding arrival times. The first arrival is the rays which penetrates down to around 300m, the second arrival is the due to the many rays which are trapped within the duct, the third and fourth arrivals are due to bottom interacting rays. The first and second arrival is separated by around 0.2 s.

A similar interpretation can be made in the case of 120 km from the source which have been plotted and interpreted in Fig. 4.8. In this case the first and second arrival is separated by almost a second. By lowering the source down to 500 m 38 eigenrays are found, there is no surface duct trapped rays all rays penetrates at least down to 500 m with at most 3 surface interactions. By indroducing absorbing bottom the bottom interacting rays are removed and 10 eigenrays are found. There is five groups of rays, two eigenrays in each which have different penetration depths from around 600 m and down to 2000m. The rays hits the surface 3 times.

If the source is lowered down to 1000 m. In the case of reflecting bottom 29 eigenrays where found. Most of these rays are bottom interacting and therefore if one try to model the arrival time structure at deep receives one need a proper handling of the sea floor. By introducing an absorbing bottom only two eigenrays where found.

Conclusion

It was found that by positioning the source at 500 m a better insonification of the Atlantic Intermediate Water (AIW) was found. By using RAY it was also seen that the ducted signal (mode 1) and the deeper penetrating signal is well separated in time by almost 1 s at 120 km from the source.

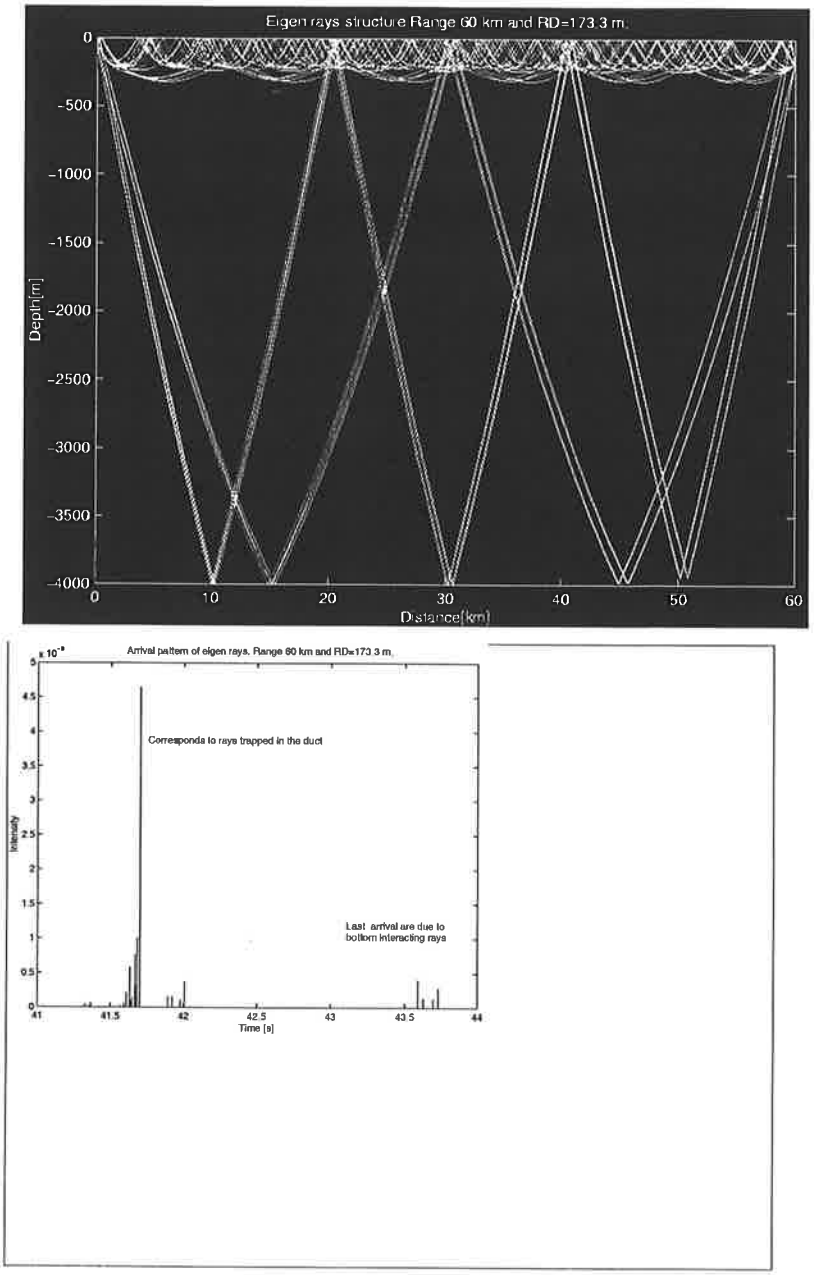

Figure 4.7. Ray arrival structure for the oceanographic field in the beginning of TAP-B. Source depth 60 m. The receiver is positioned 60 km from the source and 173.3m below the surface. 27 eigenrays was found. using angles between -30 and 30 degrees and 1000 rays are shoot.

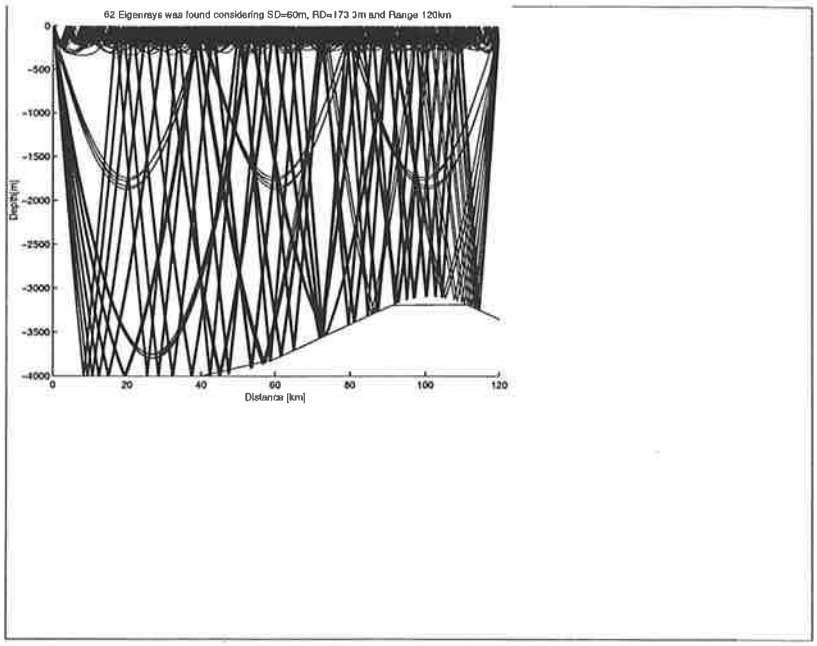

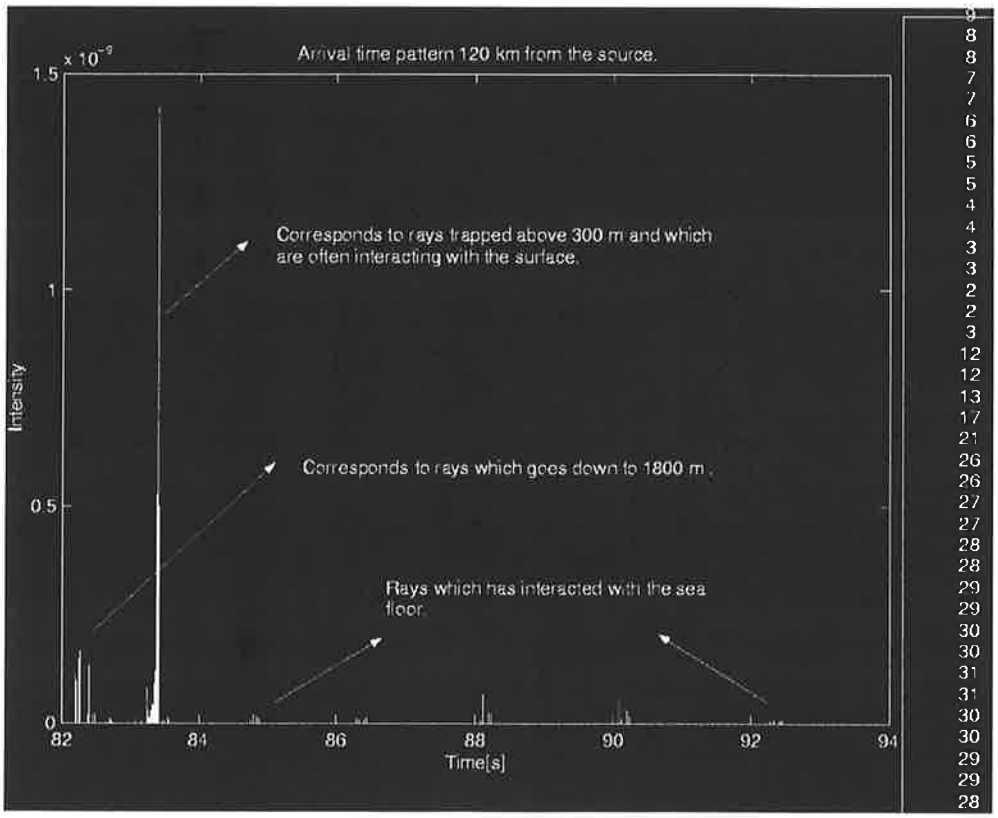

Figure 4.8. The ray arrival structure for the oceanographic field for the first 120 km of the TAP-B track. The receiver is positioned 120 km from the source and 173.3m below the surface. 27 eigenrays was found using angles between -30 and 30 degrees and 1000 rays are shot.

4.2 SEASONAL AND DECADAL VARIATIONS

Environmental data input to the Acoustic models

It has been observed both in data and in climate modeling that the strongest variations in the sea ice cover is found north of Greenland. Significant changes in the temperature field have been observed in connection to the in and out flow through the Fram Strait. Therefore, the main attention in Task 3 has been on the

- TAP-B track, which starts North east of Svalbard and ends up in the Lincoln Sea. The length of the track is around 980 km long. The TAP-B track starts at 83 30' ^{0} N and 23 ^{0} E ends at the receiver camp "NARWHAL" at 83 62.5' ^{0} N, 26 ^{0} E.

- TAP A track, which starts North east of Svalbard and ends up in the Beaufort Sea. The length of the track is around 2623 km

Sound speed input has been established for each of the four decade mean present on the US-Russian Atlas CD. The sound speed fields used as input to the range dependent OASES model, RAM and RAY. The sound speed fields used as input to the acoustic propagation models for TAP-B are presented in Fig 4.9 – 4.12. Topography from data bases was obtained from TOPO5 for RAY and RAM, and for simplicity a hard bedrock condition were used.

The typical Arctic sound speed structure is characterized by a surface layer with generally constant sound speed, a strong vertical gradient limits the duct downwards from 50 to 200 m, and a smaller vertical gradient is seen from around 200 m down to 1000 m (Atlantic Intermediate Water (AIW)). In the deeper water masses below 1000m the sound speed increases linearly with depth. For the TAB-B track the historical data show that the main changes during the last 40 years has occurred in the watermasses between 200-800 m this is also the watermasses with the strongest horizontal variations and seasonal variations. The largest horizontal gradients are seen in the eastern part of the TAP-B track, these gradients are due to the inflow of warm Atlantic water. According to the data considered in our study, the inflow of Atlantic water is found to be largest in the summer of 60s and winter 80s. A seasonal variation is seen on Greenland side where the upper 600m are colder in the summer season due to increased melting and river run-off.

Develop interface between acoustic models and environmental data

A considerable effort has been used to develop the interface between oceanographic data and the acoustic models. Software, using MATLAB, have been developed and data from US-Russian data atlas [Environmental Working Group, 1997, 1998] are available for use in RAY, OASES and RAM. The sound speed profiles are not interpolated for use in OASES due to a rapidly increasing need of computer time when the number of sectors increases. In the case of RAY the sound fields and bathymetry are interpolated within the program. The RAM program are provided with an interpolated sound speed field, and a program doing this has been developed. Bathymetry is available from TerrainBase for use in RAY and RAM.

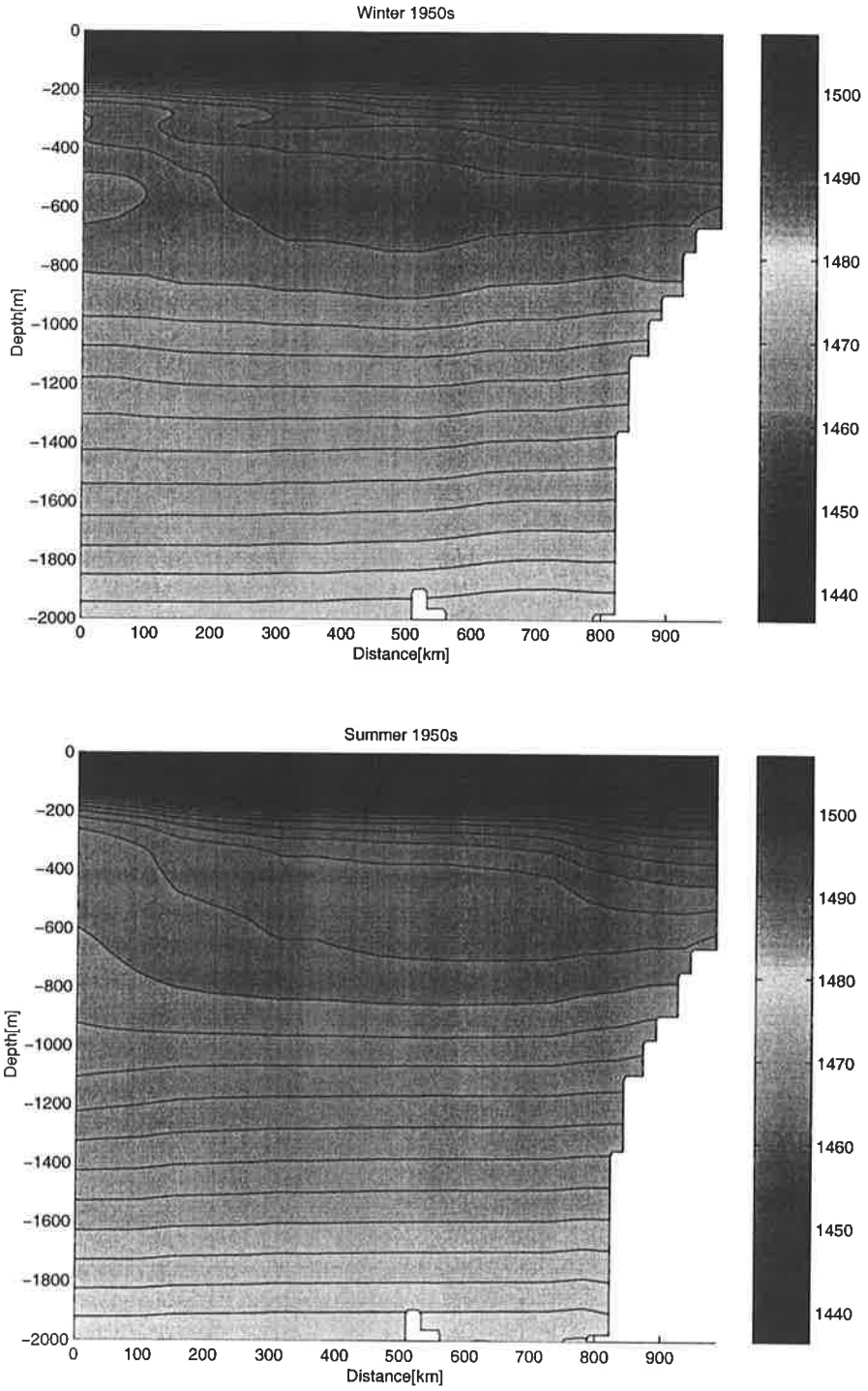

Figure 4.9. Sound speed derived from oceanographic data included on the US-Russian environmental CD for 1950s for the TAP-B track The TAP-B track starts at 83 30' ^{0} N and 23 ^{0} E ends at the receiver camp "NARWHAL" at 83 62.5' ^{0} N, 26 ^{0} E.

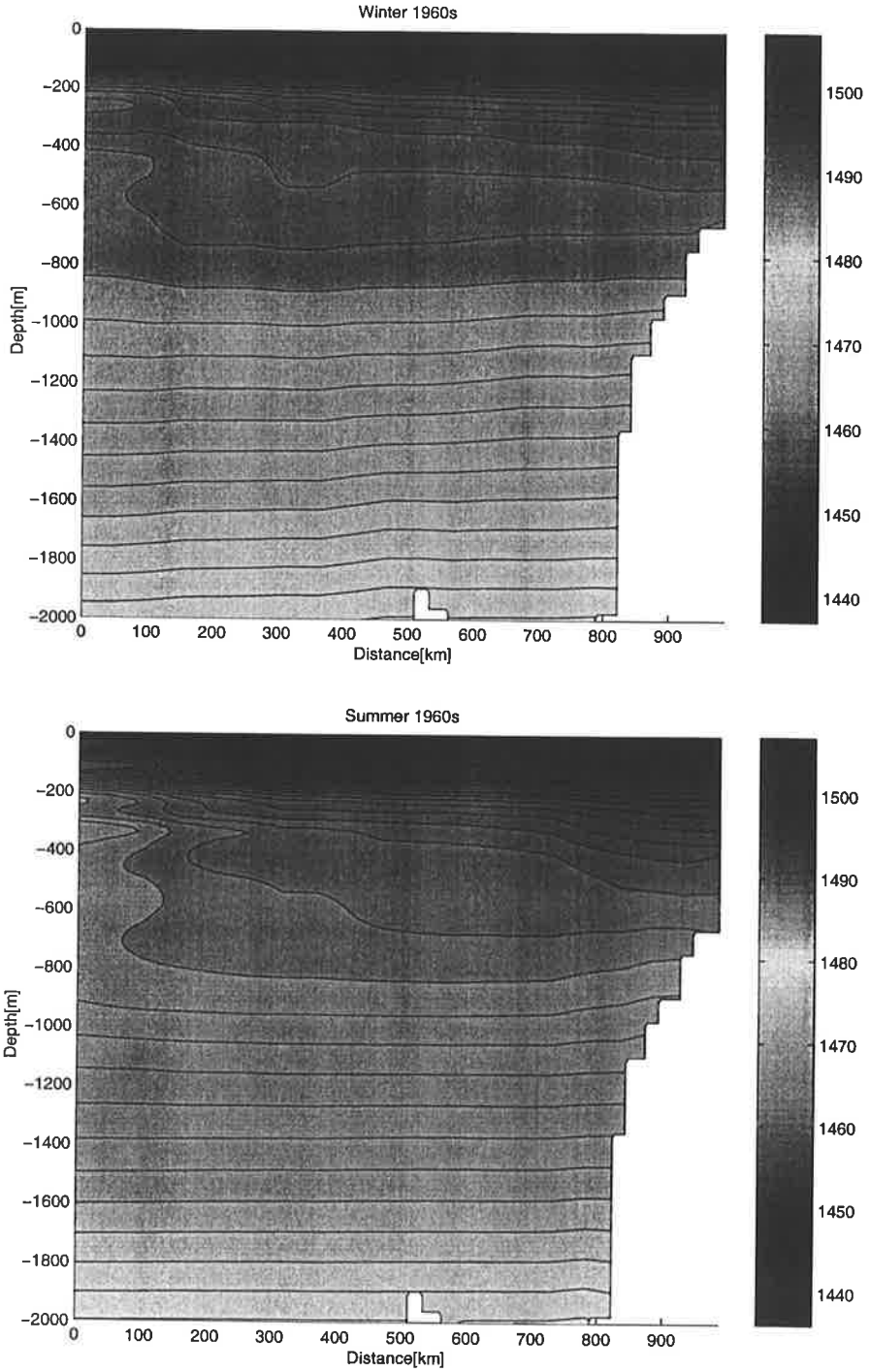

Figure 4.10. Sound speed derived from oceanographic data included on the US-Russian environmental CD for 1960s for the TAP-B track The TAP-B track starts at 83 30' ^{0} N and 23 ^{0} E ends at the receiver camp "NARWHAL" at 83 62.5' ^{0} N, 26 ^{0} E.

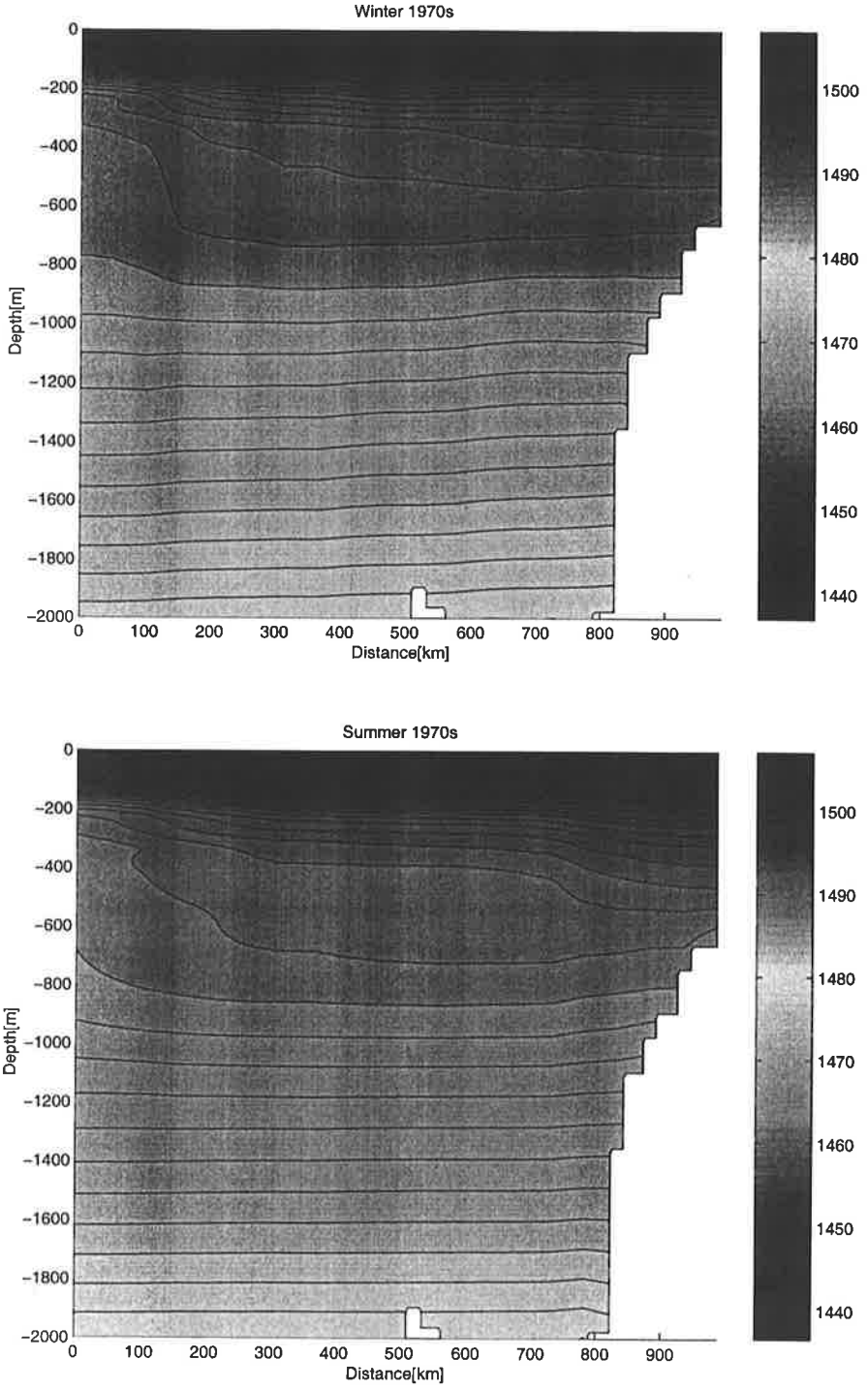

Figure 4.11. Sound speed derived from oceanographic data included on the US-Russian environmental CD for 1970s for the TAP-B track. The TAP-B track starts at 83 30' ^{0} N and 23 ^{0} E ends at the receiver camp "NARWHAL" at 83 62.5' ^{0} N, 26 ^{0} E.

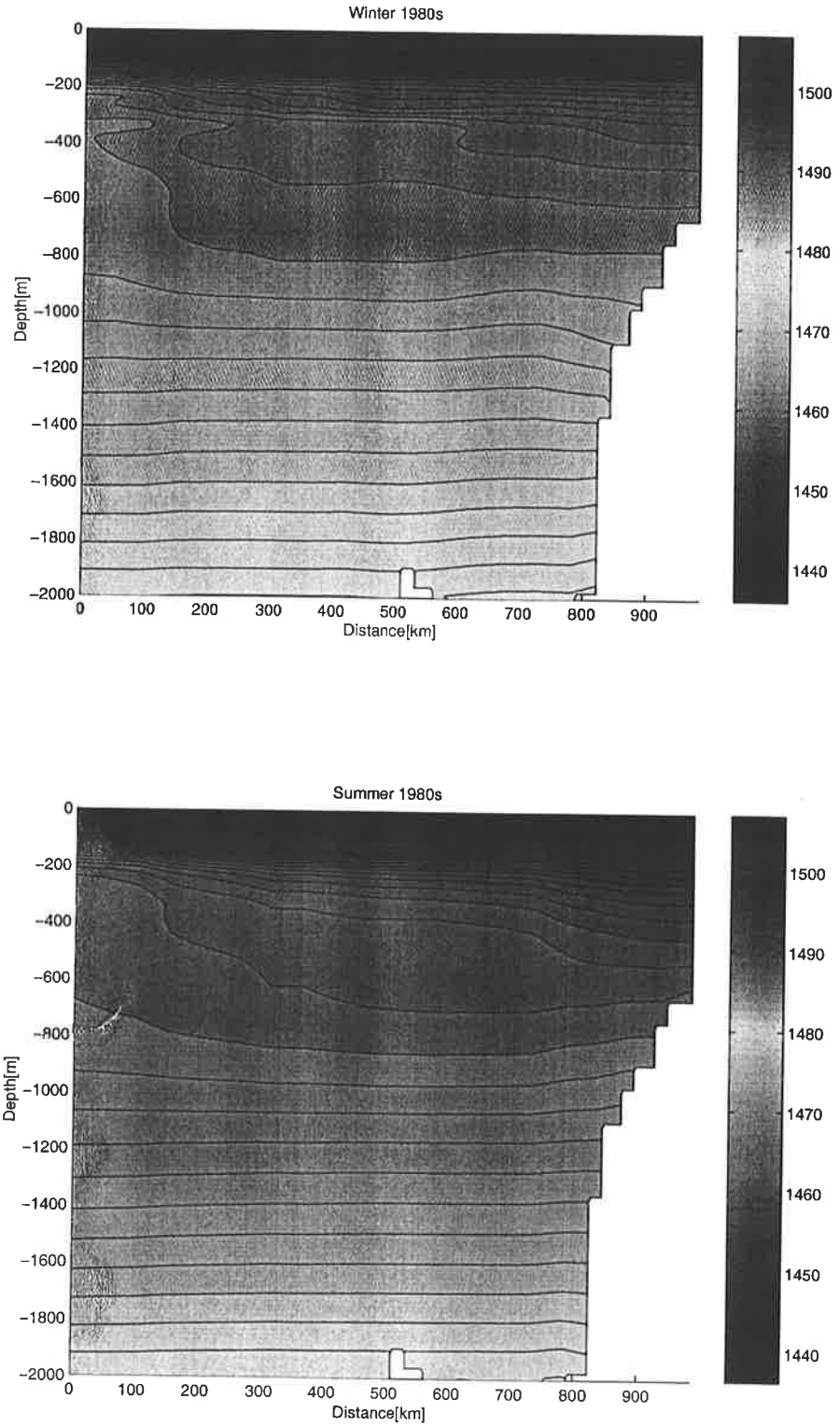

Figure 4.12. Sound speed derived from oceanographic data included on the US-Russian environmental CD for 1970s for the TAP-B track The TAP-B track starts at 83 30' ^{0} N and 23 ^{0} E ends at the receiver camp "NARWHAL" at 83 62.5' ^{0} N, 26 ^{0} E.

Acoustic Models

The range dependent calculations have been carried out interfacing OASES, RAM and RAY models to the oceanographic data described above. The horizontal resolution in the environmental input to the acoustic models is 50 km, which is the resolution in the US-Russian oceanographic data. The TAP A track have 50 sectors, while the TAP B track have 21 sectors.

In order to generate a range dependent solution the OASES model match the solution found in two consecutive range independent sectors in the vertical every quarter of the smallest wavelength involved (at 20 Hz every 18 m). The computer time became very high and increasing with frequency. The simulation time was 25 CPU hours for TAP-B using a single frequency source. OASES was found to be generally impractical for the sensitivity to ocean temperature study, especially in the time domain for long ranges. Therefore, the ray trace model, RAY, has been used for the time domain study in a combination with OASES. For the transmission loss study the RAM model was used in addition to the OASES model. The KRAKEN model was considered, but according to H. Schmidt this model would be just as time consuming as OASES (Schmidt personal communication, 1999). RAM- is used for transmission loss calculations to study the insonification of the water masses.

Due to the lack of ice effects in RAM and RAY, the OASES model has been used in the sea ice sensitivity study. In the ice sensitivity study the problem with long simulation times in the time domain was solved by selecting shorter ranges (120-300 km). Therefore we selected to use the OASES model exclusively for the ice thickness sensitvity study to estimate the errors introduced in the results using a simpler acoustic model which did not include sea ice.

Presentation of seasonal/Decadal variations

Due to very long computer times for long range propagation for pulses using OASES, the RAY model has been used to study the influence of changing oceanographic fields on travel time. The RAY model does not include the effect of the sea ice, and a changing ice cover will studied later in this report for the low frequency (20 Hz) source considered in this subtask.

The ray model has been used to calculated the eigenrays and corresponding arrival times for TAP A and TAP B using the sound speed profiles presented in the sections above for different source depths (60m and 500 m) and receiver depths (50m, 173.3 m and 500 m). The ray launch angles ranges from -15 to 15 degrees, and 2000 rays were shot. The calculations were carried out for oceanographic decade means for summer and winter conditions.

A ray with a given launch angle will trace the water masses according to the horizontal and vertical gradients present in the oceanographic input data. Eigenrays are rays which goes from the source to a given receiver position. RAY have been used to find the eigenrays for different source and receiver positions/depths for the TAP A and TAP B tracks. RAY calculates the arrival time and path length for each eigenray, those parameters are used to find the averaged sound speed for each eigenray. The averaged sound speed along a given ray is closely related to the temperature and salinity conditions along the path. Rays passing through the cold upper water masses (<200m) are slower than the rays passing through the deeper and warmer water masses (250-1500 m).

TAP-A analysis.

As an example twelve eigenrays were found for the TAP A track when the source was positioned at 60 m and the receiver at 500 m. Seven of the eigenrays are plotted in the left plot in Fig. 4.13 which shows that these rays passes through water masses between 0 down to 1500 m. The corresponding arrival times for the eigenfronts are shown in the left plot, indicating that arrivals come in every 0.5 s for 3 seconds and then a late arrival 1.5 s after the previous arrivals.

The upper plot in Fig.4.14 show the calculated mean travel time, the first arrival and the last arrival for the same configuration as used in Fig. 4.13. This plot (Fig.4.14) shows that there is no trend in the mean arrival time, while some trend can be observed considering the first arrival which seems to be faster in the 70s and 80s than in the 50s and 60s. This may indicate that the deeper water masses has become warmer. The lower plot in Fig. 4.14 shows the calculated mean sound speed along each of the eigenrays for each seasonal decadal mean. In this plot it is seen that there are more eigenrays with higher sound speeds found in the winters of 70s and 80s than earlier which also may indicate a warmer condition during winters in this period than during the two first decades. On the other hand no changes are observed in the summer time.

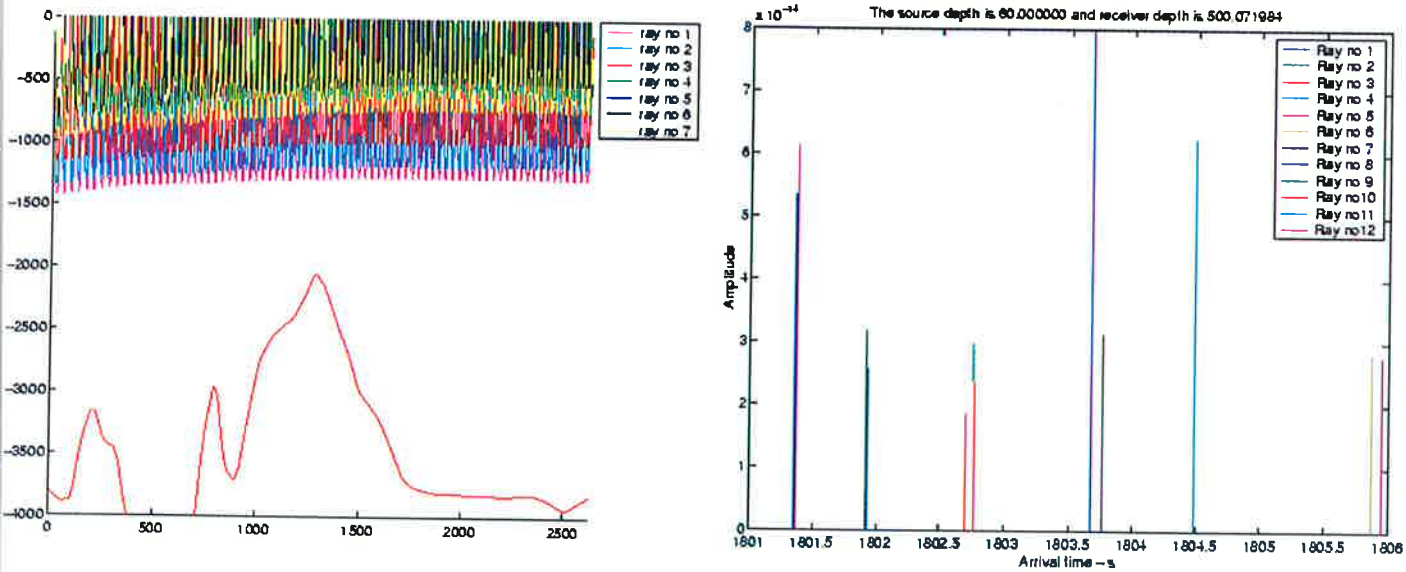

b)

Figure 4.13. (a) Seven of the twelve eigenrays are calculated by RAY for TAP-A using 1950s oceanographic data from the US-Russian data Atlas for a 2623 km long section. (b) The corresponding travel times for the 12 eigenrays. Source depth was 60 m and receiver depth 500 m.

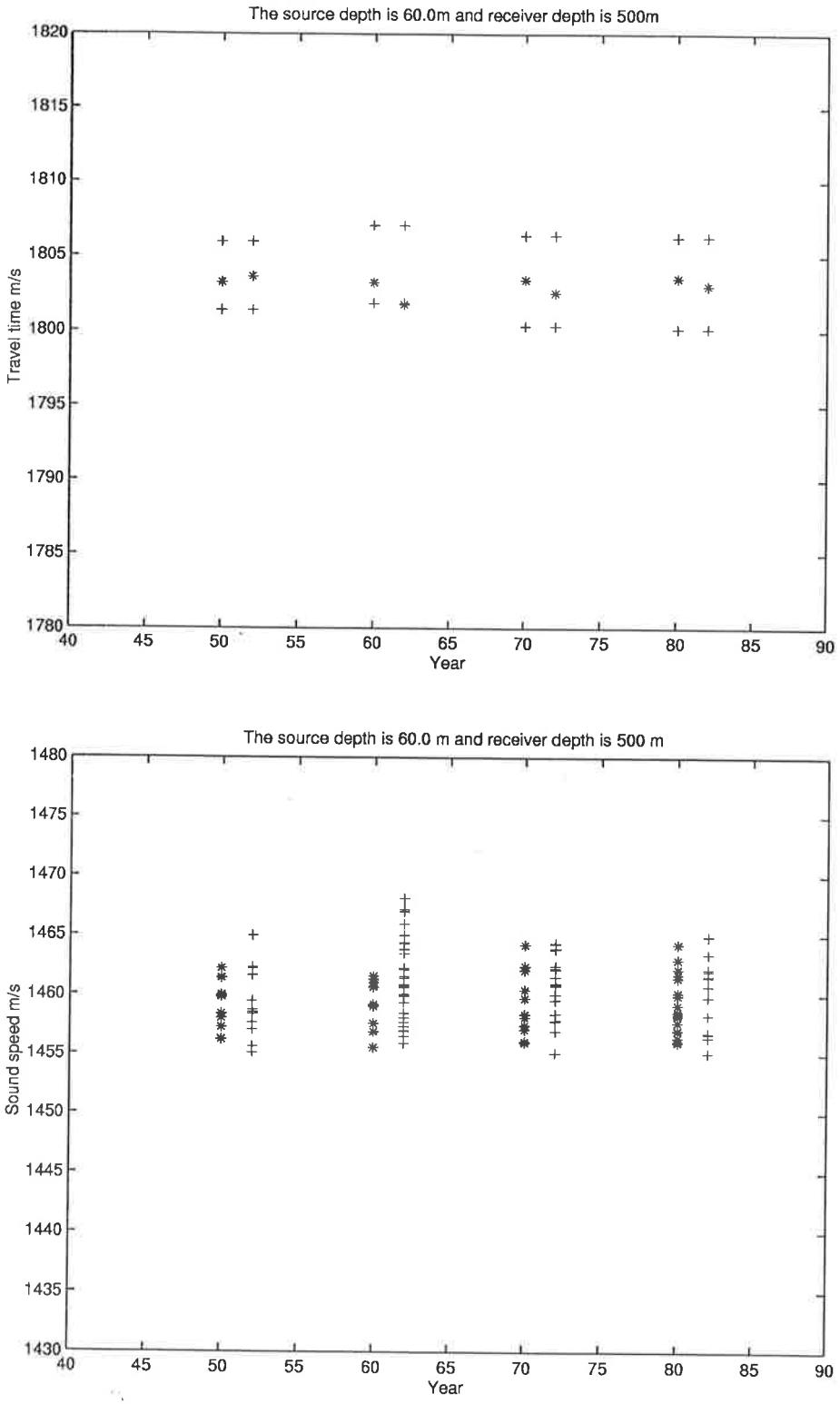

Figure 4.14. TAP A: SD=60m and RD=500 M. Upper plot is mean arrival time, first arrival time and last arrival time. The lower plot shows the averaged soundspeed along each eigenray found for each season/decade. . '+' is summer and '*' is winter.

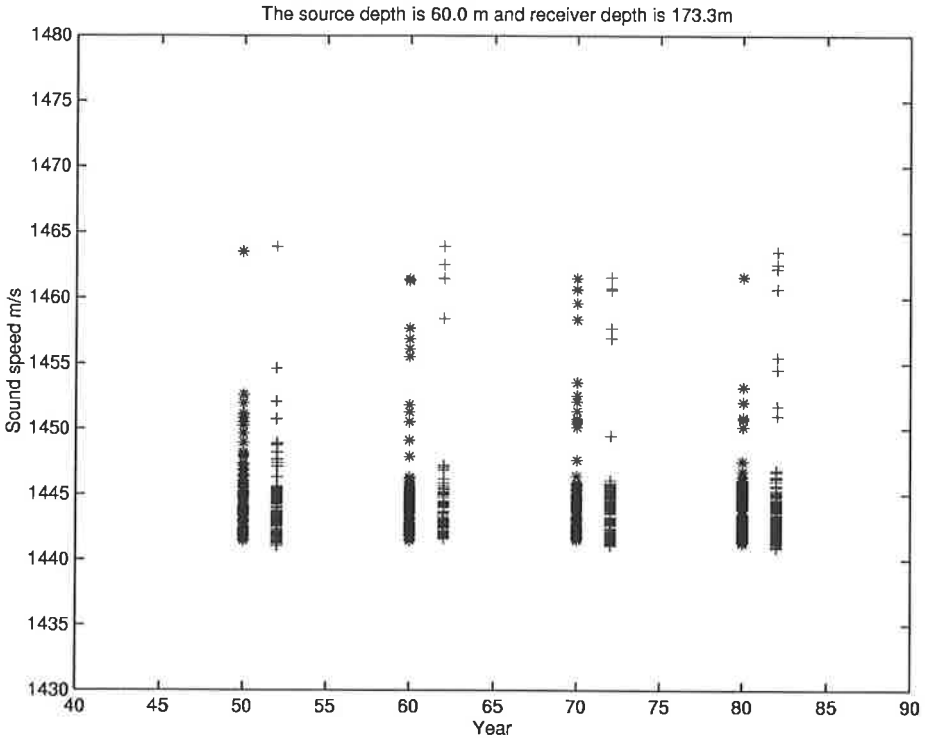

Figure 4.15. TAP-A: Sound speed along the eigen rays found for SD=60m and receiver depth 173 m. . '+' is summer and '*' is winter.

In Fig. 4.14 a shallower receiver is considered and a lot more eigenrays are found. The bunch of lower sound speeds corresponds to the rays which are trapped close to the surface. There is no clear trend of increasing sound speeds in this case. In Fig. 4.16 the source depth is 500 m and no clear trend of warming is found in this case either.

TAP-B analysis

The same study of historical oceanographic data has been done for the TAP B track. In Fig. 4.17 the averaged sound speed has been calculated for each eigenray found for a source positioned at 60 m and two receivers 980 km away from the source (RD=173.3m and 500 m). In Fig. 4.17 a shallow source (60 m) have been used. The upper plot show the soundspeeds found in the case of a 173.3 m deep receiver the lower plot shows the same for a deep receiver at 500 m. The calculations has been carried out for winter and summer means of the 1950s, 1960s, 1970s and 1980s.

For the shallow source and receiver, in Fig. 4.17, a very high number of eigenrays are found, and the sound speeds have a large spread in sound speed. A high number of eigenrays trapped within the upper 200 m of the ocean arrives the receiver later then the deeper going rays. The fastest rays

disappear from the winter season in the 1970s and 1980s, and winter conditions becomes more similar to the summer condition which seems to trapp more rays in the duct.

In the lowest plot in Fig. 4.17 a deep receiver is considered, and the bottom filtering of the rays passing through the intermediate water masses is significant and only a couple of eigenrays are obtained. By moving the receiver to deeper water more eigenrays will be obtained. In climate monitoring this will be important because the rays which traces the intermediate Atlantic water masses is very important. The two first decades there is a clear difference between summer and winter. The winters have a higher sound speed and a less spread in sound speeds than found in the summer, because the rays penetrate deeper during the winter time. In the 1970s and 1980s the winter sound speeds becomes more similar to the sound speeds found in the summer time, as the rays in the winter time becomes more shallow going. This may indicate a shaper vertical gradient separating the cold surface water from the warmer intermediate water.

In Fig. 4.18 results for a deep source (500m) and shallow receiver (173.3 m) is plotted in the upper plot and a deep receiver in the lower plot. There is no clear climate change trend. The same bottom filtering of rays is observed for the deep receiver. The few eigenrays which are left indicate a stable situation because the remaining rays have gone through the same watermasses.

Conclusion

Seasonal variations are observed in the mean sound speed along eigenrays using US-Russian data as climatology. On the otherhand no distinct climate change can not be observed either for the TAP-A and TAP-B.

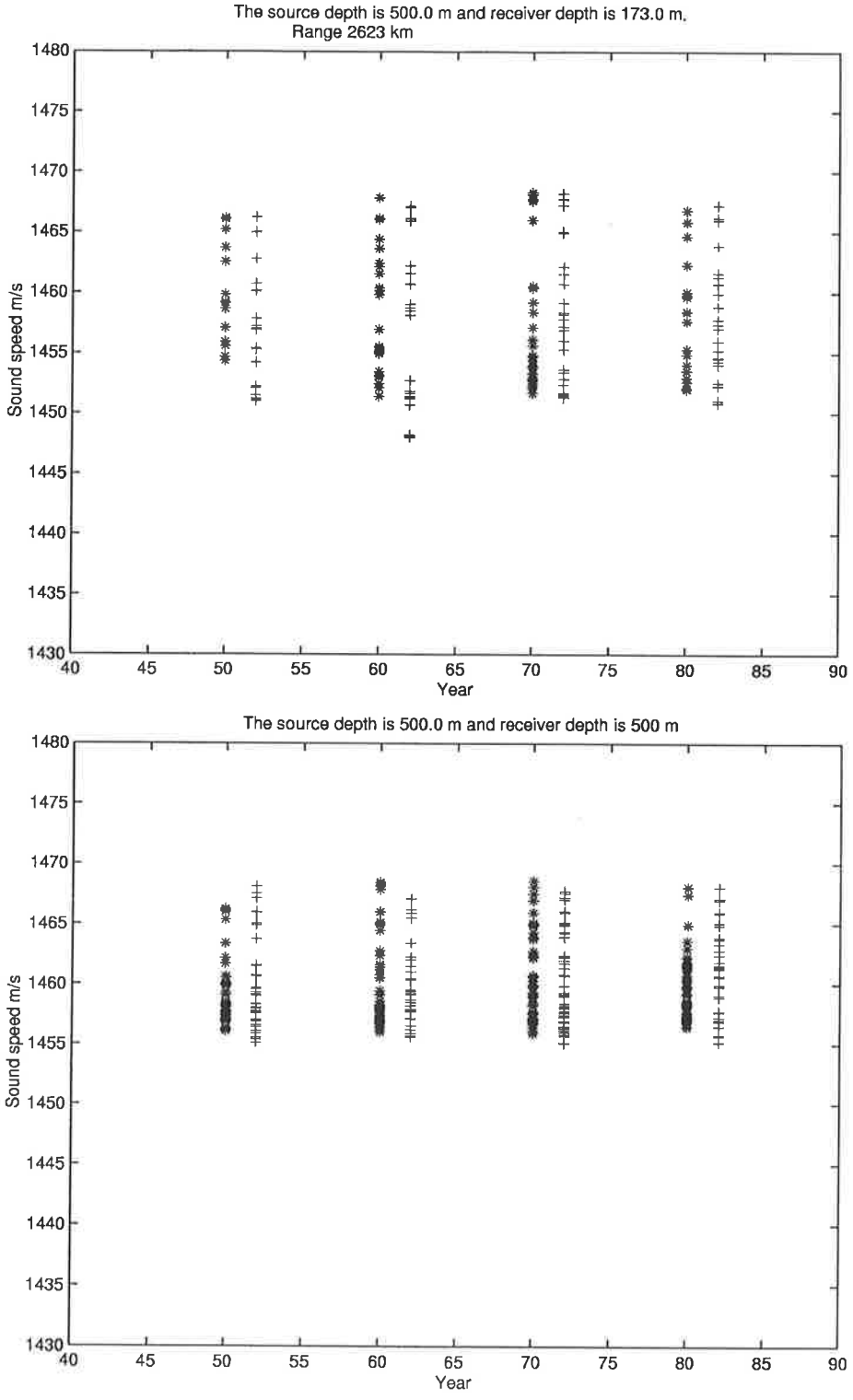

Figure 4.16. TAP-A: Sound speed along the eigen rays found for SD=500m and receiver depth 173 m in the upper plot and 500 m in the lower plot. '+' is summer and '*' is winter.

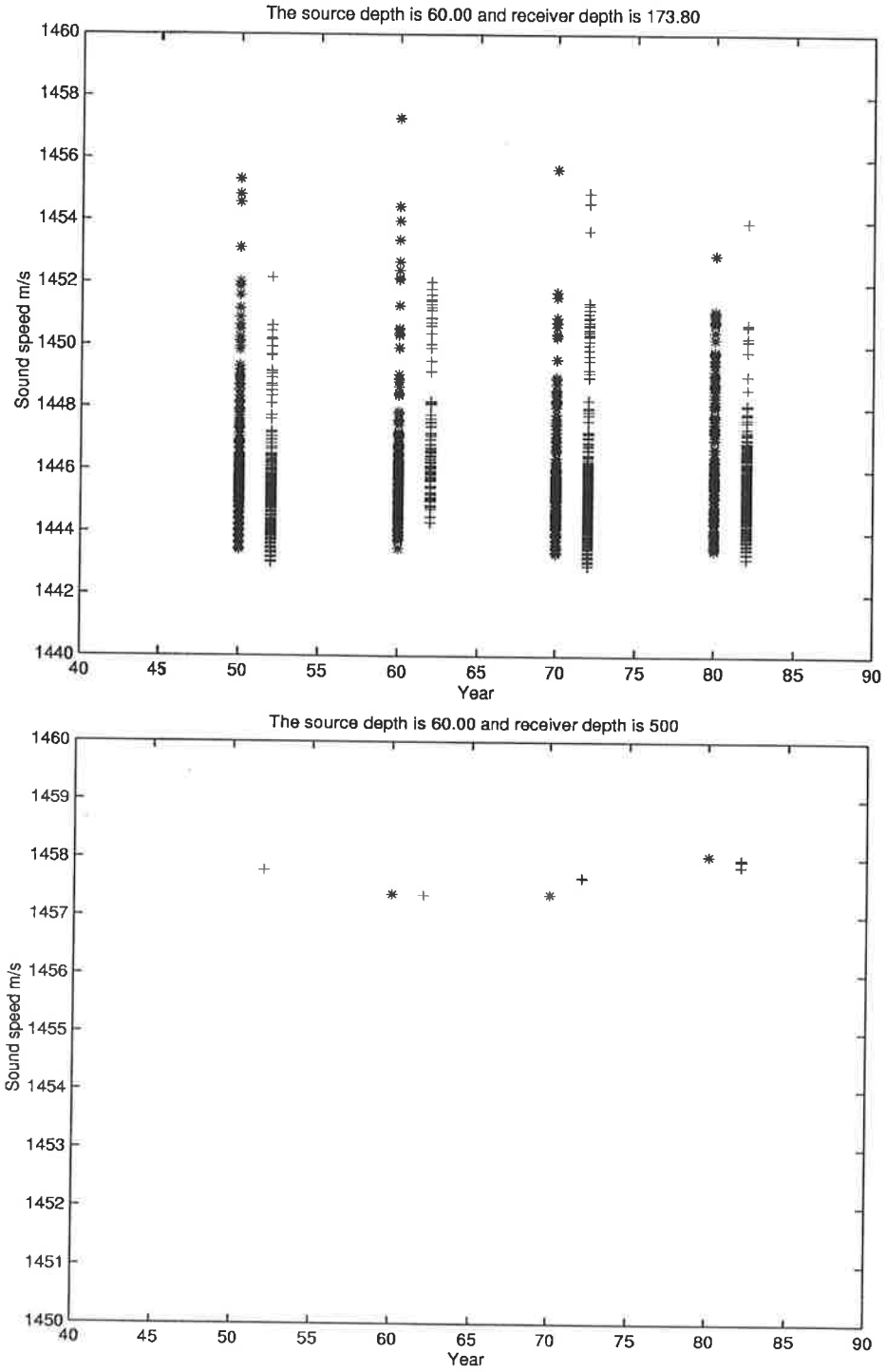

Figure 4.17. TAP-B: Sound speed along the eigen rays found for SD=60m and receiver depth 173 m in the upper plot and 500 m in the lower plot. . '+' is summer and '*' is winter.

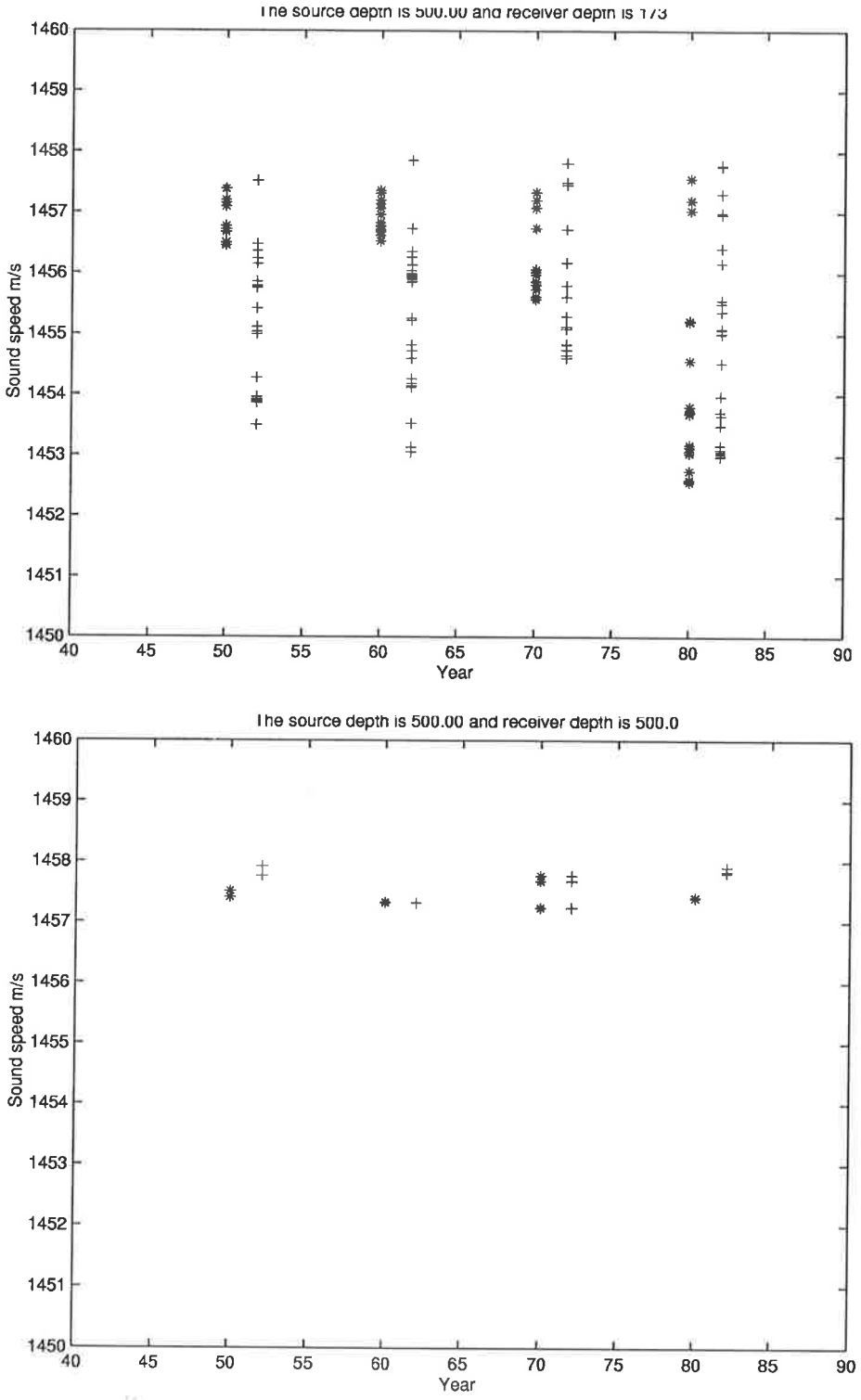

Figure 4.18. TAP-B: Sound speed along the eigen rays found for SD=500m and receiver depth 173 m in the upper plot and 500 m in the lower plot. . '+' is summer and '*' is winter

4.3 ACOUSTIC SENSITIVITY TO SEA ICE PROPERTIES

Due to the strong surface ducts found in areas of freezing processes and regions already covered by ice, sound above a cutoff frequency (increasing with surface duct depth) is trapped within the duct and repeatable interacting with the ice cover. At long distances, after several bounces with the sea ice, the sound has been exposed to several losses due to specular reflection and scattering, which will cause signal attenuation and phase change according to reflectivity properties of the sea ice. The phase changes are related to changes in the travel time. Therefor by measuring changes in signal attenuation and travel times the received signal will potentially contain integrated information about the sea ice properties.

In the TAP 1994 a source with a center frequency of 19.6 Hz was used for basin wide Arctic propagation, and based on the results from this experiment a new source has been deployed north east of Svalbard. This source transmits a signal every fourth day at 00:00 Z. This signal has been received by a vertical receiver array in the Lincoln Sea for more than 2 years now (Mikalevsky et al. 1999). Mikalevsky and co-workers claimed that the attenuation of the acoustic mode 1 and mode 2 contain information about the sea ice properties, and therefore propose to use low frequency sound as a tool for monitoring averaged sea ice properties.

One of the objective of this chapter is to investigate if this source, or other low frequency sources, can be used to find sea ice thickness estimates measuring travel time and perturbations and attenuation's along 60-2000 km long tracks.

Can the effect of sea ice be separated from the effect of changes in ocean temperature?
The main activities has been to study

- how sensitive the acoustic reflectivity from sea ice is to the mean sea ice thickness, to sea ice roughness and to some extent the internal properties of the sea ice, using the acoustic propagation model OASES.
- the sensitivity to changes in ice thickness in travel time/phase changes.

In the first section we will briefly consider the reflectivity properties of the sea ice for frequencies between 10 to 5000 Hz, and in the next section the effect of changing ice conditions on travel time at 19.6 Hz.

Specular reflection

The complex reflection coefficient is in general form written as:

$$R_c = |R_c| e^{\varphi}, \text{ where } \varphi = \operatorname{atan} \frac{\Im(R_c)}{\Re(R_c)}$$

In this study we will consider the sensitivity to ice parameters in modulus, and the phase function, as the modulus is related to the transmission loss through the reflection loss and the phase function is related to the travel time changes through beam displacement.

Theoretical expressions of the reflection coefficients of different complexity can be found in the book by Brekhoskikh (Waves in layered media). Considering for example the expression for reflection from a elastic plate floating on top of water and overlaid by a vacuum (Fig. 4.20, the

reflection depends first of all on the frequency and angle of incidence and further more on the parameters describing the sea ice such as layer thickness, density, compressional and shear wave velocity, and the wave attenuation rates in the media. In stead of studying this complicated expression analytically we will rather use the numerical model to study how the thickness and the internal properties of the sea ice influence the plane wave reflectivity. In this study the main attention is to sound at 19.6 Hz, which corresponds to wavelengths of 73 m in water and 183 m within the sea ice cover. Therefore it there is no point in detailed modelling of the sea ice with regard to finer stratification, and simple one layer sea ice model is considered.

The reflection loss module of OASES -**oasr** calculates the plane-wave reflection coefficients for an arbitrarily stratified fluid/solid halfspace (Fig. 4.20). The reflection coefficient is presented by reflection loss defined as R_{dB}=-20 Log $|R_c|$, where R_c is the complex plane wave reflection coefficient.

In this study we will first consider the reflection loss as function of grazing angle and frequency. Then we will have a look at the phase as a function of grazing angle or frequency.

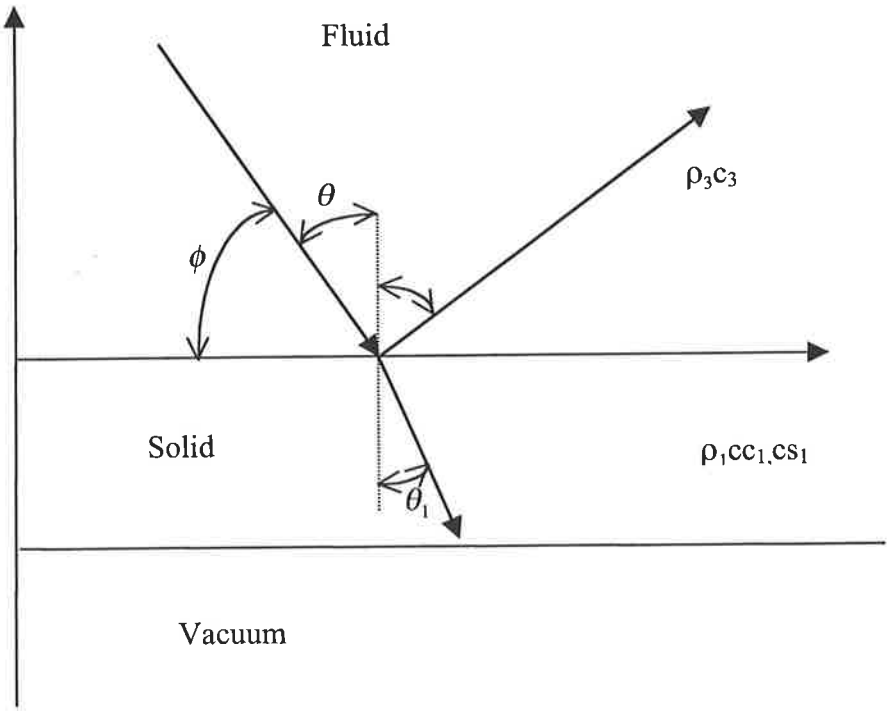

Figure 4.20. This figure defines the parameters found in the reflection coefficient between three homogeneous layers. Grazing angle is defined by ϕ and incidence angle by θ.

Reflection loss calculation using OASES

The reflection loss module of OASES -oasr calculates the plane-wave reflection coefficients for an arbitrarily stratified fluid/solid halfspace.

The reflection loss is defined as

R_{dB}=-20 Log $|R_c|$, where R_c is the complex plane wave reflection coefficient. In this study we will first consider the reflection loss as function of grazing angle and frequency. The sea ice properties used in the simulations shown in this report is listed in Table 4.1.

Table 4.1 Sea ice wave speeds and roughness for the figures of reflection loss. The water layer has a sound spped of 1440m/s

Fig number	CC compressional speed [m/s];	CS shear speed [m/s];	AC compressional attenuation dB/wavelength	AS shear attenuation dB/wavelength	RO density [g/cm^3]	RMS Roughness	CL Correlation length
Figure 4.21	3600	1800	1.0	2.5	0.92		
Figure 4.22 a,b	3000	1600	0.6	1.9	0.92		
Figure 4.22 c	3000	1450	0.6	1.9	0.92		
Figure 4.22 d	3000	1450	0.6	2.5	0.92		
Figure 4.23 a,b,c,d	3000	1450	0.6	2.5	0.92	0.1	0.2
Figure 4.24 a,b,	3000	1450	0.6	2.5	0.92	0.5	infinite

Reflection from a homogeneous elastic plate with different ice thicknesses.

The reflection loss have been calculated as a function of grazing angle (angle relative to the horizontal) and frequency for 3m, 2m, 1m and 0.5 m ice thickness. The results are plotted in Fig. 4.21 where the white color corresponds to close to total reflection. The plots show that the reflection loss as function of grazing angle depends strongly on the frequency. Furthermore, the plots reveals a strong sensitivity in the reflection coefficient function to changes in ice thickness when keeping the other sea ice properties constant, see Figure 4.21. Thinner ice moves the hole reflection loss pattern towards higher frequencies whiteout any other changes. In other words the thickness regulates the frequency filtering which can be described as follows:

- Below a given frequency, **f**, the reflection is total or close to total at all angles except at angels close to the critical angle for compressional waves, 61.3 degrees. The frequency **f** increases with decreasing ice thickness. The reflection loss for angles close to the critical angle of compressional waves is due to the transmission of acoustic energy into compressional shear waves in the ice cover.

- At larger frequencies than **f** the reflection loss increases rapidly for a grazing angles larger than 10^0-20^0. From 10^0 the losses increases up to a singularity close to the critical angel of incidence which in our case is 36.7 degrees (Figure 4.21). The losses between 10^0 up to angles close to the critical angels of the compressional waves (63^0) corresponds to transmission of acoustic energy into elastic shear waves in the ice cover.

This indicate that the details of the reflection loss pattern are given by the wave speeds and attenuation, this will be studied in the next section.

At long distances the acoustic field is composed by the the rays which propagates close to the horizontal, those rays corresponds to the plane waves with grazing angles between 0^0 and $10\text{-}20^0$. This part of the acoustic field is trapped in the surface channel and will propagated without any significant reflection losses. This part of the acoustic field is insensitive to ice thickness. Furthermore at frequencies below 70 Hz the reflection is total for all angles for all the thicknesses considered here. Therefore, the acoustic signal from a source with frequency below 70 Hz will not provide thickness information by measureing transmission loss .

The dark lines drawn in Figure 4.21 gives the frequency where the reflection losses starts to be more than 3 dB at angles close to the critical angle of shear waves. As the ice thickness is reduced the frequency domain with significant losses is switched towards higher frequencies. Comparing 3 m ice with 2 m ice the lower frequency limit (F) increases with 122 Hz from 234 Hz 356 Hz. If the ice thickness decreases to 1 m the frequency increases to 630 Hz and to 1480 Hz for 0.5 m thick ice. This shows that the changes from 1m to 0.5m is more dramatic than the changes from 3 m to 1 m.

Since the attenuation of sound, which is trapped in the surface duct, is generally due to the losses due to reflection from the underside of the sea ice cover we suggest to develop methods for measuring transmission loss as function of frequency. Such measurements will provide information about the frequency dependent filtering processes which have been shown to be sensitive to changes in ice thickness. Sources to be used in such measurments have to be broad band sources (explosives) or coded signals which contains frequencies sensitive to different ice thickness regimes. It is important that the sources contains frequencies between 100 Hz upto 1500 Hz so that it is possible to discriminate between ice in the range from 3 m down to 0.5 m.

The effect elastic properties

Compared to Figure 4.21 the compressional and shear wave speed in the two upper figures of Fig. 4.22 have been reduced from 3500 m/s to 3000 m/s and 1800 m/s to 1600 m/s, respectively. Ice thicknesses considered are 6 m to the left and 3 m to the right. The change in wavespeeds causes a corresponding reduction of the critical angles for both compressive and shear waves, to 57 and 18 degrees, respectively. From the figures it is seen that the losses decreases at grazing angles between $3\text{-}10^0$.

The changes in wave speeds causes a slight change in frequency filtering where the significant losses are introduced at slightly higher frequencies (for 3 m ice the frequency increases from 234 to 254 Hz). In the lower left plot the shear wave speed has been reduced from 1600 m/s to 1450 m/s, the new critical angle is now 6.7 degrees. This causes significant changes in the singularity corresponding to the transmission of shear wave, which is now located at 10 degrees. Furthermore the frequency filtering at low angles now starts at 200 Hz, 50 Hz lower than in the previous case.

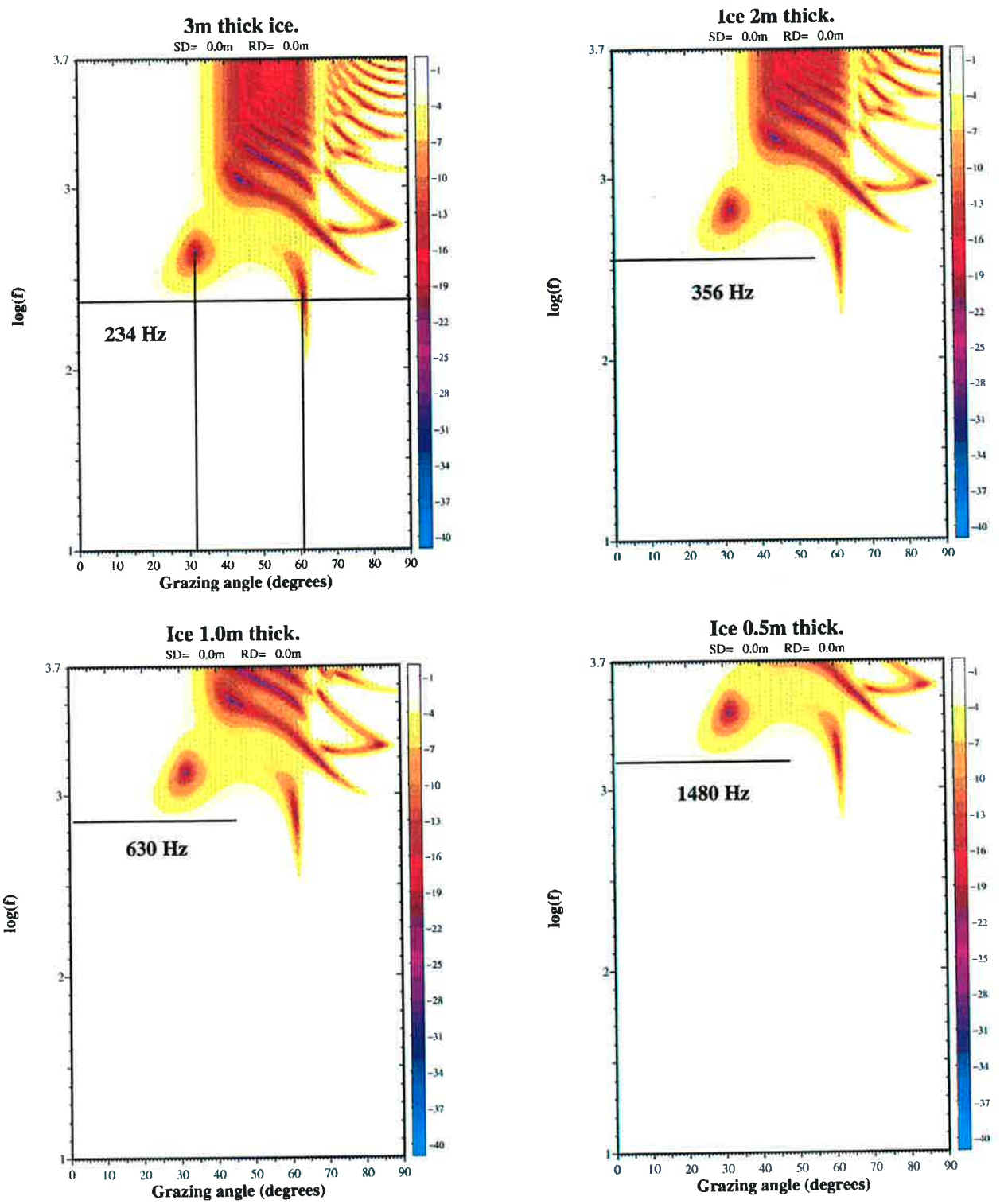

Figure 4.21 The refelection loss calculated for four different ice thicknesses : 3m, 2m, 1m, 0.5 m. The material constants are Cc=3600 m/s, cs=1800 m/s, ac=1.0 dB/wavelength as=2.5 dB/wavelength, density=0.92 g/cm^3. Sound Speed in water is set to 1440 m/s. Critical angle of reflection for the compressional waves are 61.3 degrees, and critical angle of shear waves 36.9 degrees.

In the last plot the shear wave attenuation has been increased to 2.5 dB/wavelength. This change do not cause any big changes. This shows that in an ice thickness inversion scheme additional information about the elastic properties is needed.

Scattering from ice

If the roughness is small compared to the acoustic wavelength and stationary in time and space a perturbational approach can be used so that the boundary conditions given at a rough surface can be transformed to a mean surface. In the case of free surfaces this is called Method of Small Perturbation first used by Rayleigh. This has been generalized by Kupermann and Schmidt, 1989 to rough interfaces between solid/fluid and fluid fluid layers. This approach is implemented into the modules of OASES. It has been shown by Fricke (1991,1993) that the inclusion of elastic properties are essential.

In OASES one can select between.

- Kirchoff approximation: corresponds to infinite correlation length and small scale roughness.
- Non-Kirchoff scattering: corresponds to finite correlation length

Small perturbation

In Fig. 4.23 four different ice thicknesses (6.0, 3.0, 1.0, and 0.5 m,) with a rms roughness of 10 cm and a correlation length of 20 cm is considered. The same elastic parameter values as considered in the lower left plot in the Fig. 4.22 are used for these plots and only the ice thickness is changing from plot to plot. By comparing the last plot in Fig. 4.22 with the upper right plot it is seen that there are no significant changes below 1000 Hz, while clear changes are observed at frequencies above 1000 Hz by introducing small perturbations in Fig. 4.23. As the ice thickness is further reduced the same switch of the frequency filtering towards higher frequencies as for smooth ice is observed in this case. Therefore the ice thickness changes dominates over the small scale roughness.

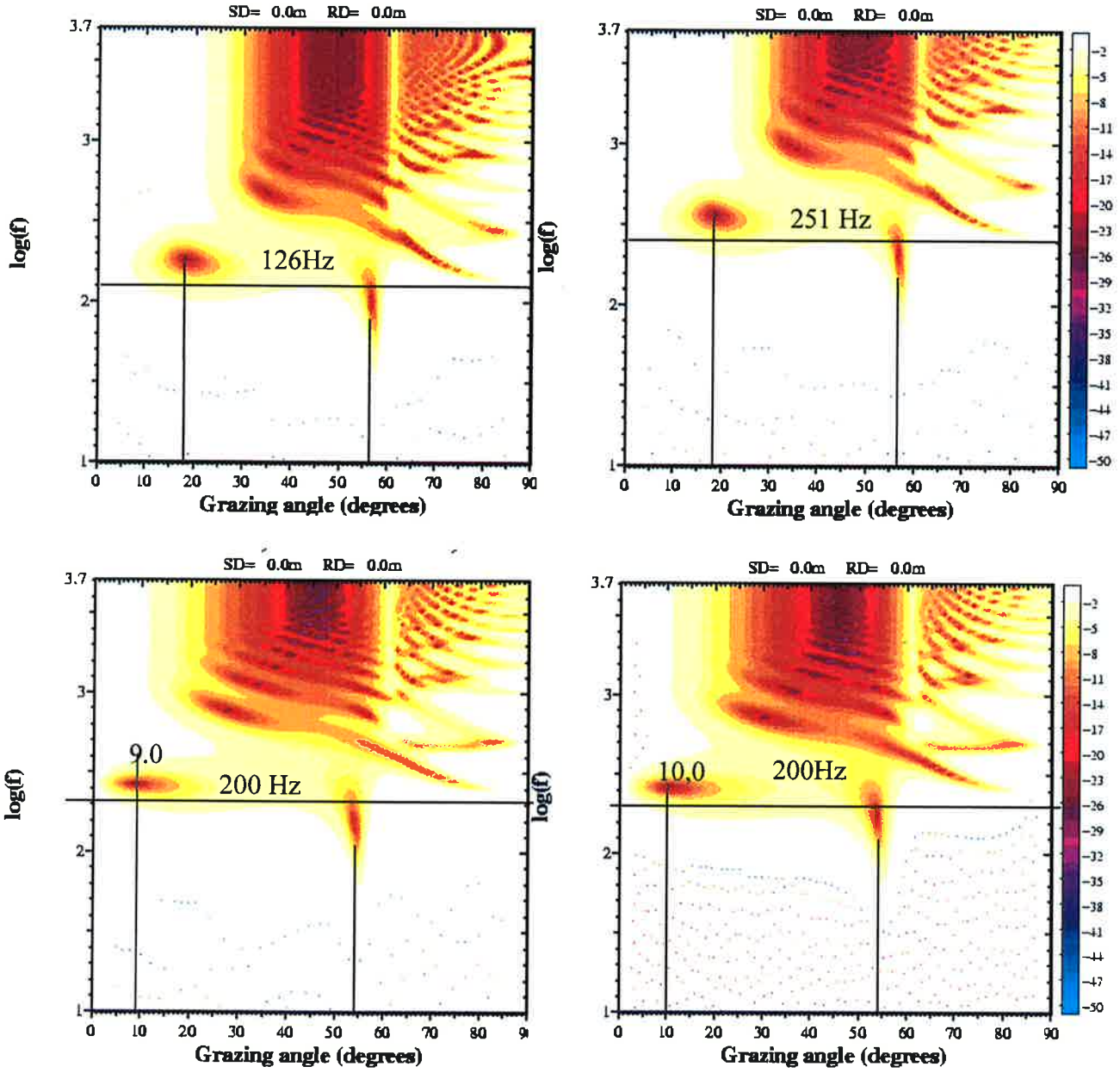

Figure 4.22 Reflection loss as function of frequency and grazing angle

In Fig. 4.22 one by one parameter is changed. The reflection loss calculated 6m thick ice in the upper left with the material constants are Cc=3000 m/s, cs=1600 m/s, ac=0.6 dB/wavelength as=1.9 dB/wavelength, density=0.92 g/cm^3.In the upper right plot the ice thickness is reduced to 3 m. In the lower left figure the cs speed is reduced to 1450 m, and finally in the lower right figure the attenuation of shear waves is increased to 2.5 dB. There is no scattering in these plots.

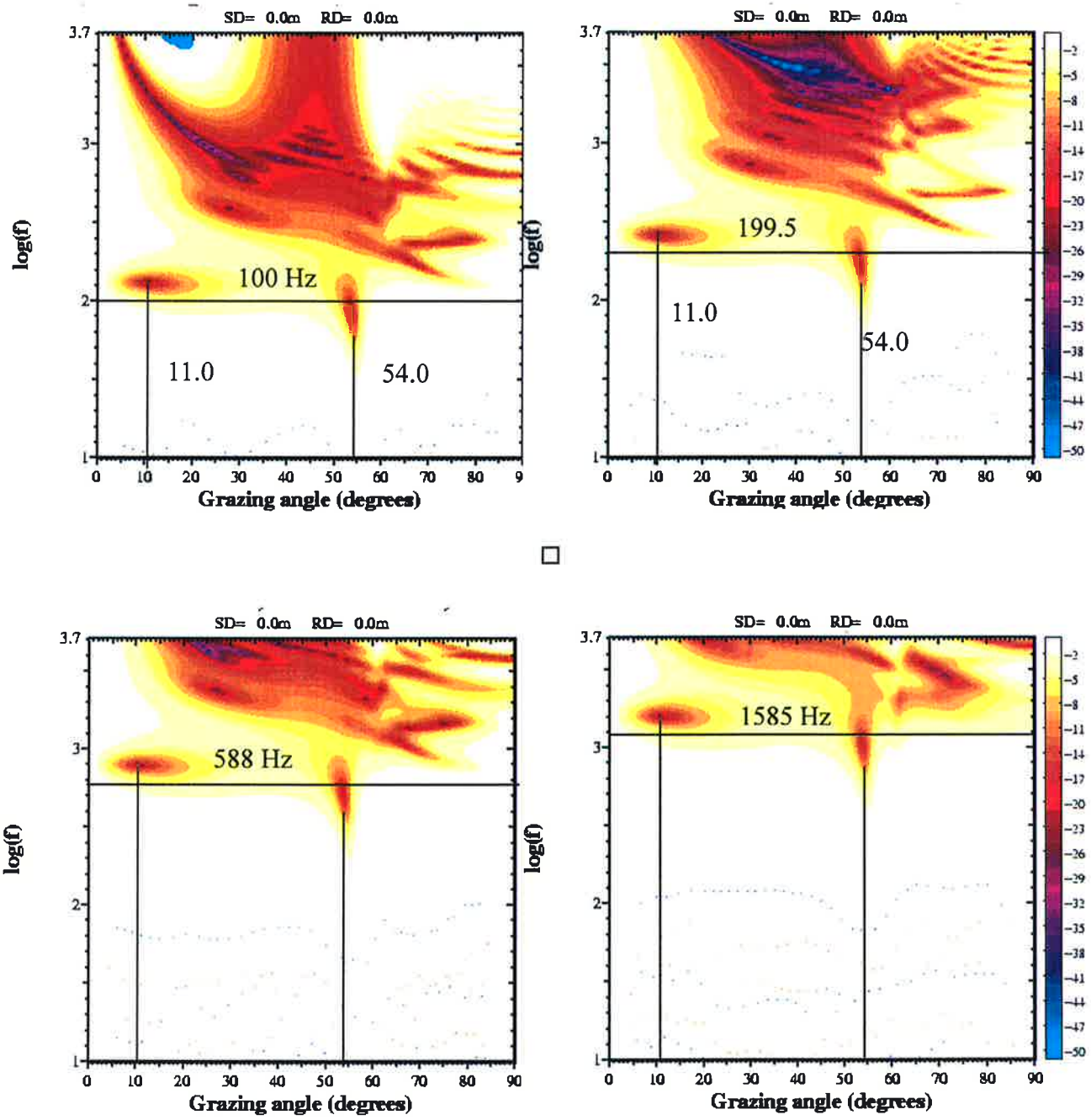

Figure 4.23 Reflection loss as function of frequency for different ice thicknesses

The reflection loss in Fig. 4.23 calculated for four different ice thicknesses : 6m, 3m, 1m, 0.5 m. The material constants are Cc=3000 m/s, cs=1450 m/s, ac=0.6 dB/wavelength as=2.5 dB/wavelength, density=0.92 g/cm^3

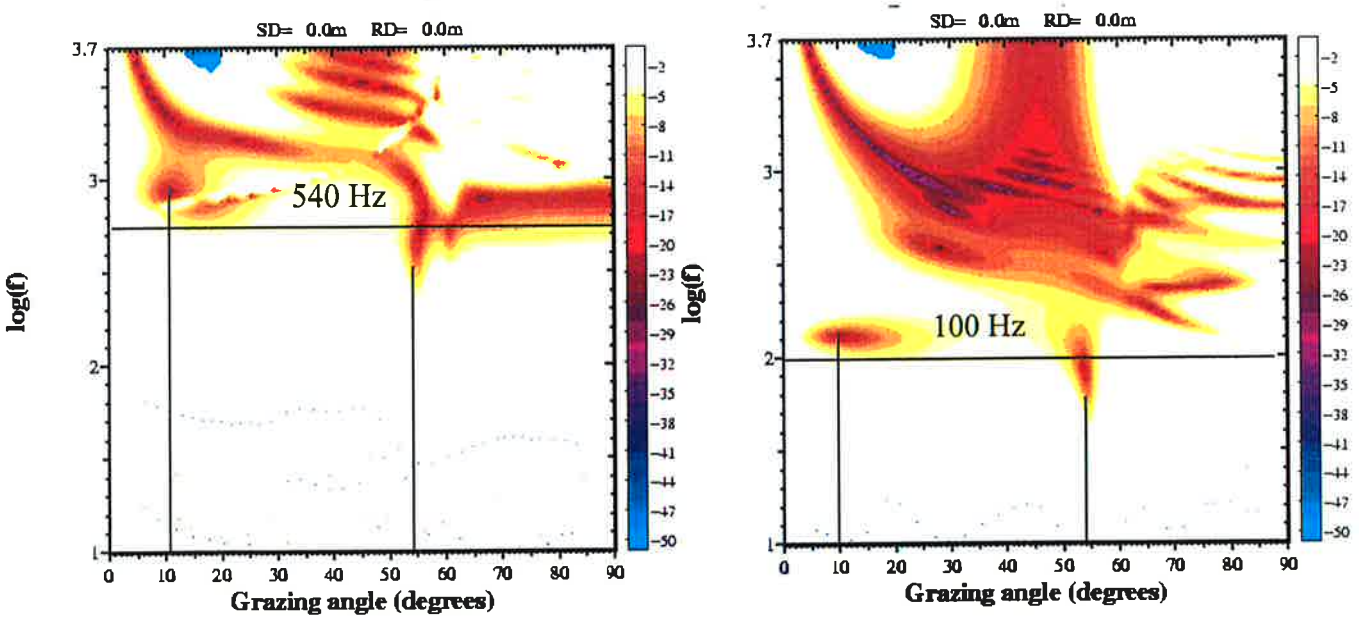

Figure 4.24 Reflection loss for 1 m (left) and 6 m (right) thickness

The reflection loss in Fig. 4.24 is calculated for ice thicknesses: 1m and 6 m. The material constants are Cc=3000 m/s, cs=1450 m/s, ac=0.6 dB/wavelength as=2.5 dB/wavelength, density=0.92 g/cm^3. RMS roughness 0.5 m and infinite correlation length.

Kirchoffs scattering

In Fig. 4.24 small scale perturbation with infinite correlation length has been introduced. In the left the ice thickness is 1 m which is comparable to the introduced rms roughness of 0.5 m. In this case the pattern of the reflection loss function is significantly changed, while the frequency F (540 Hz) is comparable to the 1 m case for small perturbation (588 Hz). When the ice thickness is 6 m the pattern is similar to the case with small scale perturbation and short correlation length.

The phase of the reflection coefficient

The second derivative of the phase function in the reflection coeffisient is important for the beam displacement/lateral waves. It is assumed that lateral waves occurs at the ice water interface and repeated interaction with the ice cover will cause significant integrated travel time changes which depends on the ice thickness. By calculating and plotting the phase function as function of grazing angle for different ice thicknesses at 19.6 Hz (As used in TAP and ACOUS) inn Fig. 4.25 it is seen that there is no big changes or ocillations in the phase function which indicate that the is no beam displacement present at this frequency. Before we conclude that there is no travel time or phase sensitivity to sea ice thickness at frequencies around 20 Hz further detailed investigation of the fullwave signal has to be carried out.

In Figure 4.26 the phase function has been calculated for two ice thicknesses (1 m, 3 m) for three different frequencies. This figure show that the sensitivity to sea ice thickness in the phase increases with frequency.

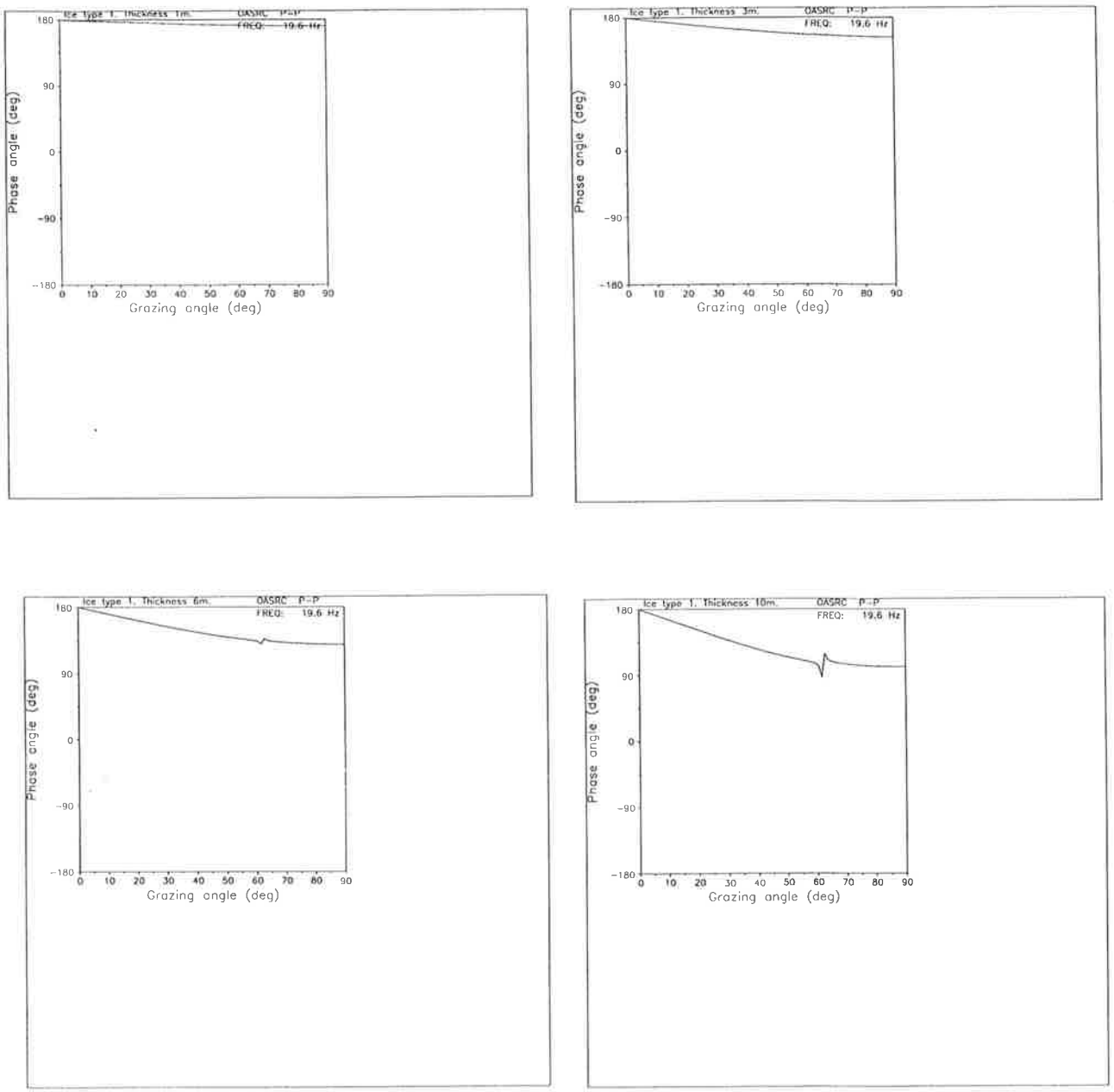

Figure 4.25. Phase as function of grazing angle. Winter ice condition with different ice thickness. Source frequency is 19.6 Hz.

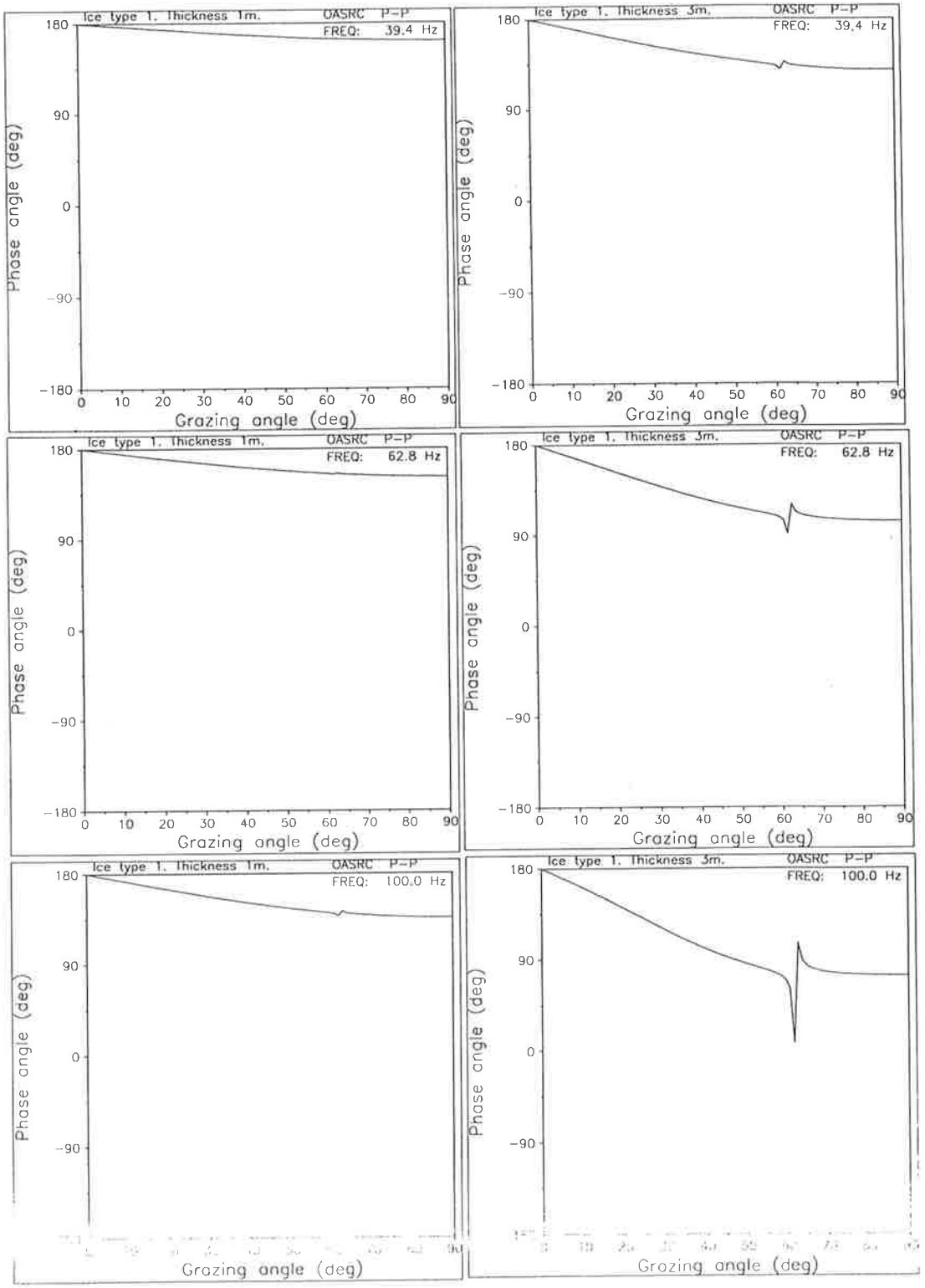

Figure 4.26. Winter ice conditions. Phase as function of grazing angle for 1m (left) and 3m (right) for selected source frequencies (close to 40, 60 and 100 Hz)

Summary of results

The reflection loss have been calculated as a function of grazing angle (angle relative to the horizontal) and frequency for different ice thicknesses using typical sound speeds for Arctic ice. The results are:

- The reflection loss function with respect to grazing angle depends strongly on the frequency.
- At frequencies below 70 Hz the reflection is total for all angles for ice thicknesses up to 9 m.
- The study of reflection loss plots reveals a strong sensitivity in the reflection coefficient function with respect to frequency to changes in ice thickness. Thinner ice moves the whole reflection loss pattern towards higher frequencies without any other changes (Sagen, 1998), and this to happen both with scattering and without scattering.
- For a low frequency source (20 Hz) the phase and modulus of the reflection coeffisient is insensitive to ice thickness.
- Rays with an interaction angle lower than 10^0 do not suffer of significant losses due to a smooth ice cover and will not feel the ice thickness. The acoustic field far from the source will therefore consist of the rays which are insensitive to the sea ice with respect to transmission loss.
- In order to obtain information about the internal ice properties and ice thickness, acoustic measurements have to be made at frequencies or in frequency bands which is sensible to the sea ice. According to our study the optimum frequencies for retrieving ice information are between 100-3000 Hz using transmission loss measurements.
- To develope ice thickness inversion routines from acoustics the sensitivity to changes in elastic properties and roughnesses has to investigated in detail, including the effect of a non-homogeneous ice plate. From our results it is most likely that a inversion scheme will need additional information about ice extent and ice classification (available from remote sensing from space) and corresponding elastic properties of the different classes of ice (detailed measurements are required).

4.4 PULSE PROPAGATION IN AN ARCTIC ENVIRONMENT

The specific objective in this section is to study the pulse propagation in a typical Arctic environment. The solution of the time dependent wave equation can be obtain by a Fourier transform of the frequency domain solutions as

Equation 1

$$p(r,z,t) = \frac{1}{2\pi}\int S(\omega)P(r,z,\omega)e^{-i\omega t}d\omega$$

where S(ω) is the source spectrum and P(r,z,ω) is the spatial transfer function. The main effort is to compute the transfer function at a number of discrete frequencies within the band of interest. This calculation of the transfer function can be done by existing propagation models for example OASES, KRAKEN or others. The evaluation of p(r,z,t) is then done by and FFT at each of the spatial positions (r,z) where the pulse respones is wanted.

In our study the OASES-OASP module calculates the depth dependent Greens function for a selected number of frequencies and determines the spatial transfer function (wide band transfer functions) at any given receiver position by evaluating the wave number integral. Then the frequency integral p(r,z,t) in Equation 1 is calculated in the post processor PP.

The source function used

In this study the OASP uses the default explosive source (point source) normalized to unit pressure at 1 m distance. The calculation of P(r,z,ω) is independent of the source function, while this function is very important for the calculation of the pulse function in the time domain. In this study we use a predefined source function in OASES, generated as a Hanning windowed sine wave with a duration corresponding to the bandwidth of the transfer function. This source minimizes artificial ringing of the response due to the truncation of the transfer function and is the recommended pulse type for narrow band sources.

In this study a source with a frequency band $[f_{min}, f_{max}]=[16,24]$ and center frequency equal to 19.6 is used. This is a relatively narrow banded source with regard to the number of frequencies included, but due to the low frequency it can be unrealistic to build in practice. This source makes it relatively simple to separate out different arrival times.

The numerical parameters

The setting of the numerical gridd in space/wave-number domain and time/frequency domains is essential for obtaining a reliable result. The procedure for selecting the correct sampling in the time domain is described in detail in the SAFARI model user manual (Schmidt, 1987) and in the book by Jensen et al., 1994.

First we define the time increment to be $\Delta t=0.00416676$s, which corresponds to a numerical frequency domain $[-F_{max}, F_{max}]=[-120,120]$. Once Δt is given the frequency domain is given. Then we need to decide the number of samples needed to cover the time necessary to receive the signal at the receivers included in the study and it has to be high enough to avoid aliasing. If the maximum range is 60 km, and lowest wave speed included is 1436 m/s then we need to cover a time interval of at least 42 s. We decide to use a sampling number of 32768, which gives a total length of 136 s and a df=0.00732 Hz. The reason for the relatively large sampling number and broad frequency domain is to play safe and avoid aliasing and truncation errors in

the time signal we consider. The frequency Fourie components are calculated between 16 Hz and 24 Hz for each specified range and depths, $P(f,x_i,z_j)$. In our case at 60 positions. The calculation time (CPU) of P(f,x,z) at 60 positions is 8849 s (2,5 hours) on the ORIGON 2000 super computer. The computation time is mainly dependent on the range parameter and time resolution.

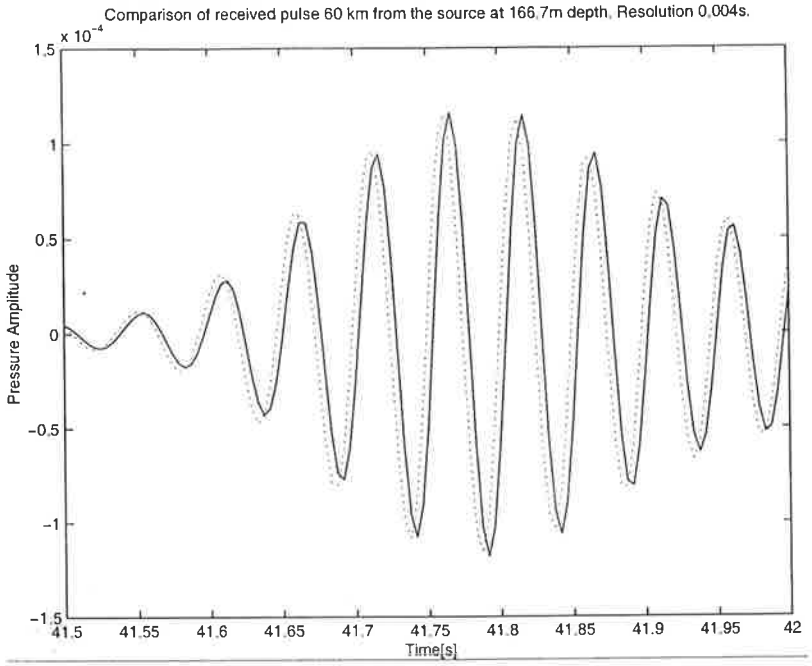

Resolution is 0.004 s.

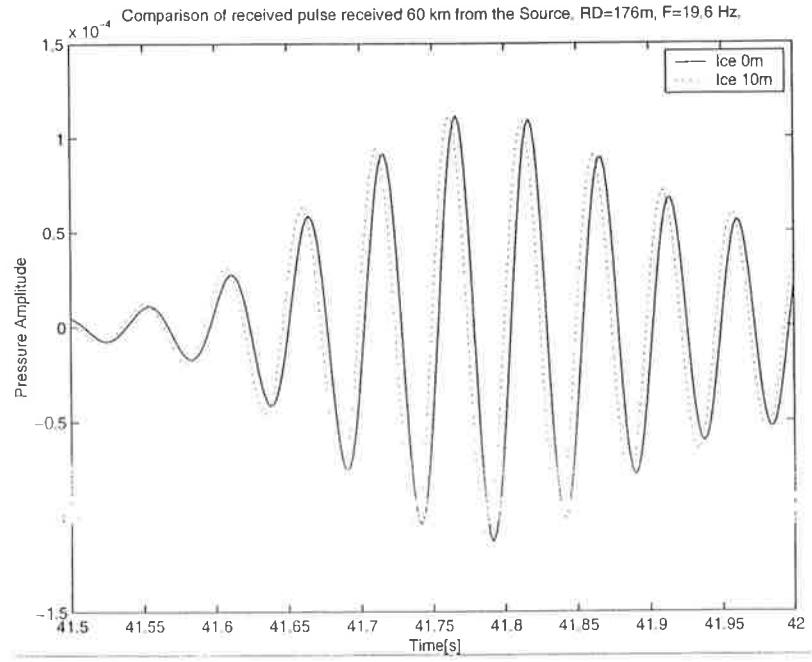

Resolution is 0.002s

Figure 4.27. Plots of received signal 60 km using different time resolution. In the upper plot a resolution of 0.004 s is used in the lower plot the time resolution is 0.002s.

In case that the time resolution is to poor to observe the time changes due to a sea ice cover for example Δt=0.00208338 s the corresponding numerical frequency domain is -240 up to 240 Hz. In order to keep the same quality in the signal sampling we have to adjust the number of sampling with the same factor (in this case a factor 2). This gives 65536 samples.

Due to very long computer times if full range dependence environments are used as input to OASES, and due to the many parameter that we have to consider the approach is as follows:

- Ranges considered is limited to be between 60 km and 120 km
- The seafloor/ocean/ice/environment is range independent
- Maximum receiver depth is at 1500 m

Then the travel time delay is calculated by comparing the ice covered oceans results with open ocean results for receivers at different depth and ranges. Based on these results estimates are calculated for full sectors, those will be evaluated for usefulness and if those perturbations will cause any problems for the monitoring of ocean temperature.

Oceanographic profile and Sea ice model

The oceanographic model is kept constant and range independent to study the effect of changing ice thickness. The sound speed profile (Fig. 4.28) is obtained from the US Russian Environmental Atlas, and is an average of stations collected during winters in the 1980s at locations "close" to 83.5 N 26.0 E. The profile is typical for the Arctic basin, and a strong surface duct is seen to go down to 250 m from where the sound speed increases fairly linearly with depth. The surface duct will trap even low frequency sound close to the sea ice and make it to interact with the sea ice cover several times.

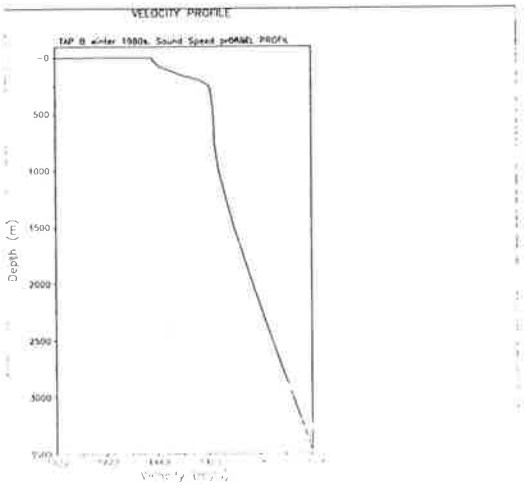

Figure 4.28. The sound velocity profile used in the acoustic pulse simulations.

The sea ice cover is modelled as a homogeneous elastic plate, this is reasonable due to the low frequency (20 Hz) considered her. The plate have a uniform thickness on which statistical roughness is introduced in the last part of the study. In order to study the effect of changing ice thickness and ice type, the plate thickness is changed between 1m and 10 m with steps of 1m for three different central Arctic ice types. The ice types is defined in Table 4.2, and the parameters are used as input to the range independent version of OASP.

Table 4.1 Definition of the different ice types considered in pulse modelling.

Ice type	cc [m/s]	cs [m/s]	ac[dB/λ]	as [dB/λ]	density $\left[\left(\frac{g}{cm^3}\right)\right]$
Winter Ice	3500 m/s	1800	0.214	0.1102	0.91
Winter Ice 2	3500 m/s	1800	0.0012	0.0072	0.91
Summer Ice	3000 m/s	1600	0.214	0.1102	0.91

Modelling changes in ice thicknesses

Three ways of introducing changes in ice thickness can be used:

1. An increase in ice thickness will reduce the thickness of the surface duct correspondingly, and travel time changes will be influenced both by the changes in surface duct thickness and ice thickness. Conservation of total volume. Mass is reduced when the ice thickness increases, because ice is less dense than water.
2. The sea ice plate thickness is just put on top of the oceanography without changing the thickness of the duct. Conservation of the ocean model. This will give of the effect of the sea ice thickness cover alone, but new mass is introduced to the system when ice thickness increases.
3. When modelling changes in ice thickness due to transformation from water to ice (or vice versa) one assume no additional mass in the system from free surface down to the sea floor. In other words mass is conserved in the process and

Equation 2

$M_{transformed\ water}=M_{new\ ice}$

The thickness of the transformed water layer is

Equation 3

$H_{water}=d_{ice}/d_{water}*H_{ice}$ (2)

In practice this mean that if you have an open water situation with the layering function $H_{water}(z)$ and there is introduced a ice plate of thickness 2 m the transformed water layer will be 1.84 m thick.

In OASES this is done by putting the 2 m Ice cover on top and the water layer thickness from the sea/ice interface to the first sound speed given in water $H_{water}(z)$ -1.84 m. Correspondingly the total depth from sea ice surface down to the bottom has gained 16 cm by introducing the 2 m sea ice cover, while the mass is kept constant.

Travel time changes

The time change is defined as the difference between travel time obtained without ice and the travel time obtained with ice:

Equation 4

$\Delta T = T_{\text{no ice}} - T_{ice}$.

The pulse arrival pattern

The arrival pattern at receiver 60 km from the acoustic source.

In Fig. 4.29 and 4.30 the pulse arrival pattern 60 km from the source has been plotted as a function of depth. The upper plot in those figures show the puls arrivals at receivers within the duct while the lower plot show the arrivals both within the duct and down to 1500 m. In Fig.4.29 there is no ice, whereas a 10 m thick ice plate has been introduced by removing 10 m of the watermasses in Fig. 4.30 . The two figures do not resolve any significant change in the arrival pattern when introducing the extreme ice thickness. At the receivers within the duct the first pulse arrival corresponds to the ducted part of the signal which in mode theory is reperesented by Mode. The second and third arrivals correspond to the deeper penetrating acoustic field which is represented by Mode 2 and 3. The later arrivals are bottom reflected part of the signal. The pulse pattern below the duct is plotted the lower plot in Fig. 4.29 and 4.30 and is very different from the arrival structure within the duct. The acoustic field is described by bottom and surface reflected signals.

The arrival pattern at receiver 120 km from the acoustic source.

In Fig. 4.31 the pulse arrival pattern within the duct 120 km from the source is plotted. The arrival pattern is significantly different from what was observed at the receiver 60 km from the source. The ducted acoustic field now corresponds to the third arrival, while the two first arrivals corresponds to the mode 2 and mode 3 which penetrates down to watermasses with higer sound speeds.

In Fig. 4.32 the pulse which propagate in an environment with ice is compared to a pulse which propagates in an environment without ice. The comparison is done at a receiver depth of 166.7 m at to distances from the source, at 60 km in the upper plot and at 120 km in the lower plot. At 60 km the first arriving pulse is strongest and not significantly influenced by the inclusion of the sea ice cover.

At 120 km it is clearly seen that it is the second arrival is the strongest, and that the phase is slightly influenced by the sea ice. The first and third arrival corresponds to a signal which do not interact with the sea ice but transverses water masses with higher sound speeds than the trapped signal which interacts with the sea ice cover.

By zooming in on the first arrival at 60 km it is found that the signal with 10 m ice arrives 0.0045s before the signal in a no ice environment.At 120 km the signal arrives 0.0091 s before the no ice signal. This is significantly above the signal resolution which is 0.002s. This show that the travel time perurbation is doubled when distance is doubled

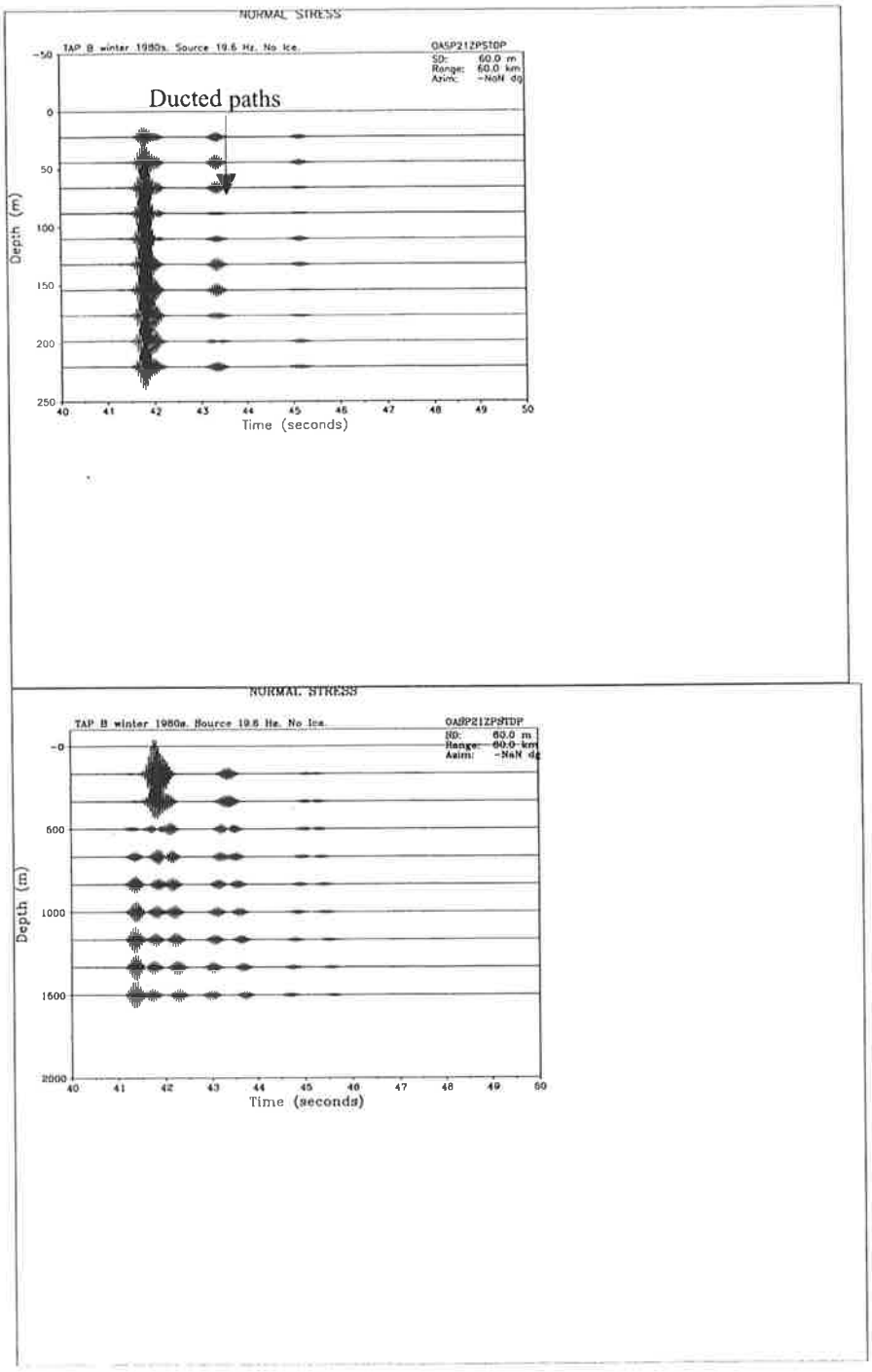

Figure 4.29 Pulse arrival structure at an receiver array positioned 60 km away from the source. In these simulations the is no sea ice cover. Oceanographic profile is given in Figure 4.28. Upper figure is the pulse arrival within the surface duct and the lower figure is the pulse arrivals at deeper receivers.

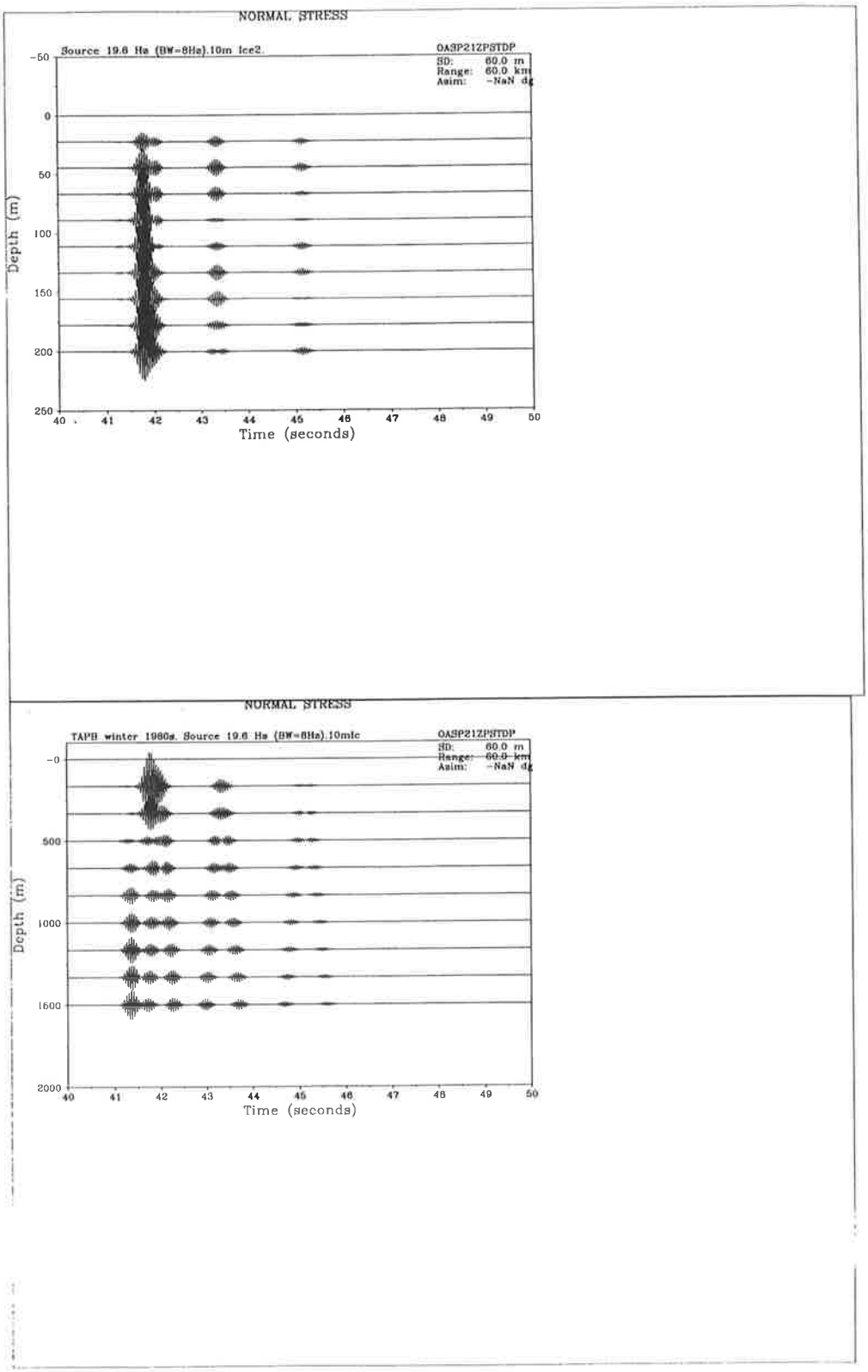

Figure 4.30 Pulse arrival structure at an receiver array positioned 60 km away from the source. Sea ice is of type 2 in Table 1 and the ice thickness is 10 m (Oceanographic profile is given in Figure 4.28. Upper figure is the pulse arrival within the surface duct and the lower figure is the pulse arrivals at deeper receivers.

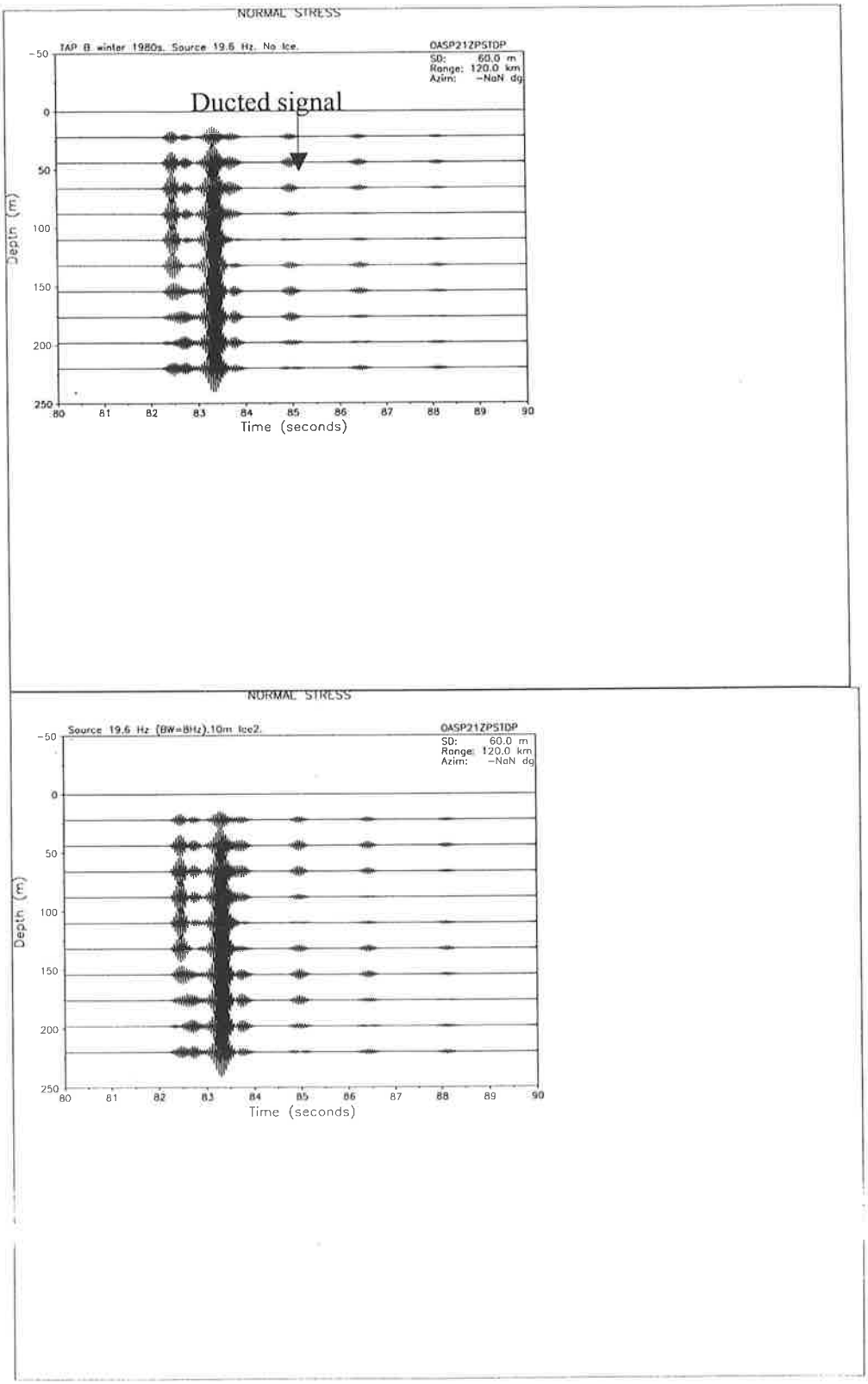

Figure 1.31 This is the pulse arrival structure within the 250 m deep surface channel 120 km from the source. The upper is with no ice and the lower is with 10 m ice.

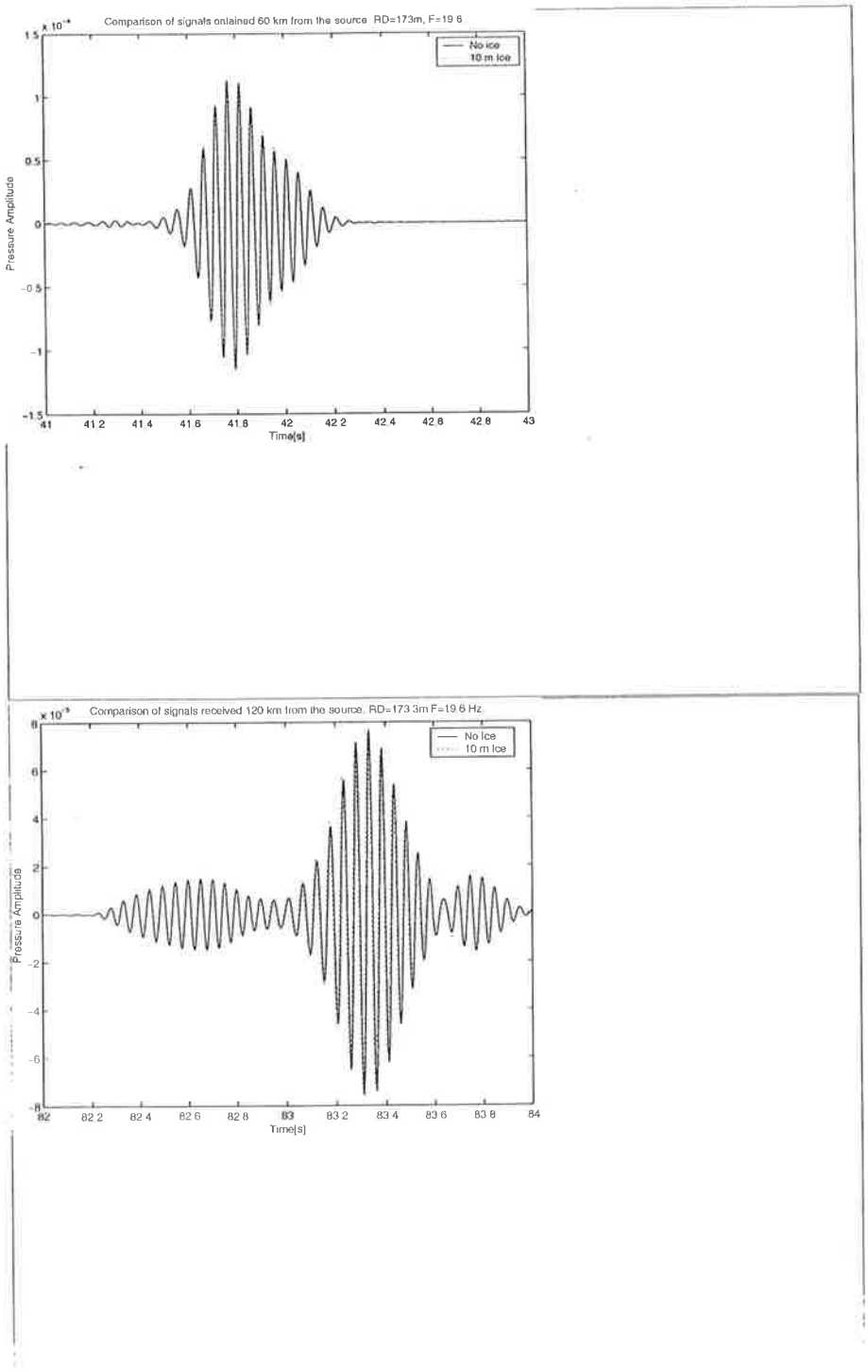

Figure 4.32 Comparison of pulse received when the summer sea ice cover is 10 m thick with a situation without sea ice. The Sea ice is put on top and corresponding adjust ment of the thickness of the upper two layers. The upper figure is 60 km from the source and the lower is 120 km from the source. The receiver depth is 173.3 m.Time resolution is 0.002s.

4.5 STUDY THE SENSITIVITY IN ACOUSTIC TRAVEL TIME TO CHANGES IN ICE CONDITIONS

Mikalevsky et al. (1999) claimed that the attenuation of the acoustic mode 1 and mode 2 contain information about the sea ice properties. We have previously shown that the "normal" ice thickness causes total internal reflection at low frequencies, and only scattering will cause any significant attenuation at this frequency. The phase of the reflection coefficient is more sensitive to ice thickness and can potentially cause travel time or phase perturbations when ice thickness changes.

The objective of this activity is to *study if travel time measurements are influence by the ice thickness and if such measurements can be used to observe changes in the ice thickness.*
A typical winter profile obtained from TAP B is used for studying the travel time changes due to sea ice. The surface duct is around 250 m deep and the total water depth is 3500m. A source with a bandwidth of 8 Hz and a center frequency of 19.6 Hz. This is similar to the source used in TAP except that the frequency band used is wider then the 2.3 Hz wide band used in TAP. The broader frequency band is used because it is simpler to identify the different arrivals. The receivers were positioned 20, 40, 60, 80, 100 and 120 km from the source. Several receiver depths have been used.

The most pronounced effects seen in the simulations are that signals received within the surface duct are very stable when varying the sea ice properties although the sound interacts continuously with the sea ice. The signal received below the duct is also stable, but very different from the signal propagating within the duct. Since the signal trapped in the duct are most influenced by the sea ice our attention has be put on the ducted signal. At 120 km two major arrivals can be detected. The first arrival corresponds to the deeper going part of the sound field. The second arrival comes in 0.5 s after, and corresponds to the surface duct trapped signal.

By comparing the second arrival of the signal received at different depths within the duct, in each particular simulation, it is found that they are in phase. In the following we will compare signals obtained 120 km from the source by receivers 173.3 m below the surface.

The time change is defined as $\Delta T = T_{ice} - T_{\text{no ice}}$.
where the first term is the travel time calculated in the case of no ice and the second term is the pulse obtained when ice cover has been introduced. If the travel time change is positive, the ice have made the signal to travel faster, while if the change is negative the ice have made the signal to travel slower. Each pulse simulation takes 5 CPU hours on the supercomputer. Figure show how the signals are compared. The travel time change have been calculated for different ice types and thicknesses using figures similar to 4.33 and the formula above. The ice cover has been introduced using three approaches which will be described separately below.

The ice plate put on top of the sound speed profiles

This was in the beginning the "natural" way of including the sea ice cover given that the ice thickness was the dominant parameter, and that the oceanography was given from point z=0, as if there were no ice present. The result is plotted in Fig. 4.34 and we can see a delay, up to 0.045 s, of the acoustic signal as the ice thickness increases. A signal delay due to the sea ice is the opposite of what we would expect, since the wave speeds in ice is greater than in ice.

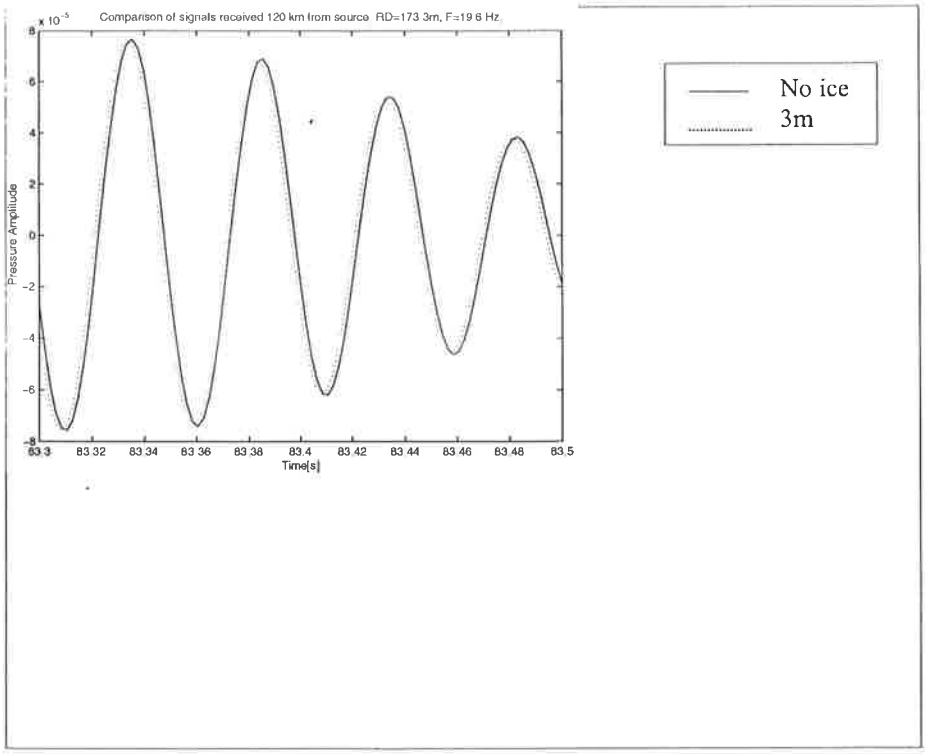

Figure 4.33 Comparison of the second arrival pulse with 3m thick ice and without ice. The receiver is positioned 120 km at 173.3 m depth. The summer ice cover has replaced the same of volume of water.

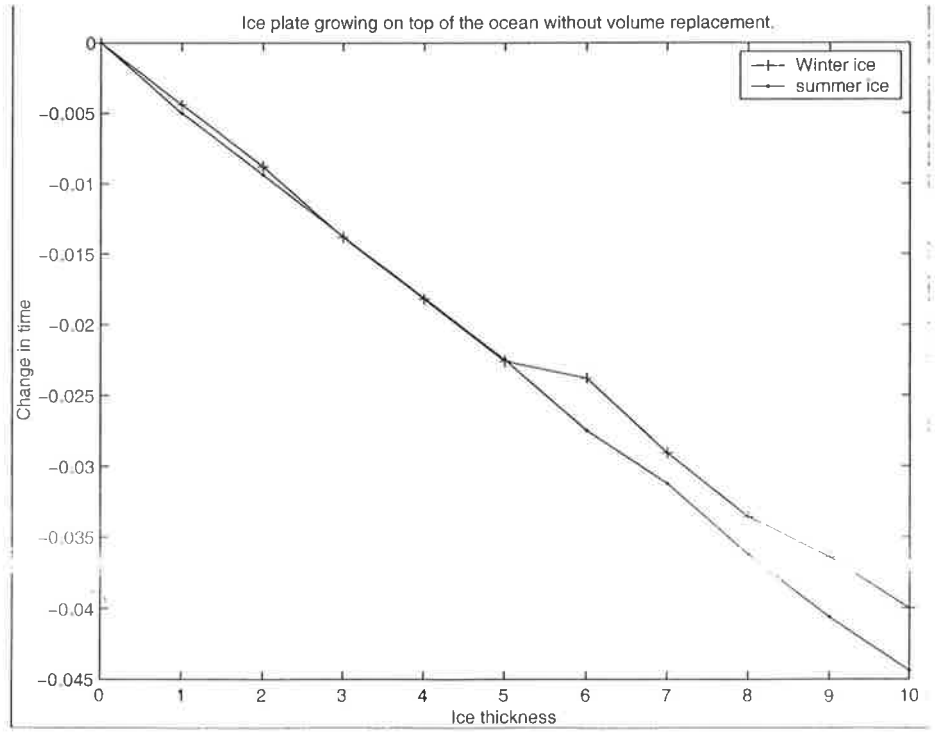

Figure 4.34 Travel time change as function of ice plate thickness. The ice plate was in these simulations put on top of the ocean without displacement of water.

The ice plate replaces the same volume of water

Ice was then introduced by letting the ice plate replace the same volume of water. The travel time changes have been calculated for different ice types, and the results are presented inFig. 4.35. From this plot it is seen that the signal travel faster as the ice thickness increases, this is also seen in Fig. 4.33. These results is similar to the results found in [11] for 250 Hz.

By tuning the ice parameters included in the reflection coefficient, the strongest effect is found when the density in ice is the same as in water. The consequence is that the water has been replaced with the same mass of ice, and in this case no travel time change was observed for ice thicknesses less than 6 m. In the other cases plotted in Fig. 4.35, the replacement of equal volumes introduce a reduction of mass.

A constant ice plate volume replaces a increasing volume of water.

In Fig. 4.36 the travel time change is plotted as a function of thickness of the displaced water layer. The simulations show that as long as the mass of introduced ice is larger than the mass of the displaced water the travel time change is negative (the ice delays the signal), while when the mass of ice introduced becomes smaller than the displaced water mass the travel time change becomes positive (the ice layer causes the sound to travel faster). The layer thickness of displaced water corresponding to no travel time change, is the thickness at which the mass of displaced water equals the mass of the introduced ice plate.

Conclusion

This leads to the result, that by assuming there is no mass change when the ice thickness change (because when ice melt it will be water implying mass conservation), there will be no travel time change. Mass conservation is a realistic assumption used in climate modeling in the Arctic. Therefore, at low frequencies open water models can be used and travel changes is due to changes in the ocean primarily temperature and to a less extent salinity. Consequently, travel time measurements using low frequency sources can not be used as a monitoring concept for sea ice thickness.

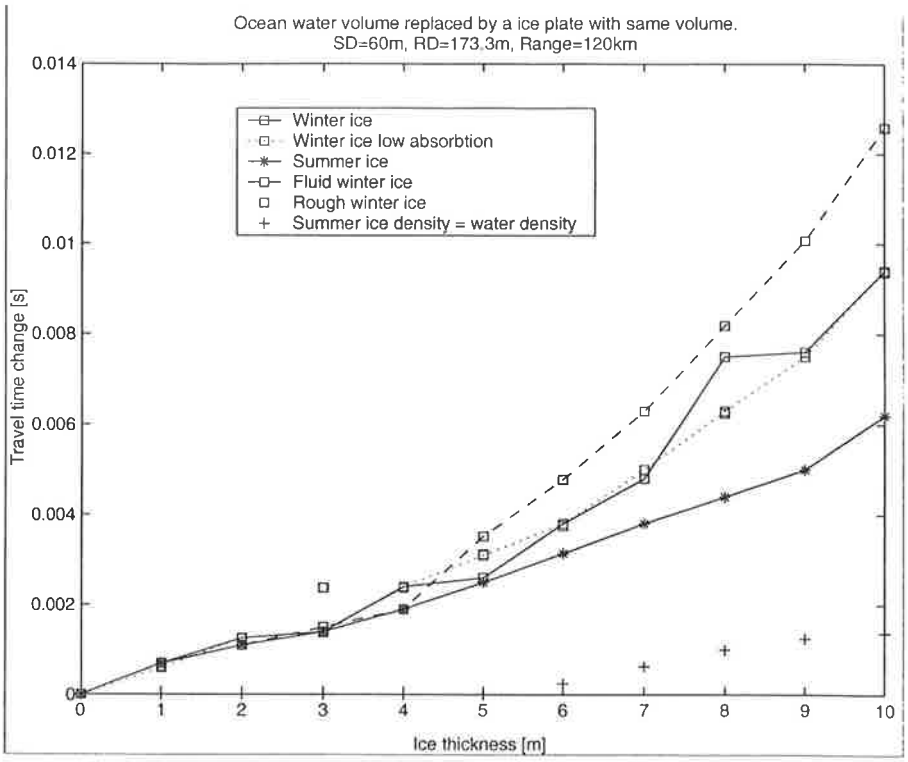

Figure 4.35 Travel time change as function of ice plate thickness. The ice plate was in these simulations displacing a water layer of same thickness, in other words volume is conserved.

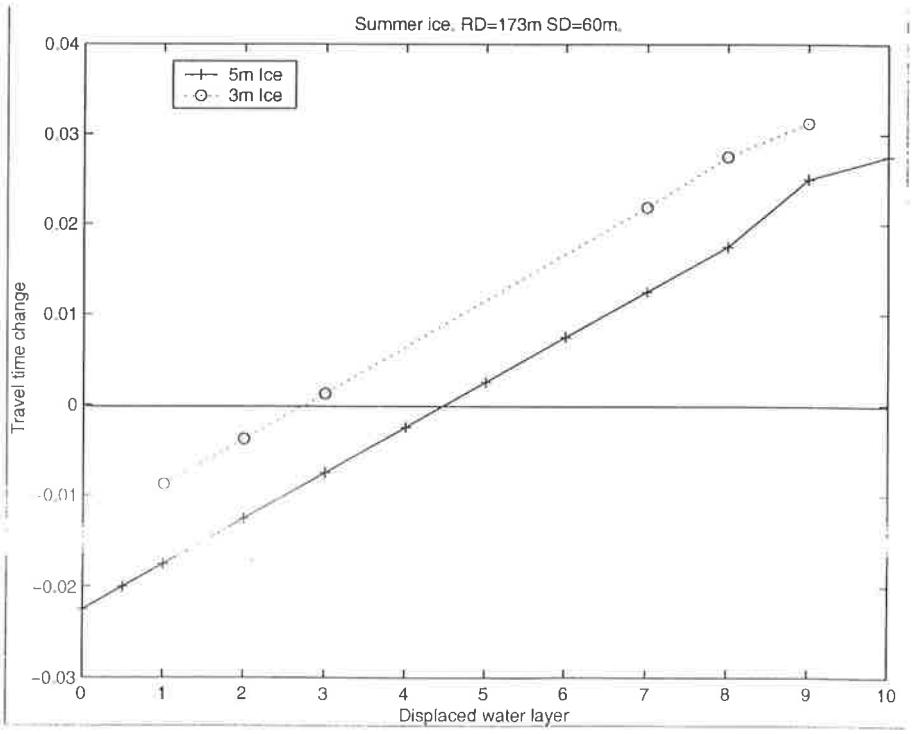

Figure 4.36 Travel time change as a function of the thickness of the displaced water layer. Two ice thicknesses have been considered for a smooth ice plate.

Chapter 5

Activity 3. Acoustic monitoring of ocean climate in the Arctic

Contents

5.1 RESULTS FROM THE ARCTIC OCEAN

Climate modelling results as input data

Two anthropogenic scenarios (including doubling of CO_2) and corresponding control runs have been provided from Task 2. The first anthropogenic scenario, delivered in June, used the wrong salinity forcing fields and a new scenario was provided in the end of October, 2000.

Each scenario provided monthly mean ocean data over 100 years where the first 25 years is spin up for the climate model. The monthly averaged temperature and salinity profiles along the three tracks are used to calculate corresponding sections of sound speed to be feeded into the acoustic model.

Acoustic experiments

The ray model calculates the eigenrays and eigenfronts for each source/receiver configuration. The traveltimes for each eigenray found for each "acoustic shot" are plotted against time. See Figure 1.The oceanographic fields and ice thicknesses were provided for three predefined tracks see Figure 1. In each acoustic experiment the eigenrays for a source located either on 60m or at 500 m and six receivers (for 50, 100, 200,300, 400, and 500m) are calculated using RAY. Each acoustic simulation takes around

1. 2.5 months for the TAP-A (2623 km),
2. 3 weeks for TAP B (700 km),
3. 8 days for eastern part of Fram Strait (200 km).

The status of the acoustic simulations is shown in the Table 5.1, as seen here less than half of the planned simulations have been done this is partly due to the late delivery from MPI and partly because we ran out of allocated calculation time at the supercomputer. The TAP-B simulations are currently being submitted to the supercomputer in Trondheim, this is a faster computer so it is expected that the allocation of 10000 CPU hours will be enough to finish the simulations for TAP-B. The completion of these simulations will be done after end of the AMOC project.

Table show overview of the Scenarios and the progress in acoustic simulations. OK means that the acoustic experiments with shallow (60 m) and deep source (500 m) has been done. The estimated times are computer time on the supercomputer ORIGON 2000 in Bergen.

Table 5.1 Climate model scenarios for use in acoustic modelling

Scenario	TAP A	TAP-B	Fram Strait	
Anthropogenic (1) (CO2)	Estimated time 2.5 monthx2	OK	OK	Received June 2000
Control Run	Estimated time 2.5 monthx2	3 weeksx2	OK	Received June 2000
Anthropogenic (2) (NEWCO2)	Estimated time 2.5 monthx2	3 weeksx2	OK	Received late October 2000
New Control	Estimated time 2.5 monthx2	3 weeksx2	OK	Received late October 2000

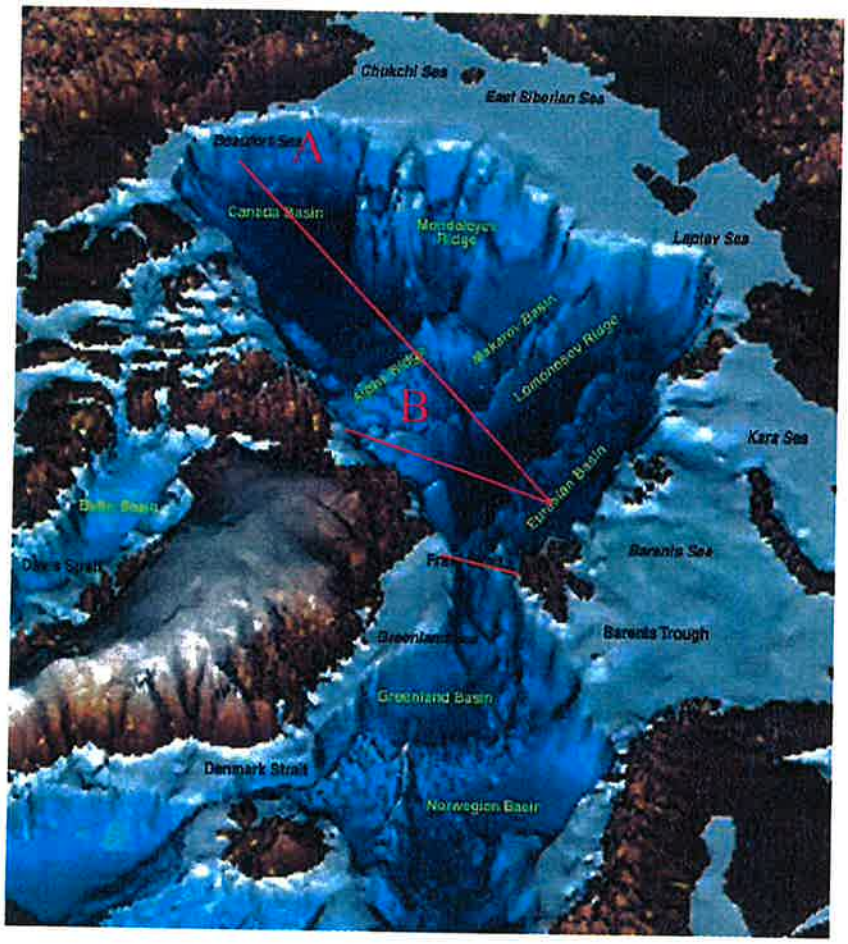

Figure 5.1. Bathymertic map of the Arctic Basin. The three selected acoustic tracks considered within AMOC. A: TAP-A, B: TAP-B and the third is the Fram Strait track along the 79 N.

TAP B simulations

The oceanographic fields

In Fig. 5.2 the averaged temperature along the TAP-B track (700 km) has been plotted as function of time. The upper panel shows the result from the control run and the lower panel shows the result from the anthophynic scenario. Comparing the Anthropongenic run with the control run it is seen that untill 2010 the development is very similar, but after 2010 the ocean becomes cooler in the control run while it becomes warmer in the Anthropogenic run. Considering the Anthropogenic run the watermasses from 200 m down to 1500m the temperature rises with 2.5 ^{0}C from the 1980s to the 2050 in the, while no strong changes in the salinity is observed, besides that less saline water penetrates deeper down as the time goes. Relatively large interannual variability in temperature can be observed in the upper 200-300 m and deeper water masses.

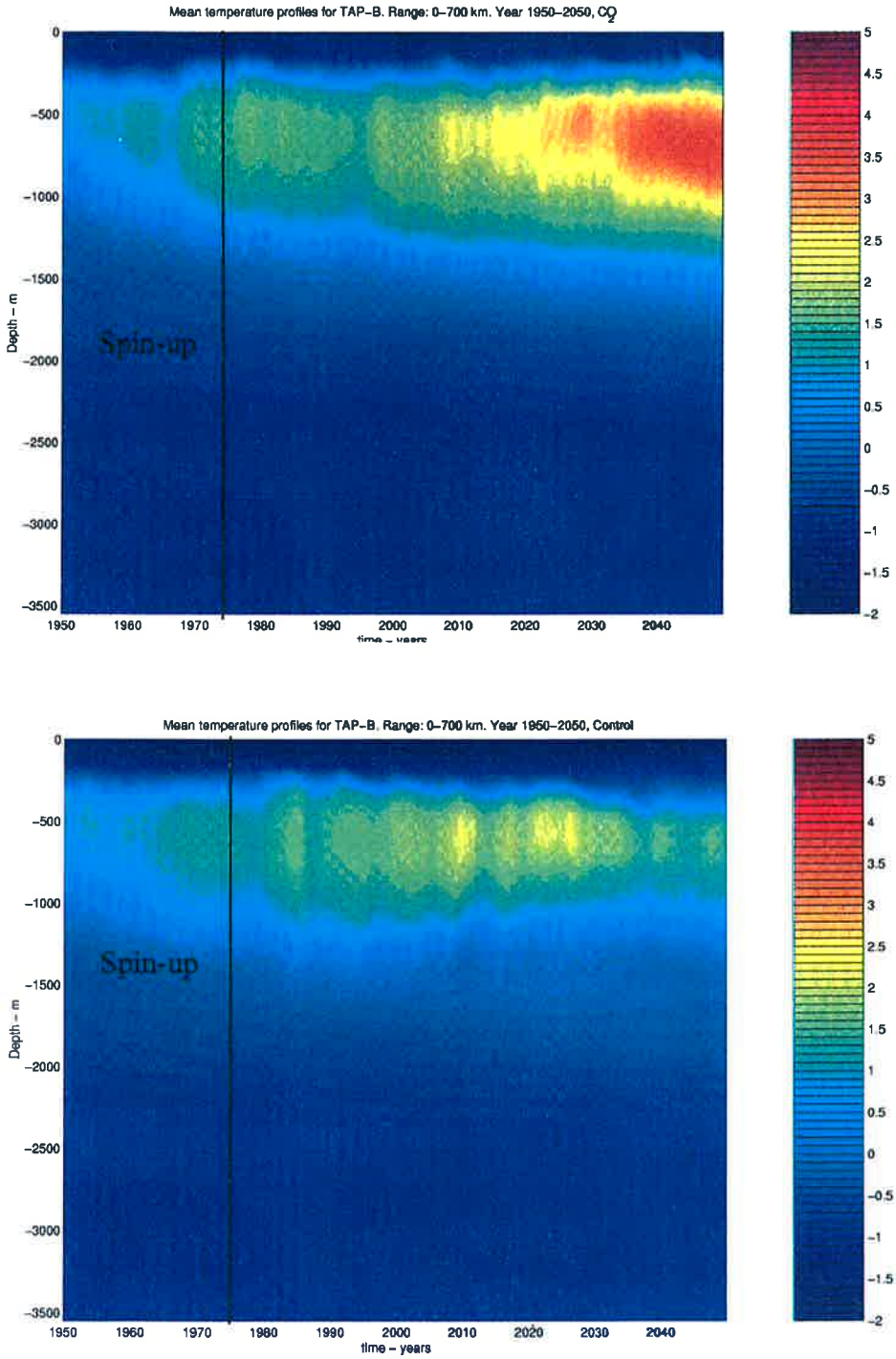

Figure 5.2 Climate model result for Anthropogenic (upper) and control run (lower) graph.

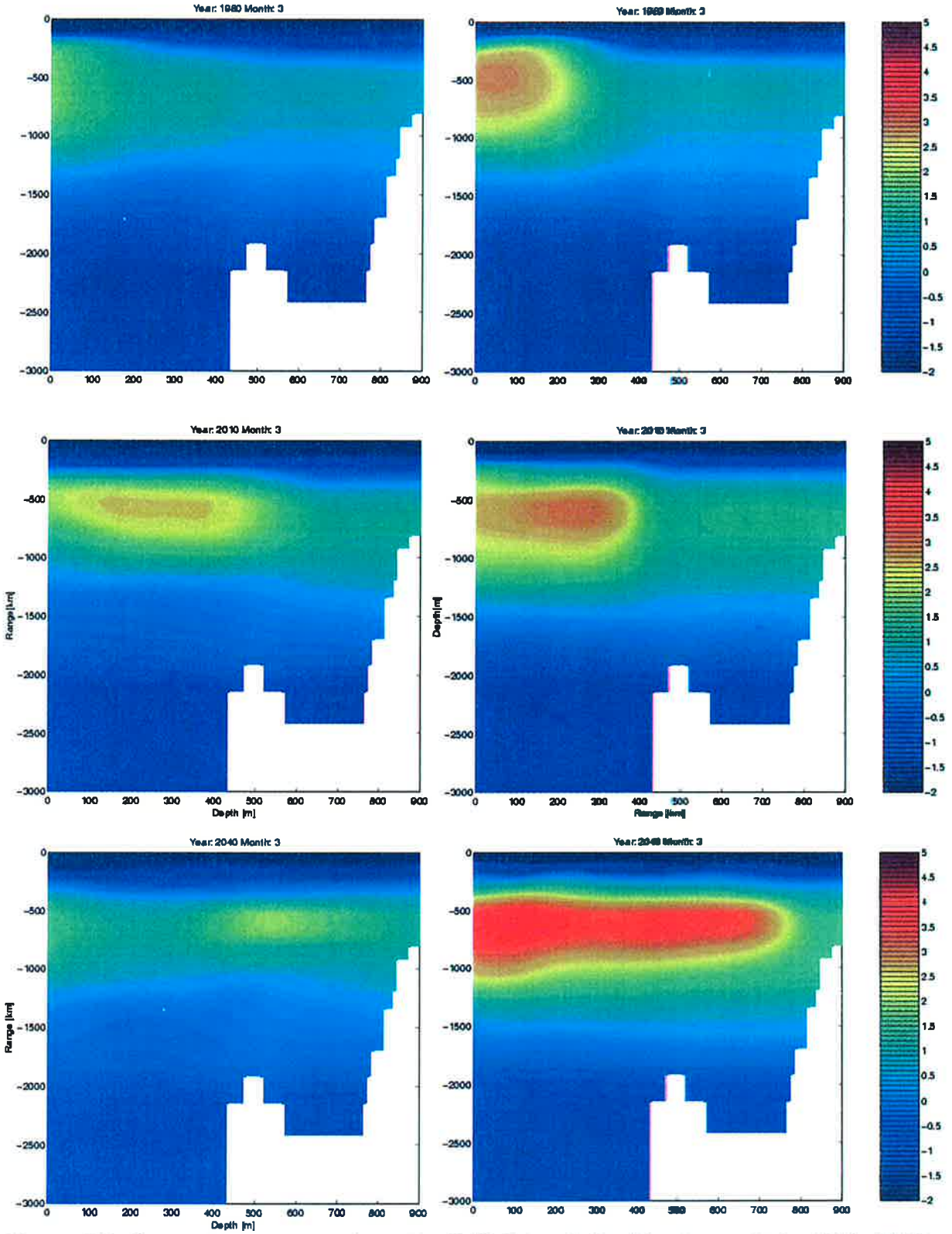

Figure 5.3. Ocean temperature along the TAP-B track for March month in 1980, 2010, and 2040.Control run (1) to the left and antrphenic (1) to the right.

Seasonal effects are not significant in temperature, while seasonal effects can be observed in the salinity in the upper 100m.

In Figure 5.3 the temperature as function of depth and range is plotted for TAP B for March month for selected years 1980, 2010 and 2040. It clearly illustrates the difference between the control run and the anthropenic run. Furthermore it is seen that by positioning the receiver 700-km from the source the climate signal is covered.

The second anthropenic run and corresponding control run, Fig. 5.4, shows a less pronounced but earlier warming in the water masses from 200m down to 1500 m. The most significant warming (roughly 1 degree) takes place between the 1980 and 2010, after this period the situation is more or less stable with some strong decadal changes. Comparing with the Control run the anthropenic run is upto a 0.5 degree warmer and the decadal variations are stronger including some enhanced events in 2010 and around 2030. As in the previous scenario the salinity situation is fairly stable.

As seen in Table 5.1 only one scenario, the first Anthropogenic, has been used as input to the acoustic model for TAP B. Although the salinity forcing fields for this scenario was wrong for this scenario some important results regarding the acoustic monitoring system can be obtained.

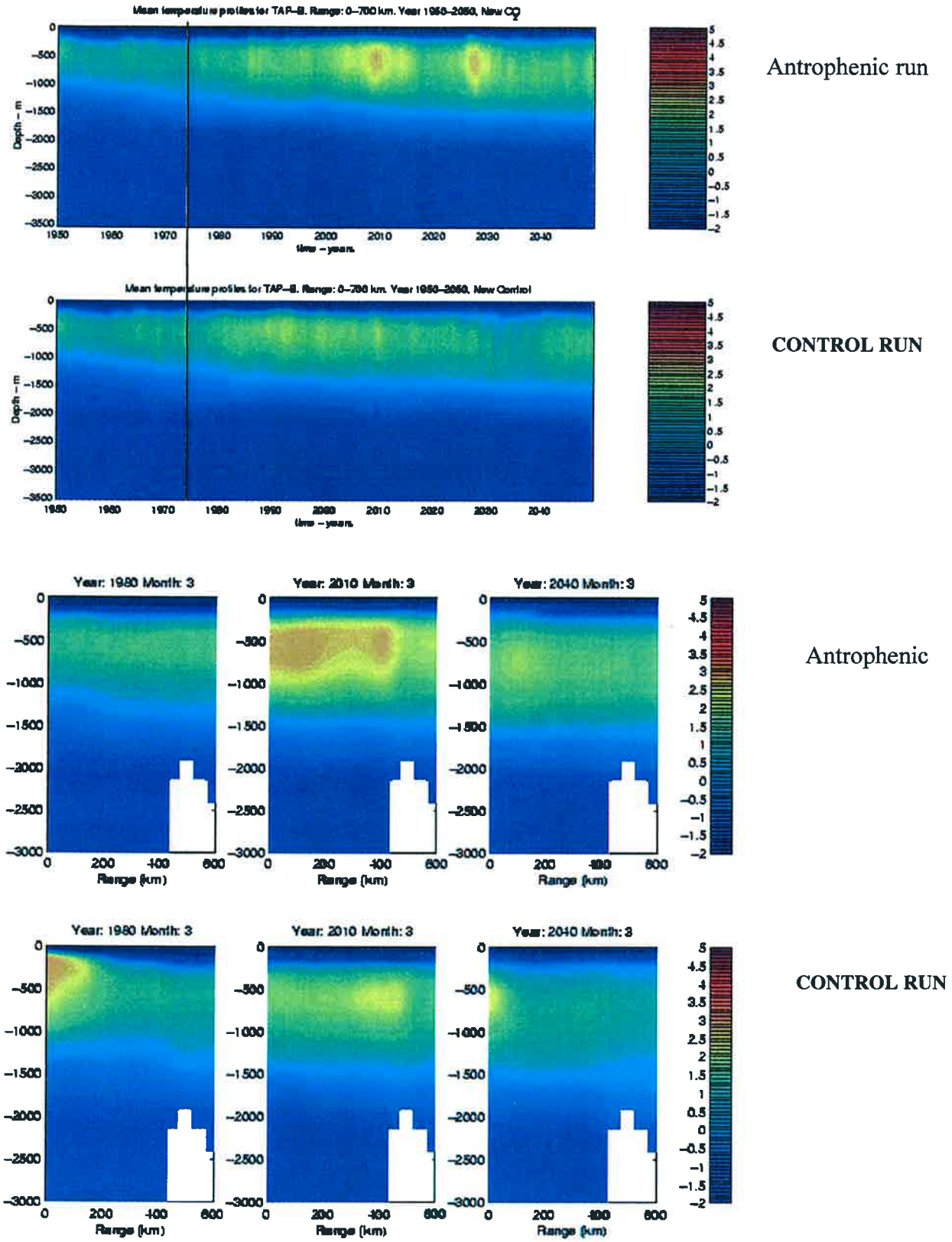

Figure 5.2. Climate modelling results from the second Antrhophenci run and control run.

The acoustic experiment

In order to avoid bottom interaction along the TAP-B track the receivers were moved away from the shelf with water depth 500 m to an area with deeper water. This gives a shorter track, 700 km long and a minimum water depth of around 2000 m. By using this track the climate signal will be mapped by rays penetrating watermasses down to around 1500 m or by the lowest acoustic modes (1-5) excited from a low frequency source (20 Hz). This part of the acoustic field will propagate without interaction with the ocean floor. According to earlier results reported in this manuscript a deep source at 500 m will provide the better information about the intermediate water masses than a shallow source (60 m). Therefore a deep source is first considered at 500 m, and then we consider a source depth of 60 m to investigate the potential of the source receiver configuration used in the experiment

Deep source

In Fig. 5.5 the travel time for each eigen ray found for SD 500 m and RD 50m and 500m is plotted against time. The calculations show the following:

- fewer eigenrays are found at the shallow receiver
- two main families of rays are seen; the first arrivals and the late arrivals. The first arrivals correspond to eigenrays that penetrates down to 1500-1700. The late arrivals correspond to the trapped rays in the upper 200-300 m.
- the first arrivals at both receivers are stable to seasonal and interannual changes but show a decreasing travel time (4.5 s) with time. The mean temperature in the water masses from 200-1500 m increased by about 2.5° C from 1980s till 2050 while the travel time decreases with 4.5 s.
- The late arrivals at all receivers show no seasonal variation, but a distinct and large decadal variation. The climate change does not appear as a signal in the late arrivals. Relatively strong changes were observed between decades and if these changes are interpreted as climate changes this may cause an overestimated climate response.

In Fig. 5.6 the arrival times are related to the mean temperature calculated for different water masses along the 700-km long track. It is observed that the first arrival (minimum travel time) is decreasing while the mean temperature for 200-1500 m and 0-1500 m increases. This corresponds to a negative correlation factor. In Table 2 the first arrival, last arrival and mean arrival at each receiver has been correlated with mean temperature in the 0-200m, 200-1500 and 0-1500. The correlation gave a negative correlation factor around 0.7 at the deepest receiver between the first arrival and the mean temperature calculated for water masses between 200-1500 m for the 700-km long track. At the shallower receivers the correlation was still negative but decreasing in value. A better correlation than 0.7 would have been received if the bunch of first arrivals were averaged before correlation or if a regression analysis was performed on these early arrivals. The results also suggest that another interesting parameter to study is the separation time between the first arrivals and the late arrivals.

Shallow source

In Fig. 5.7 the travel time for each eigenray found for SD 60 m and RD: 50m and 500m is plotted against time. The calculations shows the following:

- the strongest part of the signal are due to the rays which are trapped in the surface duct only a few rays penetrates deeper part of the ocean and these rays are very unstable from month to month.
- It is observed in Fig. 5.4 that the number of deeper going rays are reduced with time and that the arrivals becomes steadily later as the temperature increases in the watermasses between 200-1500 m. This is reflected in the correlation between arrival times and mean temperature in the 0-200m, 200-1500 and 0-1500 which was positive and relatively low at all receivers (Table 5.2). This is caused by a strengthing of the vertical temperature gradient as the temperature increases in the watermasses below the surface duct while the temperature in the duct is constant with time. This gives causes an acoustic intensification within the duct. On the otherhand the acoustic signal contains increasingly less information about the temperature below the duct.
-

According to the above observations we conclude that there is no climate signal present at any of the receivers in the case of a shallow source. In the ongoing Russian/American ACOUS experiment a source depth of 60 m has been used, and according to our results this experiment does not contain optimal information about the changes in the AIW. The changes observed by this system are generally found to be related to decadal ocsillations in the upper water masses (0-500 m).

Our conclusion is:

By positioning the acoustic source at 500 m and the receiver array 700 km the climate change occurring in the water masses between 200 and 1500 m (Figure 5.2) is easily detected. A source positioned at 60 m will not provide this information.

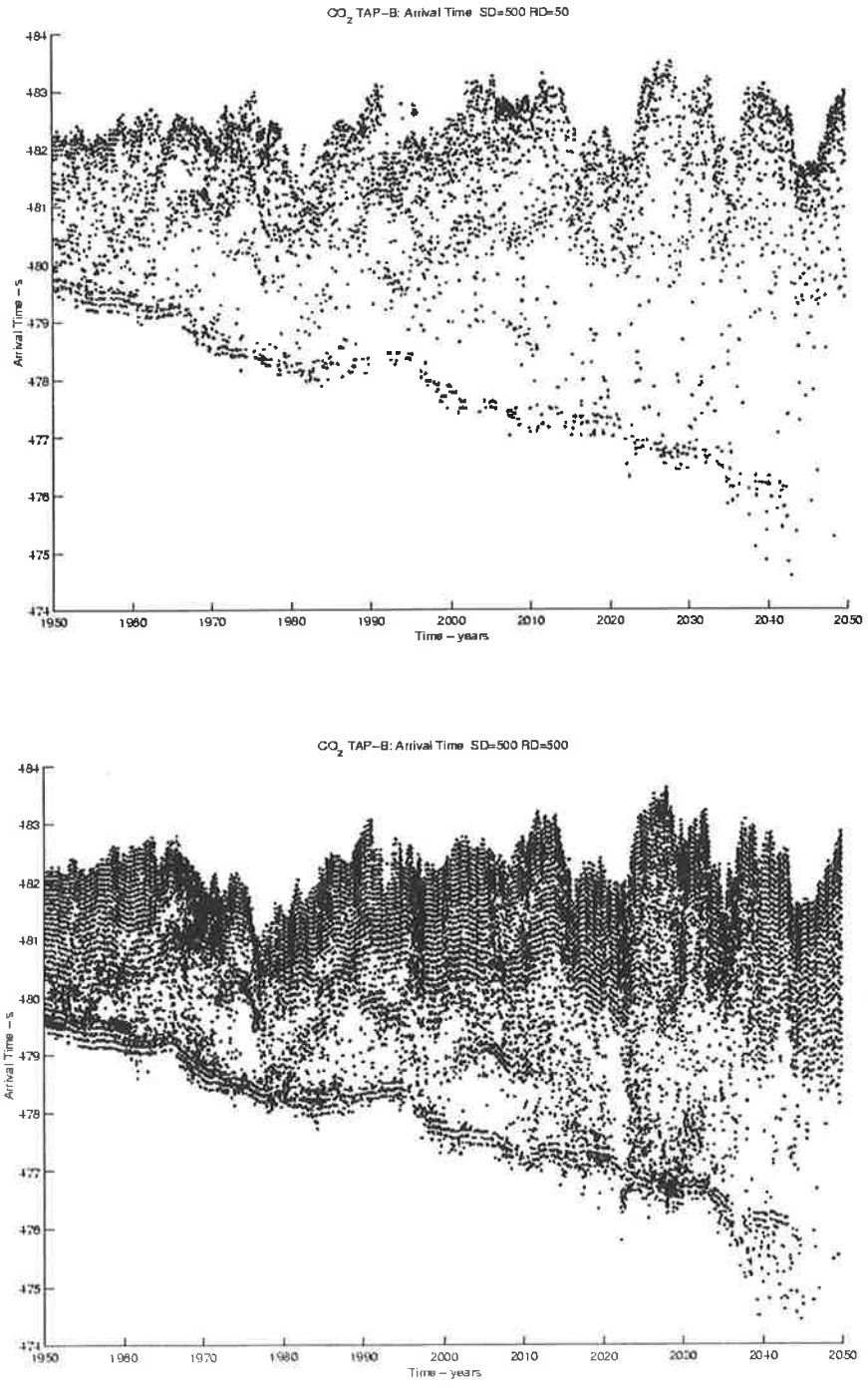

Figure 5.5 Scenario: Anthropogenic (1). Acoustic track:TAP-B. Travel time for each eigenray found for the source depth 500 m and receiver depth 50m (upper) and 500 m (lower) as function of time.

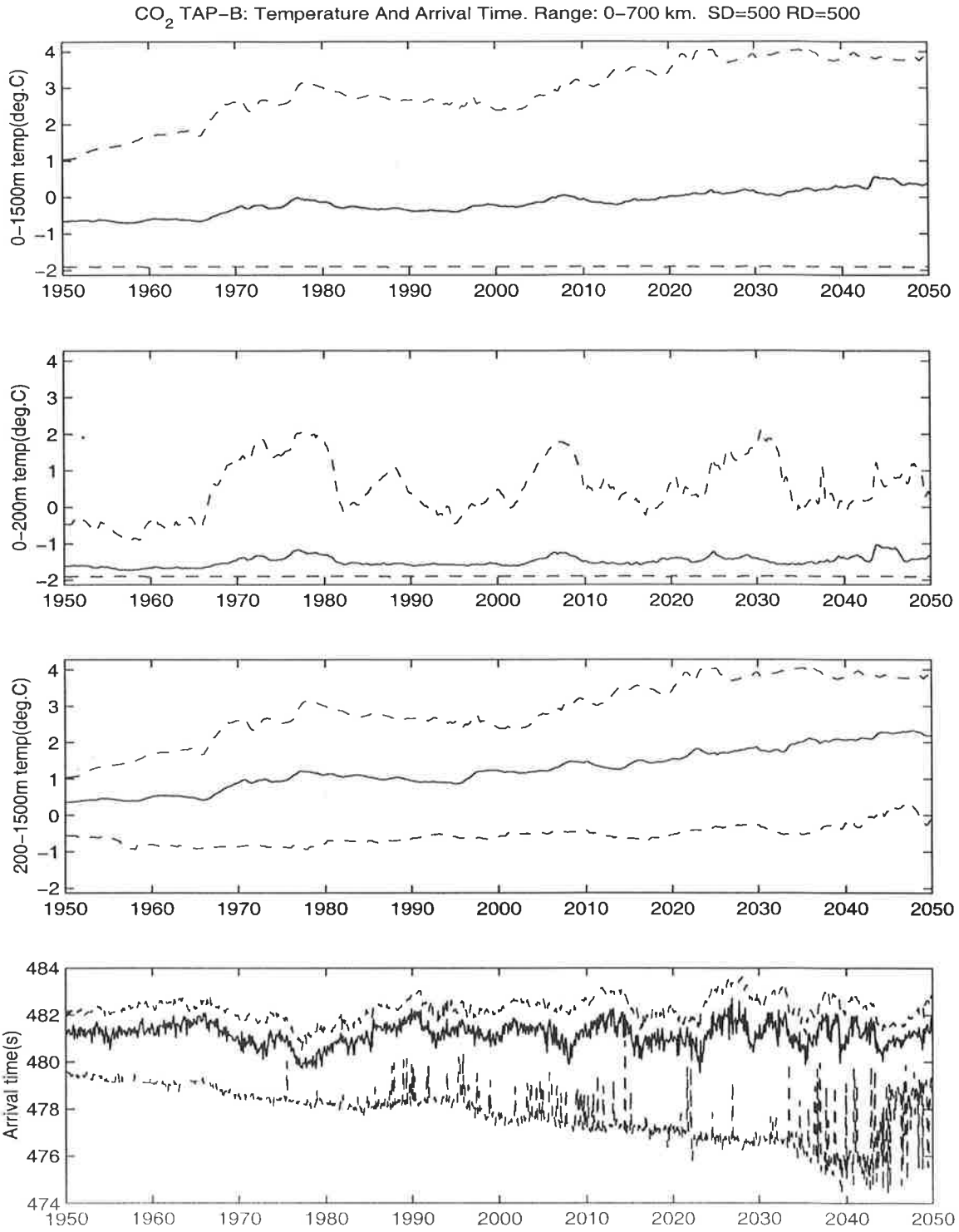

Figure 5.6 Scenario: Anthropogenic (1). Acoustic track:TAP-B. Min, Max and Mean temperature for different water masses along the 700 km long track is plotted against time. The lowest plot show the first, last and mean travel time plotted against time. Source depth is 500 m and receiver depth and 500 m.

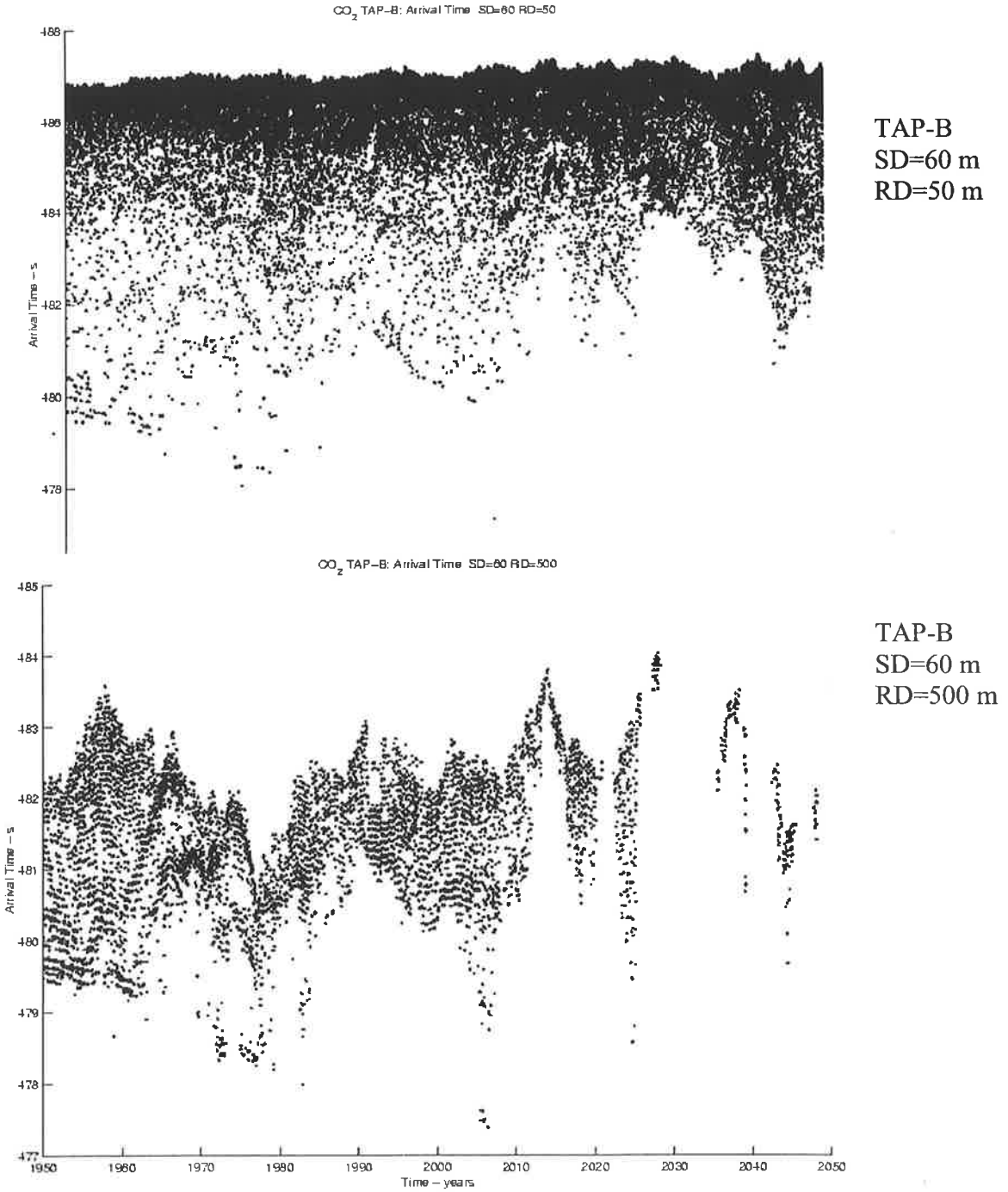

Figure 5.7 Scenario: Anthropogenic (1). Acoustic track:TAP-B. Travel time for each eigenray found for the source depth 60 m and receiver depth 50m (upper) and 500 m (lower) as function of time.

Table 5.2 Correlation matrix for TAP-B anthropogenic run for shallow (upper table) and deep (lower table) source

Correlation coefficients for arrival time vs. temperature - TAP-B

SD=60m Time=1950-2050 Scenario=CO2 Range=0-700km

Arrival Time		Temp 0-200m			Temp 200-1500m			Temp 0-1500m		
		Min	Max	Mean	Min	Max	Mean	Min	Max	Mean
	Min	-0,0582	0,1297	0,0366	0,2351	0,4559	0,3890	-0,0582	0,4559	0,3389
	Max	-0,0715	0,3881	0,4488	0,5162	0,7275	0,6458	-0,0715	0,7275	0,6493
50m	Mean	-0,0947	0,2777	0,0934	0,2799	0,5593	0,4490	-0,0947	0,5593	0,4026
	Min	-0,0872	0,1674	0,0826	0,3331	0,5735	0,5006	-0,0872	0,5735	0,4440
	Max	-0,1050	0,3466	0,3034	0,4019	0,6592	0,5549	-0,1050	0,6592	0,5395
100m	Mean	-0,1470	0,0808	-0,4047	-0,1328	0,1197	0,0063	-0,1470	0,1197	-0,0851
	Min	-0,1068	0,1913	0,1249	0,4255	0,6843	0,6205	-0,1068	0,6843	0,5554
	Max	-0,0467	-0,3677	-0,8203	-0,3991	-0,2327	-0,3187	-0,0467	-0,2327	-0,4542
200m	Mean	0,0334	-0,3881	-0,7477	-0,4287	-0,1354	-0,2703	0,0334	-0,1354	-0,3968
	Min	-0,1170	0,1838	0,1377	0,4796	0,7121	0,6547	-0,1170	0,7121	0,5874
	Max	0,0116	-0,7386	-0,7741	-0,1887	-0,1827	-0,2254	0,0116	-0,1827	-0,3647
300m	Mean	-0,0546	-0,3534	-0,4224	0,1209	0,2967	0,2052	-0,0546	0,2967	0,0801
	Min	-0,1185	0,1759	0,1258	0,4903	0,7279	0,6705	-0,1185	0,7279	0,5981
	Max	-0,0645	-0,5135	-0,5265	0,0613	0,0223	-0,0024	-0,0645	0,0223	-0,1197
400m	Mean	-0,1093	-0,0649	-0,1169	0,3744	0,5635	0,4988	-0,1093	0,5635	0,3979
	Min	-0,1213	0,1633	0,0324	0,4153	0,6705	0,5880	-0,1213	0,6705	0,5071
	Max	-0,0631	-0,2254	-0,4098	0,1060	0,1986	0,1352	-0,0631	0,1986	0,0233
500m	Mean	-0,1015	0,0334	-0,1300	0,3191	0,5546	0,4711	-0,1015	0,5546	0,3714

Correlation coefficients for arrival time vs. temperature - TAP-B

SD=500m Time=1950-2050 Scenario=CO2 Range=0-700km

Arrival Time		Temp 0-200m			Temp 200-1500m			Temp 0-1500m		
		Min	Max	Mean	Min	Max	Mean	Min	Max	Mean
	Min	-0,0339	-0,0222	-0,0423	0,0160	-0,0648	-0,0537	-0,0339	-0,0648	-0,0551
	Max	-0,0370	0,1149	0,0148	0,0306	-0,0344	-0,0156	-0,0370	-0,0344	-0,0099
50m	Mean	-0,0348	0,0928	0,0530	0,0786	0,0033	0,0254	-0,0348	0,0033	0,0335
	Min	0,0056	-0,1353	-0,0942	0,0114	-0,1571	-0,1124	0,0056	-0,1571	-0,1166
	Max	-0,0068	0,1748	0,0048	0,0215	-0,0007	0,0000	-0,0068	-0,0007	0,0011
100m	Mean	-0,0033	0,0681	0,0622	0,1308	0,0159	0,0622	-0,0033	0,0159	0,0668
	Min	-0,0196	-0,1976	-0,2243	-0,1688	-0,3889	-0,3529	-0,0196	-0,3889	-0,3501
	Max	-0,0533	0,2222	0,0073	0,0609	0,0527	0,0465	-0,0533	0,0527	0,0412
200m	Mean	-0,0533	0,0969	0,0356	0,1132	-0,0007	0,0431	-0,0533	-0,0007	0,0446
	Min	0,0199	-0,2438	-0,2742	-0,3159	-0,5461	-0,5149	0,0199	-0,5461	-0,4990
	Max	-0,0471	0,2337	-0,0090	0,0586	0,0696	0,0518	-0,0471	0,0696	0,0421
300m	Mean	-0,0037	0,0961	0,0134	0,0649	-0,0465	0,0024	-0,0037	-0,0465	0,0050
	Min	0,0130	-0,2617	-0,3093	-0,3252	-0,6239	-0,5714	0,0130	-0,6239	-0,5549
	Max	-0,0494	0,2322	-0,0191	0,0545	0,0725	0,0509	-0,0494	0,0725	0,0390
400m	Mean	-0,0143	0,1663	0,0227	0,0513	-0,0618	-0,0168	-0,0143	-0,0618	-0,0092
	Min	0,0193	-0,2571	-0,3595	-0,4595	-0,7304	-0,7072	0,0193	-0,7304	-0,6815
	Max	-0,0944	-0,1202	-0,3303	0,1426	0,0681	0,0379	-0,0944	0,0681	-0,0416
500m	Mean	-0,0846	-0,2948	-0,4616	0,0333	-0,1506	-0,1491	-0,0846	-0,1506	-0,2300

5.2 FRAM STRAIT RESULTS

Oceanographic fields.

In the Fram strait the warm water is entering the Arctic Basin on the eastern side while the cold water is exiting the basin on the western side of the strait. The temperature cross section along 79 N in the Fram Strait is plotted for various scenarios in Fig. 5.8 – 5.11. The climate signal is strongest in the first scenario, in both cases the warming is seen as warm water propagate westward from the eastern continental break of the Fram strait. In 2040 the warmer water dominates from 250 m and down to 1000 meter except on the Greenland continental shelf. It is also seen a significant warming of the surface water in March month from the middle of the Fram strait to the Svalbard side.

In this study a 200 km long section (from 300 km to 500 km) is selected for the acoustic experiment in order to monitor the changes in the inflow along the coast of Svalbard. The mean vertical profile for the watermasses between 300 and 500 km is calculated for each month in the 100 year long simulation, and presented for the first and second simulation in Fig. 5.10 and Fig. 5.11, respectively. As above the strongest climate signal is observed in the first scenario and the difference between the antrophenic run and the control run is very clear. The warming is 2-2.5 ^{0}C from 1980 to 2050 in the first antropenic run while it is 0.5 to 1.0 ^{0}C for the control run. The second scenario shows a 1 degree increase in the antrophenic run and no significant increase in the control run. In both scenarios the warming signal is observed in the water masses above 1500 m and up to the surface, and in general the warming is strongest from 2000 to 2030. The seasonal effects are very clear in both simulations including the control runs.

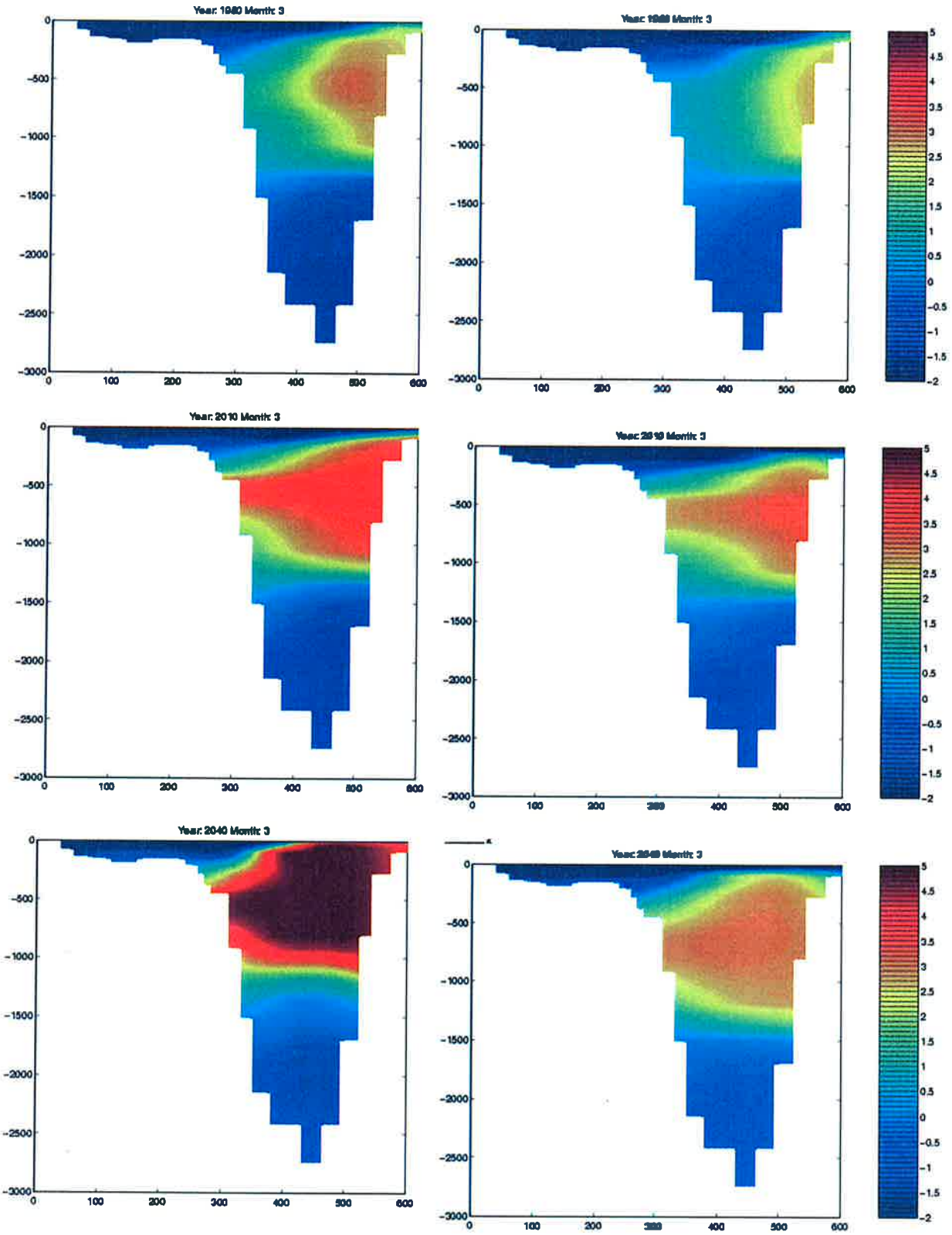

Figure 5.8 Temperature plotted as function of range for March month for the years 1980, 2010, 2040 plot along 79 N in the Fram strait. The Antropenic (1) run to the left and the control run to the right.

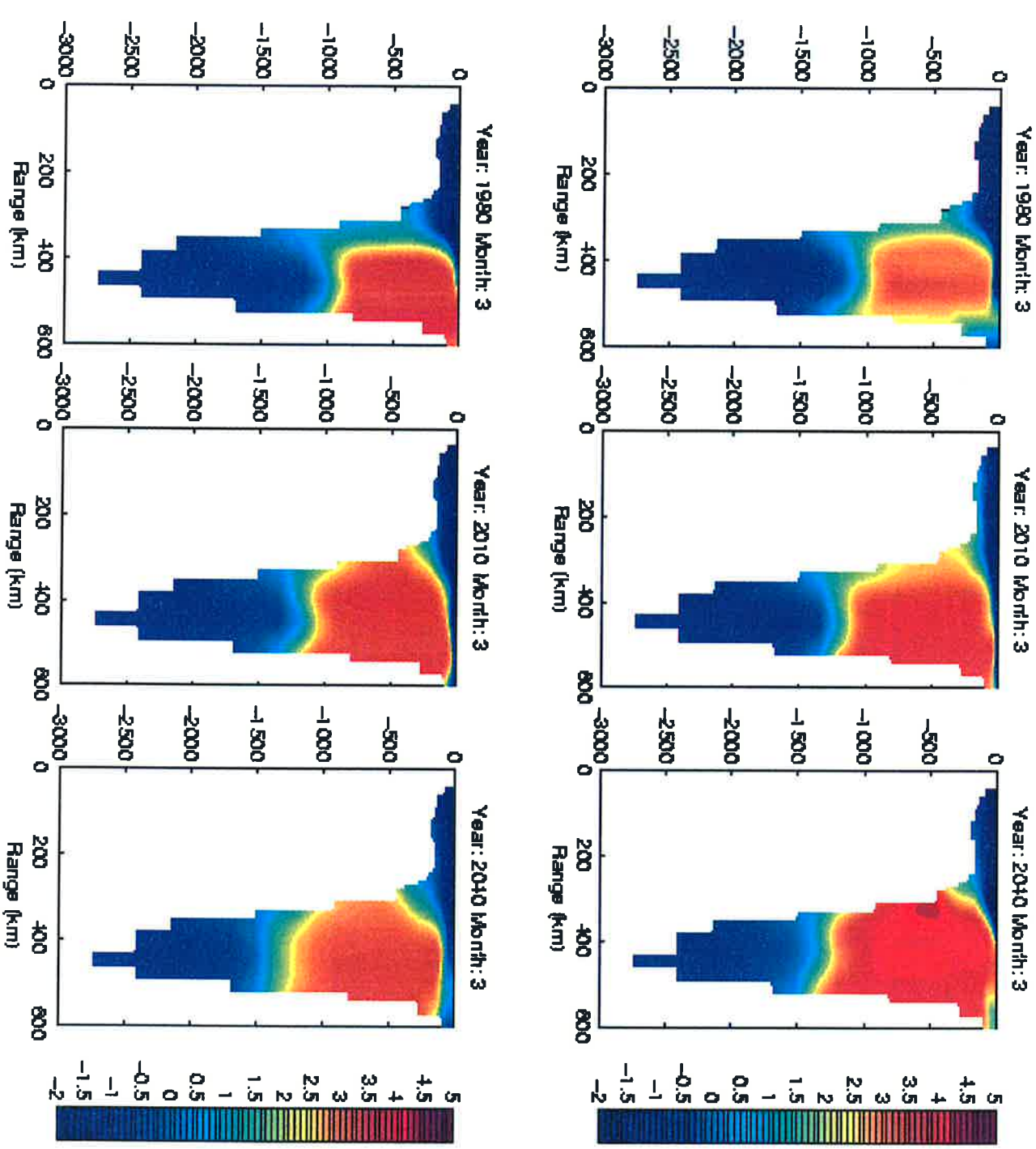

Figure 5.9 Temperature plotted as function of range for March month for the years 1980, 2010, 2040 plot along 79 N in the Fram strait. The Antropenic (2) run to the right and the control run to the left.

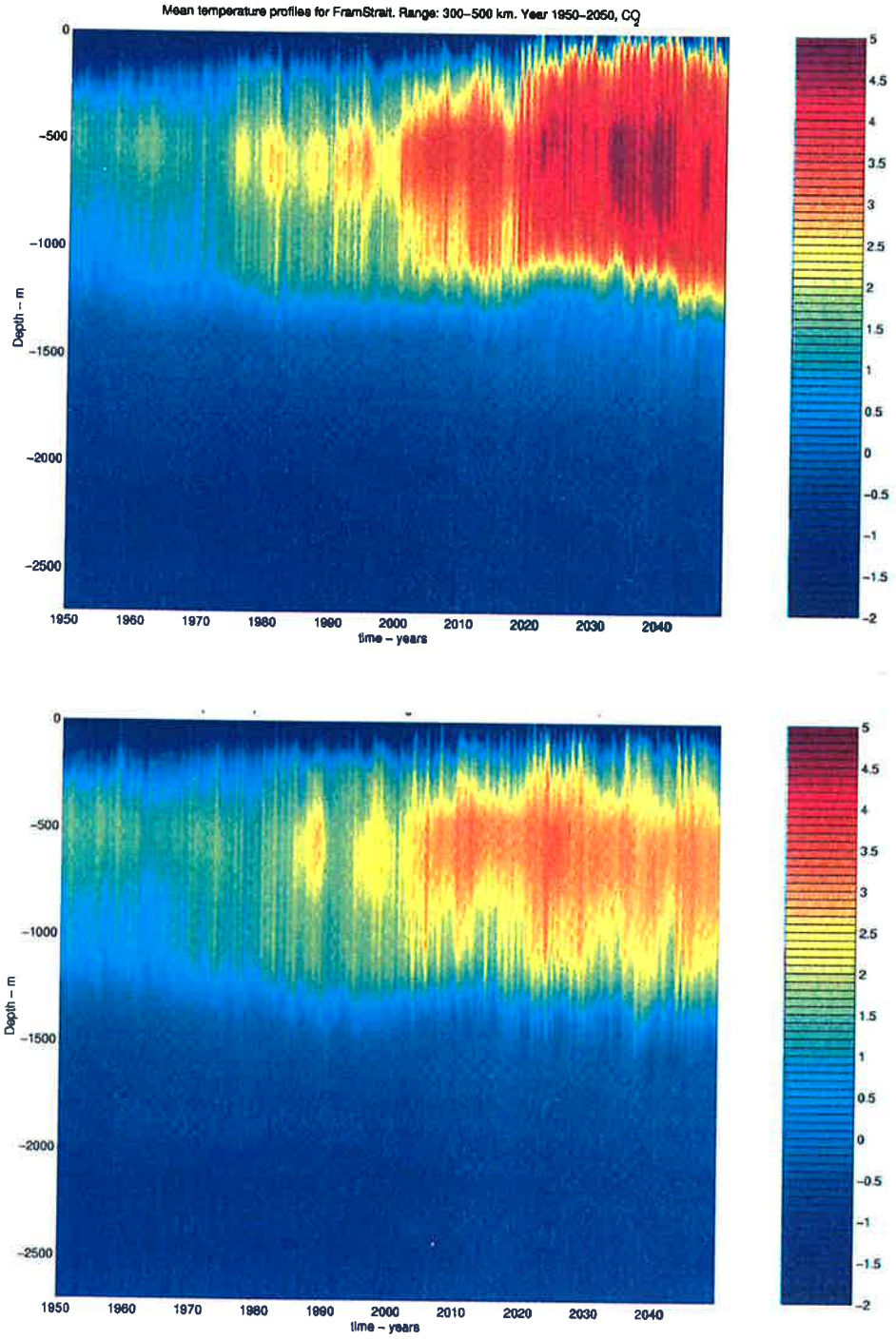

Figure 5.10. Fram Strait: Climate modelling result from the first Anthrophenic (1) run in the upper plot and corresponding control run (1) in the lower plot.

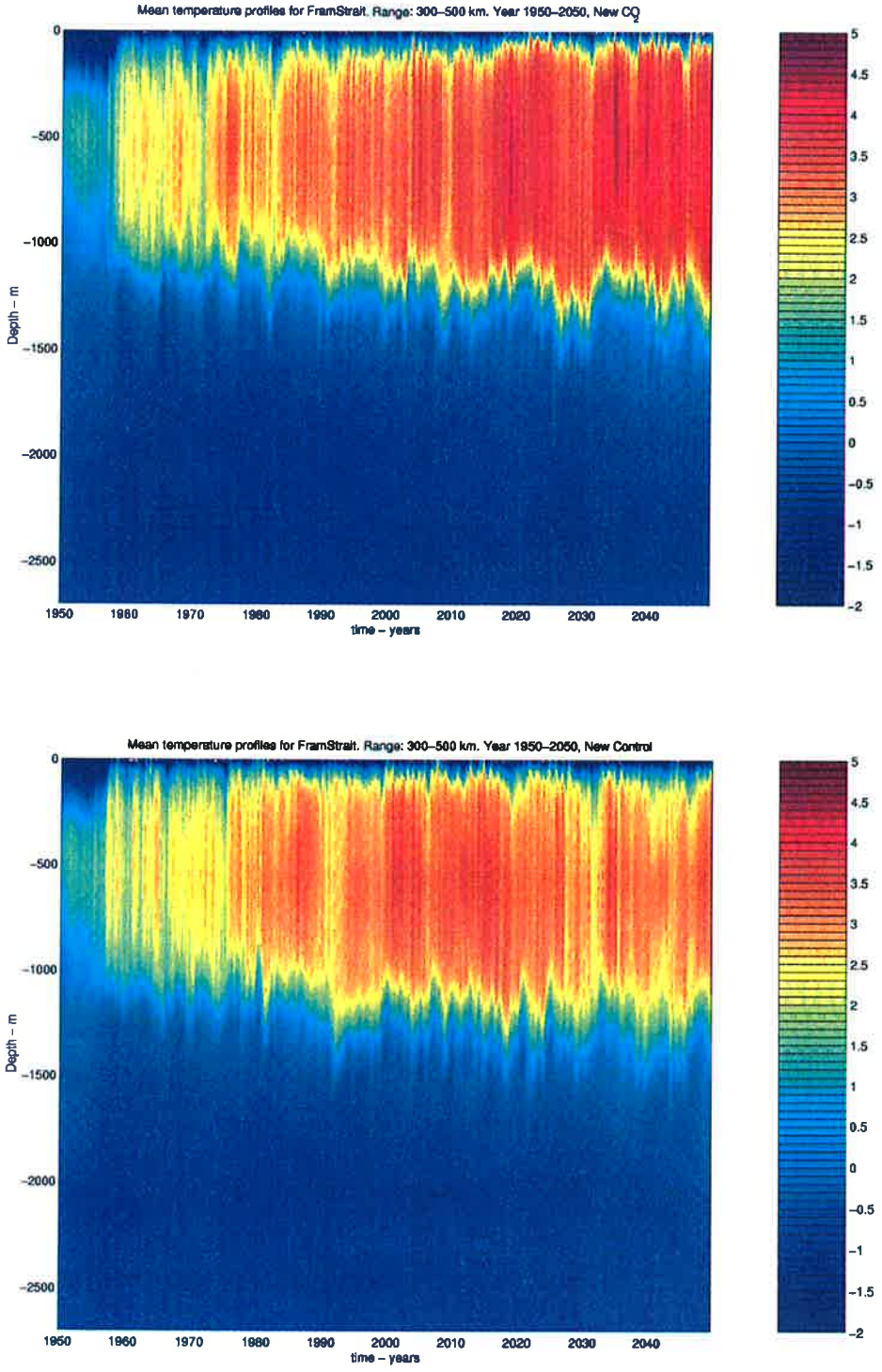

Figure 5.11 Fram Strait: Climate modelling result from the first Anthrophenic (2) run in the upper plot and corresponding control run (2) in the lower plot.

The acoustic experiments

As for the TAP-B track the source and receiver array is located in deep water areas. The acoustic track is 200 km long covering the eastern part of the strait. The source is loacted at 300 km and the receiver at 500 km. In the acoustic simulations two source depths are selected 60 m and 500 m. A vertical array with receivers at 50, 100, 200, 300, 400 and 500 m are used. Both scenorios, including control ran and anthropenic runs, has been used as input to the acoustic model. The results of the simulations are presented in Figs. 5.12 – 5.17 as arrival time for each eigenray as function of time. For each source depth the results are plotted for receiver at 50 m and 500 m (results are also available for the other receivers). The first arrival, last arrival and the mean arrival is then correlated with mean temperature in 0-200 m, 200-1500 m and 0-1500 m,

Deep Source

In the case of a deep source Fig. 5.12 and 5.14 show that the arrivals obtained at the deep and shallow receiver is similar except that more arrivals are found for the deep receiver than for the shallow receiver. Some clear events occures in the travel time (marked with numbers in Fig. 5.12 and 5.14) these events corresponds to warming events observed in Fig. 5.9 and 5.10. The climate signal is clearly observed at both receivers. In the first scenario the travel time is gradually reduced with 1.85 s during the 100 years this is 0.019s pr year. In the second scenario the travel time is gradually reduced with 0.8 s which is 0.008s pr year. The results also show that the ray stability is poor, due to the seasonal variability. Table 3 and 4 show the correlation matrix of the timeseries of first, last and mean arrival times with the time series of max, min and mean temperature in the watermasses between 0-200 m, 200-1500m and 0-1500 m. The best correlation, between -0.8 and -0.95 are found between the mean arrival time and the mean temperature for watermasses (0-1500m) and (200-1500). This is found at all receivers. This result suggests that by averaging the arrivals it is possible to obtain a stable measure of the changes in the arrival times which is very closely related to the change of temperature in the watermasses.

Shallow source

In the case of a shallow source Fig. 5.15 and 5.17 show that the arrival time structure obtained at the deep and shallow receiver is different from each other. The deep receiver picks up the climate change structure as seen for the deep source. In the first scenario the shallow receiver picks up the warming signal after the warming signal also occures in the surface water after 2015. This is also seen in the second scenario but it is less pronounced. Also for a shallow source the ray stability is poor, due to the seasonal variability. Considering the correlation in Table 3 and 4 the correlation factors are similar to the deep source and in some cases even better.

Conclusion

Our result shows that both a deep and a shallow source will provide information about the mean temperature of the water masses. In the case of the shallow source the strong seasonal variability will mask the climate signal, except at the deeper receivers. The clearest climate is observed at all receivers by using a deep source as some of the seasonal effects has been filtered out by the ocean environment. By averaging the arrivals it is possible to obtain a stable measure of the changes in the arrival times which is very closely related to the change of temperature in the water masses. The monitoring of ocean temperature in the Fram Strait is possible. A deep source

gives the best results for long term monitoring of the climate, while the shallow source will provide information about the seaonal changes.

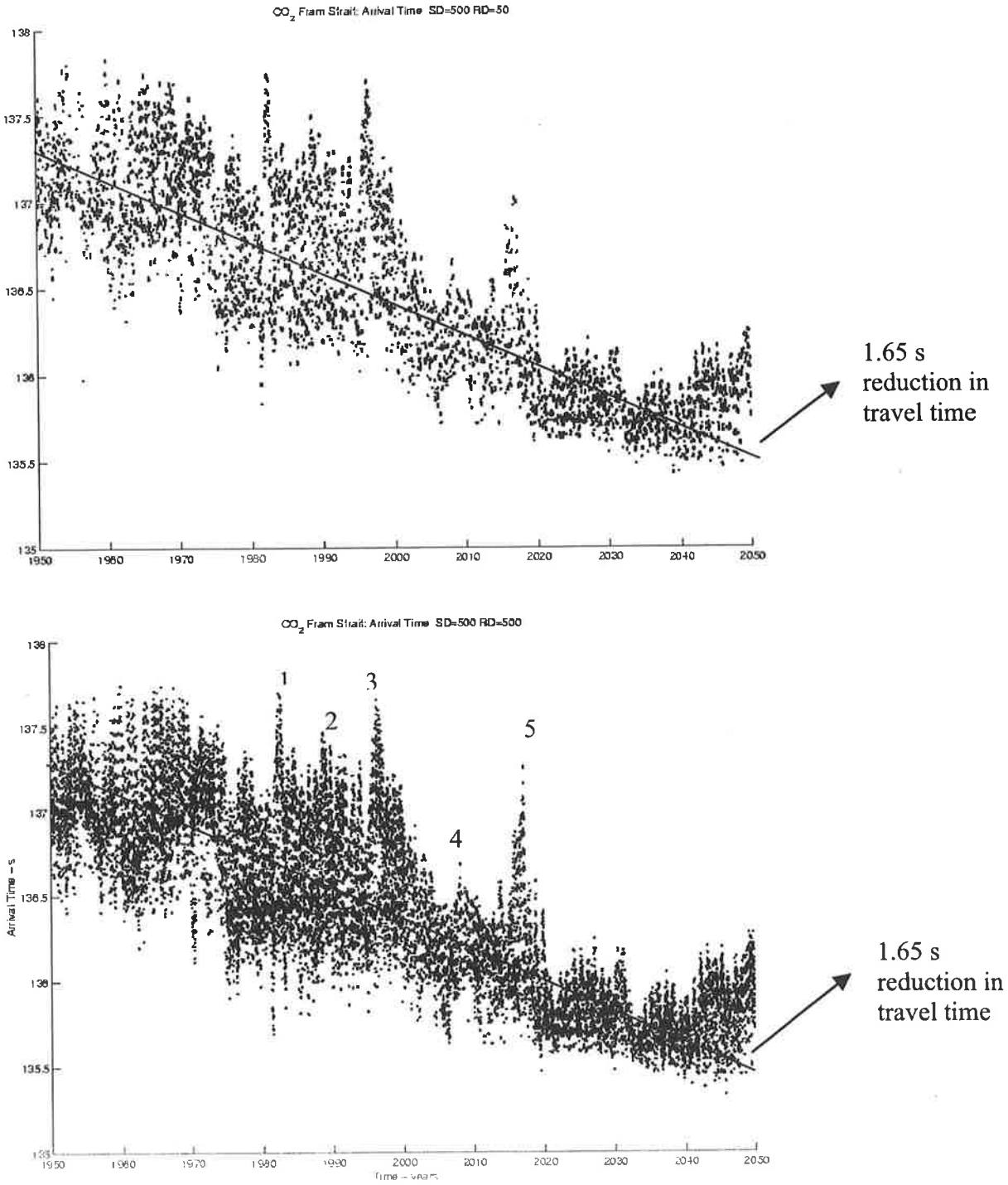

Figure 5.12 Antrophenic run (1). Source depth 500 m. Upper plot shows arrival times for eigenrays at at a receiver at 50 m and lower plot shows arrivals for the eigenrays at 500 m.

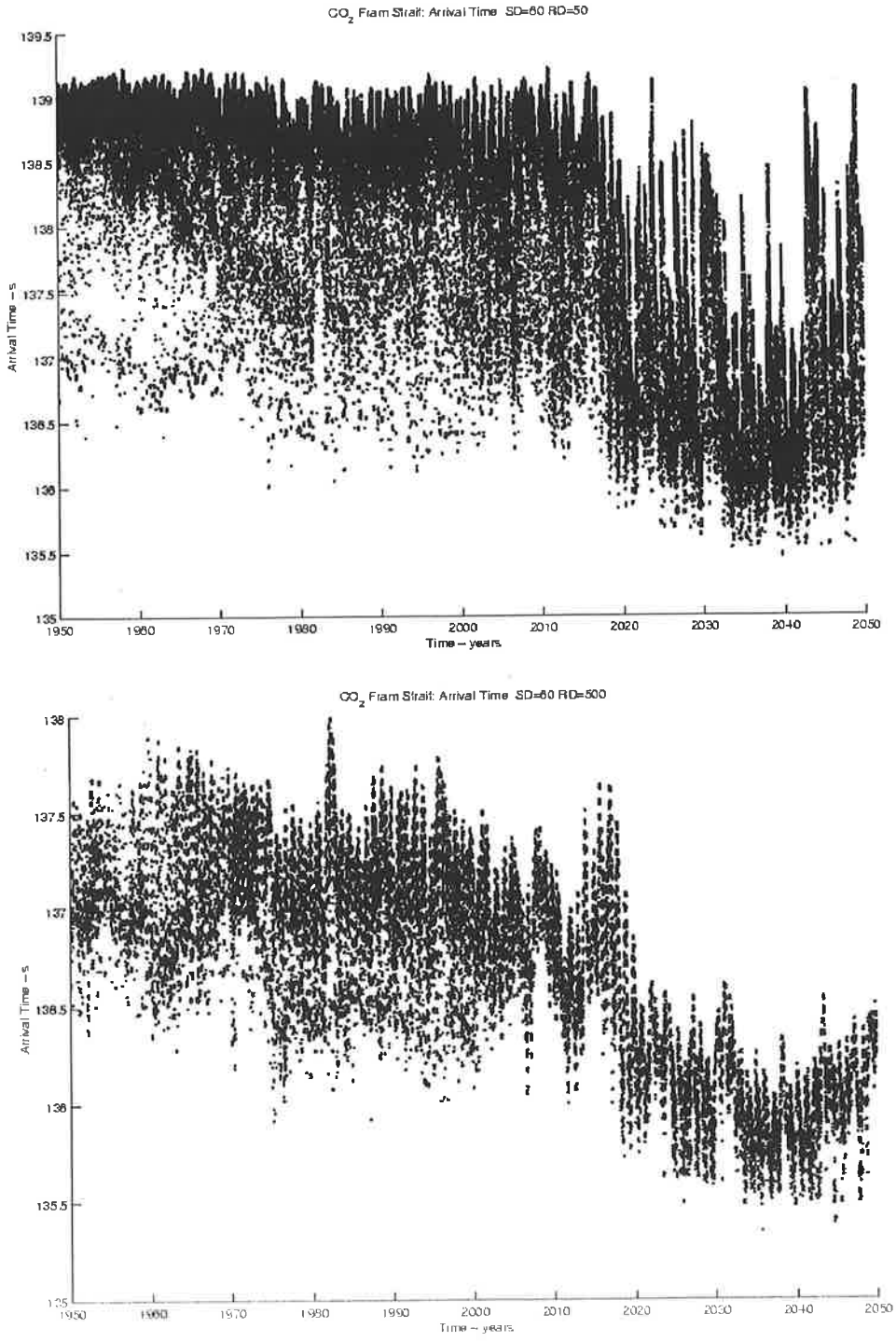

Figure 5.13 Antrophenic run (1). Source depth 60 m. Upper plot shows arrival times for eigenrays at at a receiver at 50 m and lower plot shows arrivals for the eigenrays at 500 m.

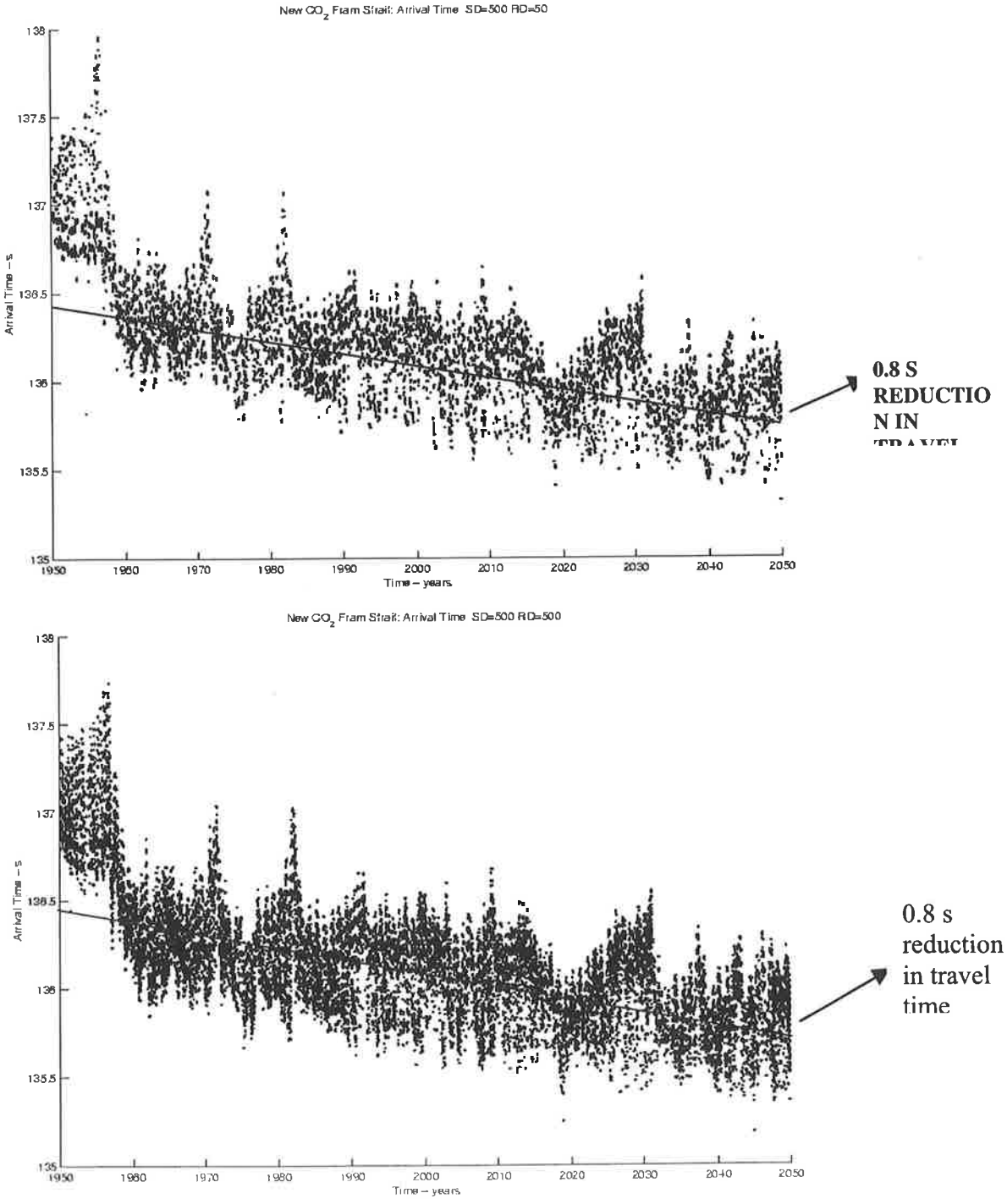

Figure 5.14 Antrophenic run (2). Source depth 500 m. Upper plot shows arrival times for eigenrays at at a receiver at 50 m and lower plot shows arrivals for the eigenrays at 500 m

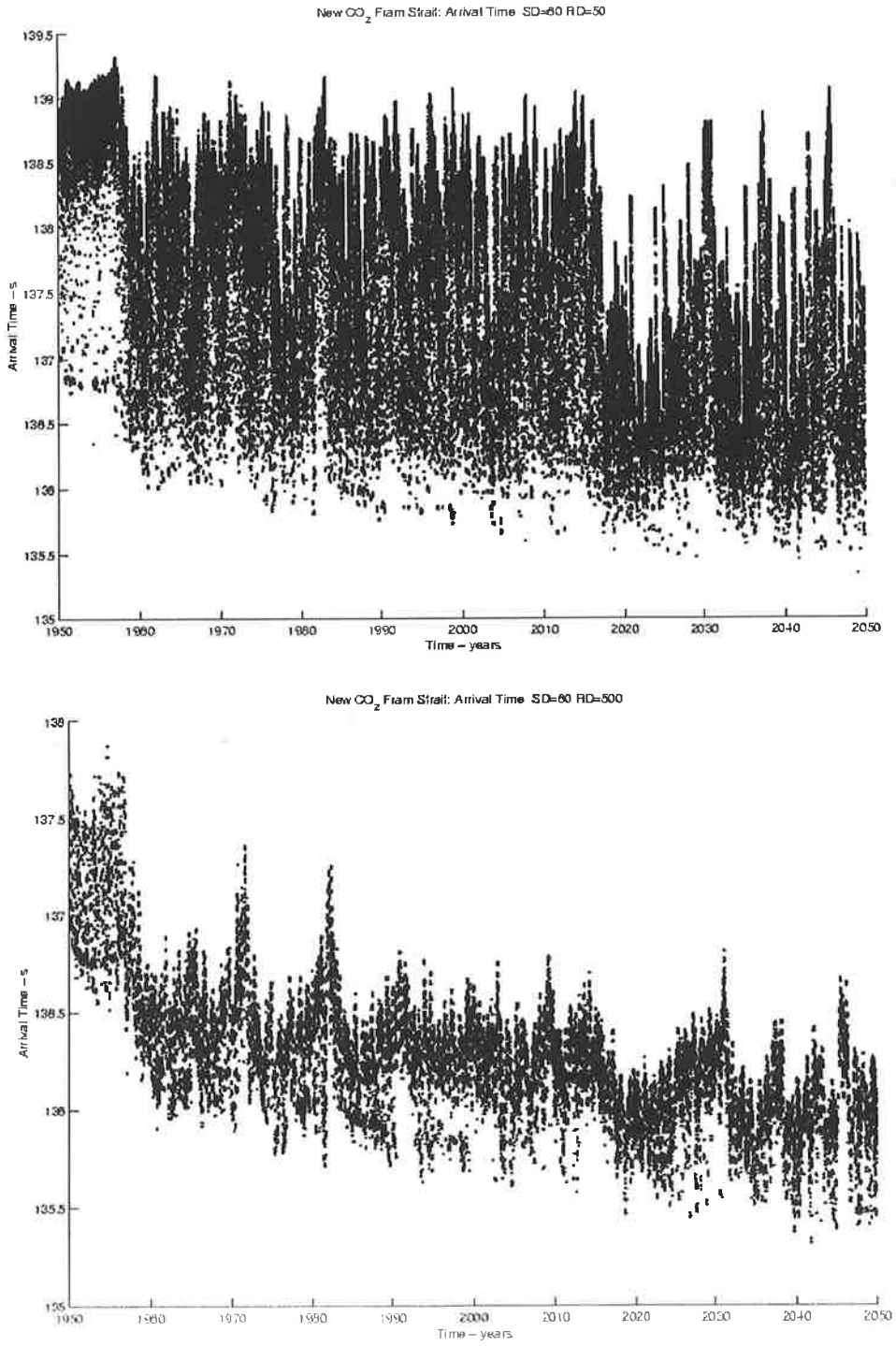

Figure 5.15 Antrophenic run (2). Source depth 500 m. Upper plot shows arrival times for eigenrays at at a receiver at 50 m and lower plot shows arrivals for the eigenrays at 500 m.

Table 3. Antrophenic run (1). Correlation between min, max, mean temperatures and first, last and mean arrivals.

Correlation coefficients for arrival time vs. temperature - Fram Strait

SD=500m Time=1950-2050 Scenario=CO2 Range=300-500km

Arrival Time		Temp 0-200m			Temp 200-1500m			Temp 0-1500m		
		Min	Max	Mean	Min	Max	Mean	Min	Max	Mean
	Min	0,1108	-0,8735	-0,8315	-0,8298	-0,8748	-0,9177	0,1108	-0,8477	-0,8863
	Max	0,0900	-0,8984	-0,8804	-0,8602	-0,9223	-0,9567	0,0900	-0,8957	-0,9323
50m	Mean	0,0981	-0,9012	-0,8744	-0,8596	-0,9227	-0,9563	0,0981	-0,8951	-0,9284
	Min	0,0982	-0,8831	-0,8329	-0,8443	-0,8845	-0,9290	0,0982	-0,8539	-0,8919
	Max	0,0927	-0,9074	-0,8902	-0,8642	-0,9271	-0,9637	0,0927	-0,9009	-0,9411
100m	Mean	0,0942	-0,9068	-0,8816	-0,8632	-0,9235	-0,9615	0,0942	-0,8966	-0,9350
	Min	0,0952	-0,8896	-0,8351	-0,8563	-0,8947	-0,9394	0,0952	-0,8613	-0,8976
	Max	0,0904	-0,9147	-0,8951	-0,8704	-0,9284	-0,9692	0,0904	-0,9020	-0,9464
200m	Mean	0,0923	-0,9133	-0,8863	-0,8700	-0,9313	-0,9695	0,0923	-0,9029	-0,9411
	Min	0,0957	-0,8922	-0,8347	-0,8630	-0,8982	-0,9428	0,0957	-0,8644	-0,8987
	Max	0,0896	-0,9223	-0,8982	-0,8730	-0,9314	-0,9733	0,0896	-0,9047	-0,9499
300m	Mean	0,0922	-0,9198	-0,8863	-0,8741	-0,9335	-0,9731	0,0922	-0,9048	-0,9427
	Min	0,0992	-0,8892	-0,8307	-0,8600	-0,8958	-0,9405	0,0992	-0,8613	-0,8954
	Max	0,0904	-0,9219	-0,8986	-0,8727	-0,9322	-0,9731	0,0904	-0,9055	-0,9501
400m	Mean	0,0959	-0,9208	-0,8862	-0,8769	-0,9340	-0,9748	0,0959	-0,9046	-0,9433
	Min	0,0961	-0,8897	-0,8272	-0,8601	-0,8905	-0,9383	0,0961	-0,8566	-0,8923
	Max	0,0900	-0,9194	-0,9036	-0,8748	-0,9334	-0,9742	0,0900	-0,9073	-0,9536
500m	Mean	0,0946	-0,9222	-0,8901	-0,8800	-0,9346	-0,9765	0,0946	-0,9060	-0,9464

Correlation coefficients for arrival time vs. temperature - Fram Strait

SD=60m Time=1950-2050 Scenario=CO2 Range=300-500km

Arrival Time		Temp 0-200m			Temp 200-1500m			Temp 0-1500m		
		Min	Max	Mean	Min	Max	Mean	Min	Max	Mean
	Min	0,0291	-0,7982	-0,8313	-0,6928	-0,7315	-0,7887	0,0291	-0,7380	-0,8325
	Max	0,0474	-0,8038	-0,9438	-0,6703	-0,7557	-0,7891	0,0474	-0,8239	-0,9010
50m	Mean	0,0699	-0,8661	-0,9707	-0,7406	-0,8057	-0,8539	0,0699	-0,8555	-0,9443
	Min	0,0156	-0,8062	-0,8517	-0,7022	-0,7476	-0,8000	0,0156	-0,7545	-0,8496
	Max	0,0380	-0,8723	-0,9758	-0,7648	-0,8132	-0,8690	0,0380	-0,8554	-0,9536
100m	Mean	0,0431	-0,9156	-0,9724	-0,8089	-0,8397	-0,9081	0,0431	-0,8617	-0,9678
	Min	-0,0063	-0,8072	-0,8716	-0,7052	-0,7549	-0,8046	-0,0063	-0,7660	-0,8636
	Max	-0,0003	-0,9091	-0,9703	-0,8012	-0,8437	-0,9026	-0,0003	-0,8583	-0,9643
200m	Mean	0,0095	-0,9300	-0,9641	-0,8174	-0,8562	-0,9206	0,0095	-0,8584	-0,9680
	Min	-0,0159	-0,8056	-0,8826	-0,7009	-0,7588	-0,8010	-0,0159	-0,7733	-0,8688
	Max	-0,0071	-0,9103	-0,9671	-0,8103	-0,8607	-0,9138	-0,0071	-0,8618	-0,9670
300m	Mean	-0,0006	-0,9106	-0,9686	-0,8142	-0,8613	-0,9180	-0,0006	-0,8619	-0,9697
	Min	-0,0225	-0,7965	-0,8787	-0,6918	-0,7526	-0,7929	-0,0225	-0,7678	-0,8630
	Max	0,0147	-0,9145	-0,9713	-0,8428	-0,8866	-0,9413	0,0147	-0,8815	-0,9810
400m	Mean	-0,0017	-0,8873	-0,9686	-0,8112	-0,8656	-0,9140	-0,0017	-0,8673	-0,9680
	Min	-0,0388	-0,7731	-0,8679	-0,6677	-0,7328	-0,7708	-0,0388	-0,7511	-0,8473
	Max	0,0056	-0,8744	-0,9609	-0,8221	-0,8782	-0,9224	0,0056	-0,8758	-0,9668
500m	Mean	-0,0178	-0,8481	-0,9594	-0,7809	-0,8500	-0,8889	-0,0178	-0,8564	-0,9519

Table 5.4. Antrophenic run (2). Correlation between min, max, mean temperatures and first, last and mean arrivals.

Correlation coefficients for arrival time vs. temperature - Fram Strait

SD=500m Time=1950-2050 Scenario=New Control Range=300-500km

Arrival Time		Temp 0-200m			Temp 200-1500m			Temp 0-1500m		
		Min	Max	Mean	Min	Max	Mean	Min	Max	Mean
	Min	-0,0928	-0,5077	-0,6873	-0,4576	-0,4691	-0,7641	-0,0928	-0,3850	-0,7588
	Max	-0,0242	-0,7864	-0,8638	-0,1899	-0,7837	-0,8373	-0,0242	-0,6599	-0,9001
50m	Mean	-0,0491	-0,7065	-0,8333	-0,2839	-0,6932	-0,8422	-0,0491	-0,5795	-0,8834
	Min	-0,1197	-0,4924	-0,6858	-0,5290	-0,4454	-0,7925	-0,1197	-0,3573	-0,7702
	Max	-0,0201	-0,8016	-0,8780	-0,1963	-0,7986	-0,8504	-0,0201	-0,6725	-0,9147
100m	Mean	-0,0498	-0,7139	-0,8424	-0,3089	-0,6955	-0,8589	-0,0498	-0,5850	-0,8962
	Min	-0,1273	-0,4809	-0,7004	-0,6032	-0,4154	-0,8259	-0,1273	-0,3309	-0,7938
	Max	-0,0238	-0,8067	-0,8847	-0,1965	-0,8017	-0,8536	-0,0238	-0,6749	-0,9202
200m	Mean	-0,0542	-0,7201	-0,8581	-0,3283	-0,6967	-0,8725	-0,0542	-0,5819	-0,9119
	Min	-0,1474	-0,4704	-0,7033	-0,6141	-0,4144	-0,8404	-0,1474	-0,3202	-0,8019
	Max	-0,0242	-0,8084	-0,8864	-0,1984	-0,8027	-0,8556	-0,0242	-0,6748	-0,9222
300m	Mean	-0,0659	-0,7135	-0,8598	-0,3419	-0,6899	-0,8813	-0,0659	-0,5701	-0,9168
	Min	-0,1590	-0,4693	-0,7046	-0,6360	-0,4035	-0,8468	-0,1590	-0,3145	-0,8055
	Max	-0,0238	-0,8090	-0,8876	-0,1986	-0,8044	-0,8556	-0,0238	-0,6756	-0,9229
400m	Mean	-0,0723	-0,7178	-0,8630	-0,3483	-0,6868	-0,8805	-0,0723	-0,5692	-0,9184
	Min	-0,1501	-0,4690	-0,7013	-0,6473	-0,4013	-0,8531	-0,1501	-0,3157	-0,8062
	Max	-0,0270	-0,8053	-0,8875	-0,2056	-0,8034	-0,8611	-0,0270	-0,6711	-0,9252
500m	Mean	-0,0637	-0,7089	-0,8573	-0,3619	-0,6832	-0,8823	-0,0637	-0,5622	-0,9157

Correlation coefficients for arrival time vs. temperature - Fram Strait

SD=60m Time=1950-2050 Scenario=New CO2 Range=300-500km

Arrival Time		Temp 0-200m			Temp 200-1500m			Temp 0-1500m		
		Min	Max	Mean	Min	Max	Mean	Min	Max	Mean
	Min	-0,0448	-0,7505	-0,8206	-0,3932	-0,7032	-0,8083	-0,0448	-0,6522	-0,8403
	Max	-0,0119	-0,6525	-0,8762	-0,3194	-0,5296	-0,6429	-0,0119	-0,6552	-0,8036
50m	Mean	-0,0237	-0,7297	-0,9122	-0,2924	-0,5984	-0,6900	-0,0237	-0,6911	-0,8455
	Min	-0,0583	-0,7509	-0,8531	-0,4257	-0,7231	-0,8425	-0,0583	-0,6683	-0,8745
	Max	-0,0362	-0,7420	-0,9211	-0,2927	-0,6250	-0,7120	-0,0362	-0,6970	-0,8601
100m	Mean	-0,0465	-0,8229	-0,9424	-0,3298	-0,7104	-0,8090	-0,0465	-0,7201	-0,9143
	Min	-0,0781	-0,7439	-0,8639	-0,4306	-0,7235	-0,8577	-0,0781	-0,6660	-0,8875
	Max	-0,0527	-0,8078	-0,9203	-0,3138	-0,7208	-0,8023	-0,0527	-0,7081	-0,8980
200m	Mean	-0,0560	-0,8567	-0,9278	-0,3599	-0,7864	-0,8757	-0,0560	-0,7378	-0,9338
	Min	-0,0798	-0,7430	-0,8706	-0,4313	-0,7138	-0,8550	-0,0798	-0,6633	-0,8904
	Max	-0,0543	-0,8461	-0,9300	-0,3628	-0,7893	-0,8793	-0,0543	-0,7377	-0,9367
300m	Mean	-0,0628	-0,8550	-0,9271	-0,3851	-0,8112	-0,9001	-0,0628	-0,7507	-0,9438
	Min	-0,0801	-0,7386	-0,8749	-0,4379	-0,7097	-0,8558	-0,0801	-0,6596	-0,8934
	Max	-0,0568	-0,8601	-0,9275	-0,3844	-0,8312	-0,9130	-0,0568	-0,7642	-0,9495
400m	Mean	-0,0636	-0,8442	-0,9263	-0,3931	-0,8191	-0,9068	-0,0636	-0,7558	-0,9462
	Min	-0,0799	-0,7346	-0,8704	-0,4424	-0,7029	-0,8543	-0,0799	-0,6553	-0,8900
	Max	-0,0466	-0,8665	-0,9218	-0,3896	-0,8513	-0,9190	-0,0466	-0,7836	-0,9486
500m	Mean	-0,0614	-0,8370	-0,9241	-0,3963	-0,8241	-0,9068	-0,0614	-0,7629	-0,9448

5.3 CONCLUSION OF THE STUDY

For TAP-B the first (early) arrivals will contain information about the climate warming if one consider a deep source. Every receiver depth considered gives this information but some signal processing has to be done. A shallow source does not provide the climate signal.
For the Fram Strait one should consider the mean arrival time. Both source depths and all receiver depths gives the information.

CHAPTER 6: SUMMARY OF RESULTS AND CONCLUSIONS

The goal of the acoustic modelling in Task 3.1 was to study the sensitivity of detecting climate change in ocean temperature by acoustic propagation along tracks in the Arctic basin.

The approach has been to use existing acoustic models such as OASES (wave number integration model), RAY (Ray trace model), SUPERSNAP (normal mode) and RAM (parabolic equation), to perform the sensitivity study by using data from Task 1 and model results from Task 2 as input. Prior to the sensitivity study software had to be established

- to efficiently produce realistic environmental input to the acoustic models of the data delivered from Task 1
- to interface the acoustic models with the large amount of climate modelling results from Task 2
- to organise the large amount of input data and results
- to present the results from the long term simulation of acoustic propagation parameters

ACOUSTIC PROPAGATION MODELS

The acoustic propagation model OASES was for the first time implemented on a super computer to do simulations for more than 1000 km long tracks. Simulations have been done for a 400 km long track in the Fram Strait and two more than 1000 km long tracks in the interior of the Arctic basin.

The OASES model has been used to calculate the transmission loss as function of range and frequency for different source and receiver depths. Comparing the results show that the optimum frequency of propagation is most sensitive to the depth of the receiver relative to the surface duct and less sensitive to the position of the source. When both the source and receivers are positioned within the surface duct (as in the upper plot) the centre of optimum frequency domain of propagation is 65 Hz. If a receiver below the surface duct is concerned the optimum frequency is around 25 Hz. The same optimum frequency is found when source and receiver is below the surface duct the optimum frequency.

The OASES model was not used for the Arctic Ocean temperature sensitivity test (neither for travel time nor intensity) due the heavy computer demand. On the other hand the OASES model was essential for the sea ice sensitivity study and to document the optimum frequency of propagation. The RAY model was used for the travel time calculations and RAM for the transmission loss calculations. SUPERSNAP has been used to interpret the results in terms of modes.

ACOUSTIC INSONIFICATION OF THE ARCTIC BASIN

The acoustic insonification of the Arctic Basin for the selected tracks have been studied by calculating the transmission loss as function of depth and range. The RAM model was used for a frequency of 20 Hz and two source depths (60 m and 500 m).. The calculations show that the transmission loss is significantly different for the two source depths. If a relatively shallow source depth is used the acoustic energy is generally trapped within the 200 m thick surface duct. Whereas for a deep source the energy is more concentrated between 300 and 1000 m, allowing these water masses to be monitored. On the other hand the shallow source should be excellent for monitoring the surface water layer.

The transmission loss at deeper depths are less influenced by the position of the source and more related to changes in the bathymetry. The part of the acoustic field which penetrates to the deeper part of the basin is influenced by the topographical conditions, while the acoustic field in the upper part of the ocean is less influenced. In order to avoid influence by the sea floor on the important part of the acoustic field (which probes the 250-1500m water masses) one should keep the receiver array away from shelves and other shallow water regions. For the TAP-B track one should be aware that positioning a receiver array in shallow water (around 500 m) will cause additional transmission loss of the modes/rays which goes through the water masses between 250-1500m.

These results will have strong impact on how a long-term monitoring system should be designed with regard to source and receiver configuration. According to our results the source should be deployed at 500 m depth rather that at 60 m, which is used in the ACOUS, in order to get the best insonification of the Atlantic Intermediate Water (AIW). Furthermore, the simulations show that in the selection of tracks for monitoring the AIW it is important to avoid shallow water regions, which will effectively filter away the part of the acoustic field that penetrates AIW water masses.

SENSITIVITY TO SEA ICE

In order to use these open ocean models within ice covered regions at low frequencies a sensitivity study to sea ice was performed at low frequencies. The result of this work showed that changes in ice thickness will not cause any travel time change compared to open water conditions if a low frequency (20Hz) source is used, and under the assumption that changes in sea ice thickness was either caused by pure melting/freezing of sea water or that in case of a snow fall the corresponding mass of water "flows away" (corresponding to the mass conservation). Furthermore, we found that roughness, as it is treated in the OASES model, does not cause significant changes in travel time.

The reflection coefficient at frequencies below 100 Hz is insensitive to ice thickness, while it is slightly sensitive to changes of the under ice roughness. On the other hand the reflection loss as function is very sensitive to ice thickness at frequencies above 100 Hz, and that a thinning of ice will cause a reduction of reflection loss at increasing frequencies.
The conclusions of this sensitivity study are that

- low frequency propagation can be modelled by using open water models like RAM and RAY without corrections for ice. This will make the basin wide calculations, for studying the effect of temperature/salinity changes in the Arctic Basin, much less computer demanding.
- basin wide estimates of mean ice thickness can not be provided by a low frequency source
- Regional estimates can potentially be provided by inversion techniques based on transmission loss (and travel time) using signals from a broad band or coded (100-5000 Hz) source positioned in the surface duct.

SENSITIVITY TO OCEAN FIELDS USING HISTORICAL DATA

The historical data from the US-Russian data Atlas for tracks corresponding to TAP A and TAP B were extracted and used as input to the RAY model to do acoustic experiments with different depths for sources and receivers. This study showed that there has not been "trendy changes" in the oceanographic fields either for TAP A, TAP-B or the Fram Strait during the period from 1950 till 1989. Furthermore these simulations shows that in order to monitor the intermediate water depths from 200-1500 m one should put the source at 500 m. If the source is put 60 m below the surface as it was done in the ongoing long term Acoustic experiment

performed by American Scientist the major acoustic energy is put into the surface duct and less energy goes into the "more important" intermediate water masses. Some rays penetrates the deeper depths but they seem to be less stable for seasons and decades. As most of the acoustic field is composed of rays which traces the mix layer (surface duct) this configuration is better for monitoring changes in the duct layer.

SENSITIVITY TO OCEAN FIELDS USING CLIMATE MODELLING RESULTS

Two anthropogenic scenarios (including doubling of CO_2) and corresponding control runs have been provided from Task 2. Each scenario provided monthly mean ocean data over 100 years where the first 25 years is spin up for the climate model. The monthly averaged temperature and salinity profiles along the three tracks are used to calculate corresponding sections of sound speed to be feeded into the acoustic model.
In each acoustic experiment the eigenrays for a source located either on 60m or at 500 m and six receivers are calculated using RAY. Each acoustic simulation took around 2.5 months for the TAP-A (2623 km), roughly 3 weeks in the case TAP B (700 km), while in the case of Fram Strait the acoustic calculations took around 8 days (200 km). Each scenario provided monthly mean ocean data over 100 years. First the 100 years of monthly averaged temperature and salinity profiles along the three tracks were used to calculate corresponding sections of sound speed, which were fed into the RAY model. The Ray model calculated the eigenrays and eigenfronts for each source/receiver configuration. The travel times for each eigenray found for each "acoustic shot" are plotted against time.

TAP-B

In the case of source depth (SD) of 500 m and receiver depths (RD) varying from 50-100-200-300-400-500m the first arrivals at all the receivers, which corresponded to the deeper penetrating eigenrays, were relatively stable to monthly and inter-annual changes. A clear decrease in travel time of 4.5 s was found as the mean temperature from 200-1500 m increased by about 2.5° C. The late arrivals corresponded to the surface ducted eigenrays which were not related to the warming of the deep water masses. The first arrival time was correlated with mean temperature in the 0-200m, 200-1500 and 0-1500, showing a negative correlation of about 0.7 at the deepest receiver. At the other receivers the correlation was still negative but decreasing in value.

In the experiments with shallow source depth (60 m) the results show that the strongest part of the signal are due to the rays which are trapped in the surface duct only a few rays penetrates deeper part of the ocean and these rays are very unstable from month to month. Furthermore, the number of deeper going rays are reduced with time and the arrivals become steadily later as the temperature increases in the water masses between 200-1500 m. This is caused by a strengthing of the vertical temperature gradient as the temperature increases in the water masses below the surface duct while the temperature in the duct is constant with time. This causes an acoustic intensification within the duct. On the other hand the acoustic signal contains increasingly less information about the temperature below the duct.

Using a shallow source at 60 m depth there is no climate signal present at any of the receivers. In the ongoing Russian/American ACOUS experiment (Mikalevsky et al., 1999) a source depth of 60 m has been used, and according to our results this experiment does not contain optimal information about the changes in the AIW. The changes observed by this system are generally found to be related to decadal ocsillations in the upper water masses (0-500 m). By positioning the acoustic source at 500 m and the receiver array 700 km the climate change occurring in the water masses between 200 and 1500 m is easily detected.

Fram Strait.

Data both from two anthropogenic and the control run were used as input to ray tracing model (RAY) for simulations across the eastern Fram Strait where the core of warm Atlantic water is a dominant feature. Seasonal as well as long term variability are observed in both the anthropogenic and the control runs. The anthropogenic simulation shows a stronger warming signal compared to the control run from 2000 to 2050.

The acoustic simulation show a clear decrease in the travel times but the travel times are less stable (due to strong seasonal effects and decadal variations) than in the interior Arctic. This indicates that an averaging of the arrivals has to be performed to pick up the climate signal earlier than when considering the "raw" data. This has to be considered more in detail when developing the inversion techniques. By correlating the first arrival, mean arrival time and last arrival with mean temperature in 0-200m, 200-1500m and 0-1500m a negative correlation factor between 0.7 and 0.94 is found. This is a good relation between increase in temperature and decrease in travel time.

CONCLUSION

The overall conclusion is that acoustic monitoring of ocean climate is possible both in the Arctic Basin and in the Fram Strait.

Chapter 7: References

Aagard, K. and E. Carmack 1994

Allison and Moritz 1995

Anderson, L.G., G. Bjørk, O. Holby, E.P.Jones, G. Kattner, K.P. Koltermann, B. Liljeblad, R. Lindegren, B. Rudels, and J. H. Swift, (**1994**), Water masses and circulation in the Eurasian Basin: Results from the Oden 91 expedition", J. Geophys. Res. Vol 99 (C2), pp.3273-3283.

Bjørgo, E., O. M. Johannessen and M. W. Miles (1997). Analysis of merged SMMR-SSMI time series of Arctic and Antarctic sea ice parameters 1978-1995, *Geophysical Research Letters*, Vol.24, no.4, pp. 413-416.

Buckingham, M.J., (**1991**). "On acoustic transmission in ocean surface waveguides" Phil. Trans. R. Soc. London. A 335, 513-555.

Bourke, R.H., A.R. Parsons. (**1993**). Ambien tnoise characteristics of the northwestern Barents Sea. J. Acoust. Soc. Am. 94 (5), 2799-2808.

Brekhovskikh, L.M., (**1980**) Waves in layered media. (Sec. Ed.) Applied mathematics and Mechanics 16. Academic Press, Inc.

Dahl, P.H., (**1989**), "Acoustic Diffraction from a Semi-Infinite Elastic Plate Under Arbitary Fluid Loading with Application to Scattering from Arctic Ice Leads", Doctoral Dissertation, WHOI-89-28.

Diachoke, O.I., (**1976**) "Effects of sea -ice ridges on sound propagation in the Arctic Ocean", J.Acoust.Soc.Am., Vol.59 (5), 1110-1120.

Dyer I., P.H. Dahl, A.B. Baggeroer, P.N. Mikhalevsky (**1987**). Ocean Dynamics and Acoustic Fluctuations in the Fram Strait Marginal Ice Zone. Science, Volume 236, 435-436.

Fricke, J.R., (**1991**). "Acoustic scattering from elastic ice, A finite difference solution", Doctoral dissertation, WHOI-91-10.

Fricke, J. R. (**1993**), "Acoustic scattering from elemental Arctic ice features: Numerical modelling results.", J.Acoust. Soc.Am. 93 (4), 1784-1796.

Fricke, J. R. and G.L. Unger (**1995**), "Acoustic scattering from elemental Arctic ice features: Experimental results.", J.Acoust. Soc.Am. 97 (1), 192 - 198.

Gerstoft, P., H. Schmidt (**1991**). A boundary element approach to ocean seismoacoustic facet reverberation. J. Acoust. Soc. Am. **89** (4), 1629-1642.

Gjevik, B., E.Nøst, T.Straume,. (1990). Atlas of tides on the shelfs of the Norwegian and the Barents Sea. Department of Mathematics, University of Oslo, P.O. Box 1053 Olso, Norway.

Goh, J. T., H. Schmidt (**1994**), "Validity of spectral theories for weakly range dependent ocean environments-Numerical results", J. Acoust. Soc. **95** (2), 727-732 .

Goh, J.T., H. Schmidt, (**1995**) "Spectral super element approach to range dependent ocean acoustic modelling", J.Acoust. Soc. Am. **98** (2) **100**, 465-472.

Goh, J.T., H. Schmidt, (**1996**) "A hybrid couples wave-number integration approach to range-dependent seismoacoustic modelling", J.Acoust. Soc. **100** (3), 1409-1420.

Goh, J.T., H. Schmidt, P. Gerstoft, Woojae Seong, (**1997**)"Benchmarks for validating range -dependent seismo-acoustic propagation codes", IEEE Journal of oceanic engineering, Vol.XX, NO.Y.

Goodman, D.J., P.Wadhams and V.A. Squire (1980), "The Flexural Response of a Tabular Ice Island to Ocan Swell", Annals of Glaciology.Hunter, S.C. (1983). "Mechanics of contineous media. Second edition.", (Ellis Horwood).

Hamre et al. AMOC Task 1 report. NERSC Technical Report no. 162, January 1999.

Jensen, F.B., W.A. Kupermann, M.B. Porter, H. Schmidt, (**1994**). *Computional ocean Acoustics*, (American Institute of Physics, New York, 1994) pp. 121-129.

Jin, G., J.F.Lynch, R.Pawlowicz, P. Wadhams. (**1993**). Effects of sea ice cover on acoustic ray travel times, with applications to the Greenland Sea tomography experiment. J.Acoust. Soc. Am. 94 (2), 1044-1057.

Johannessen, O.M., J.A. Johannessen, B. Farrelly, and E.A. Svendsen (1983). Oceanographic conditions in the marginal ice zone noth of Svalbard in early fall 1979 with an emphasis on mesoscale processes. J. Geophys. Res., 88, 2755-2769.

Johannessen, O.M, J.A. Johannessen, E. Svendsen, R.A. Shuchman, W.J. Campbell, E.G. Josberger (**1987**). "Ice- Edge Eddies in the Fram Strait Marginal Ice Zone," SCIENCE, Volume 236, 427-429.

Johannessen, J. A. , O.M. Johannessen, E. Svendsen, R. Shuchman, T. Manley, W.J. Campbell, E.G. Josberger, S. Sandven, J. C. Gascard, T. Olaussen, K. Davidson, J. Van Leer, (**1987**). "Mesoscale eddies in the Fram Strait marginal ice Zone during the 1983 and 1984 marginal ice zone experiments," J. Geophys. Res. **92**, 6754 - 6772.

Johannessen, O.M., Ø. Nesse and I. Engelsen (**1992a**) Correlation between ambient noise and environmental variables in the MIZ of the Barents Sea. NERSC Technical Report no. 52.

Johannessen, O. M., H. Sagen, Ø. Nesse, I. Engelsen and S. Sandven (**1992b**). "Ambient noise generated by ice-ocean jets, eddies and tidal current in the marginal ice zone," in *Proceeding of European Conference on Underwater Acoustics,* edited by M. Weydert (Elsevier Applied Science, 1992), pp. 28 - 38 .

Johannessen, O.M, et al (1997). Acoustic Monitoring of the Ocean Climate in the Arctic Ocean (AMOC). Technical Annex to AMOC contract with the European Commision Environment and Climate Programme, 1994-1998.

Johannessen, O.M., M. W. Miles and E. V. Shalina (1999a). Satellite evidence for an Arctic sea ice cover transformation. *Science*, Vol.286, 1937-1939.

Kowalik and Proshutinsk (1994). "The Arctic Ocean Tides." in *The polar oceans and their role in shaping the global environment, Nansen Centennial Volume, Geophysical Monograph 85,* edited by O.M. Johannessen, R.D.Muench and J.E. Overland, (American Geophysical Union, United States of America, 1994) pp. 137-158

Kupermann, W.A., H. Schmidt (**1989**). Self-consistent perturbation approach to rough surface scattering in stratified elastic media. J.Acoust. Soc. Am. **86** (4), 1511-1522.

Laible, H.A., S. D. Rajan. (1996). Temporal evolution of ice reflectivity. J. Acoust. Soc. Am., **99** (2), 851-865

LePage, K. and H. Schmidt (**1994**), Modelling of low frequency transmission loss in the central Arctic", J.Acoust. Soc. Am **96** (3), 1783-1795.

Lynch, J.F., G. Jin, R. Pawlowicz, D. Ray, A. J. Plueddemann, C.-S. Chiu, J.H. Miller, R.H. Bourke, A.R.Parsons, R. Muench (**1996**). Acoustic travel-time perturbations due to shallow-water internal waves and internal tides in the Barents Sea Polar Front: Theory and experiment. J. Acoust. Soc. Am.99 (2), 803-821.

Makris, N.C. , Dyer, I., (**1991**). "Environmental correlates of Arctic ice edge noise," J. Acoust. Soc. Am. **90**, 3288-3298.

Mikhalevsky, P., A.B. Baggeroer, H. Schmidt, K. von der Heydt, E.K. Scheer, A. Gavrilov (1995). Transarctic Acoustic Propagation. Sea Ice Mechanics and Arctic Modelling Workshop, Volume I, Anchorage, Alaska.

Mikhalevsky, P.N., A.N. Gavrilov and A.B. Baggeroer (1999). The Transarctic Acoustic Pro pagation Experiment and Climate Monitoring in the Arctic, Preprint to IEEE *Journal of Oceanic Engineering,*.

Munk, W., P. Worcester, C. Wunsch (**1995**). Ocean Acoustic Tomography. Cambridge Monographs on Mechanics.

Nagurny, V., Korostelev, V. Ivanov (1999). INTAS 97-1277 Project: Multi year Variability of Sea ice Thickness in the Arctic Basin Measured by Elastic-gravity Waves on the Ice Surface. A technical report from the Arctic and Antarctic Research Institute, St. Petersburg.

Noble, B..(**1958**). Methods based on the Wiener-Hopf Technique. Chelsea Publishing Company, New York.

Parkinson et al., 1999

Pawlowicz, R., D. Farmer, B. Sotirin, S. Ozard (**1996**). Shallow-water receptions from the transarctic acoustic propagation experiemnt. J. Acoust. Soc.Am. **100** (3), 1482-1491.

Rothrock, D.A., Y.Yu, G.A. Maykut (1999). Thinning of the Arctic Sea Ice Cover. *Geophys.Res.Lett.*23, 3469-3472.

Sagen, H., Ph D thesis, 1998

Sagen, H., O.M. Johannessen, S. Sandven. (1990). The influence of sea ice on ocean ambient noise. "Ice Technology for Polar Operation". Edited by T.K.S.Murthy, J.G. Paren, W.M. Sackinger, P. Wadhams. Computational Publications, 309-320.

Sandven, S., O.M.Johannessen. Internal waves in the marginal ice zone, JGR 1987

Schmidt, H. (**1988**). SAFARI. Seismo Acoustic Fast field Algorithm for Range-Independent environments. User's guide. Saclant Undersea Research Centre. Report.

Schmidt, H. (**1994**). "Seismo-Acoustics of the Arctic Ice Cover," in *Proceedings of the second European conference on Underwater Acoustics, Volume 1,* edited by L. Bjørnø, (European Commission, Belgium, 1994), pp. 3-14.

Schmidt, H.. (**1997**). OASES Version 2.1 User Guide and Reference Manual. Department of Ocean Engineering. Massachusetts Institute of Technology.

Vinje, T. 1998

Wadhams, P., (**1987**

Wadhams, P. (**1992**).

Wadhams, (**1994**).

Wadhams, (**1998**).